UCSF
UC San Francisco Electronic Theses and Dissertations

Title
Surface Functionalization of Liposomes with Proteins and Carbohydrates for Use in Anti-Cancer Applications

Permalink
https://escholarship.org/uc/item/3r4315s7

Author
Platt, Virginia Marie

Publication Date
2010

Peer reviewed|Thesis/dissertation

eScholarship.org Powered by the California Digital Library
University of California

Surface Functionalization of Liposomes with Proteins
and Carbohydrates for Use in Anti-Cancer Applications

by

Virginia M. Platt

DISSERTATION

Submitted in partial satisfaction of the requirements for the degree of

DOCTOR OF PHILOSOPHY

in

Bioengineering

in the

GRADUATE DIVISION

of the

UNIVERSITY OF CALIFORNIA, SAN FRANCISCO

AND

Copyright 2010

by

Virginia M. Platt

To my family, born and chosen:

I am forever changed for loving you and being loved by you

Acknowledgements (I)

The text of Chapter 1 is in part a reprint of materials published in the journal *Molecular Pharmaceutics* and the book *Hyaluronan in Cancer Biology*. Virginia M. Platt wrote the review and book chapter, F.C. Szoka assisted in thoroughly revising both.

Platt, V. M., and Szoka, F. C., Jr. (2008) Anticancer therapeutics: targeting macromolecules and nanocarriers to hyaluronan or CD44, a hyaluronan receptor. *Mol Pharm 5*, 474-86.

Platt, V. M., and Szoka, F. (2009) Exploiting the Hyaluronan-CD44 Interaction for Cancer Therapy, in *Hyaluronan in Cancer Biology* (Stern, R., Ed.) pp 379-403, Elsevier, San Francisco.

The text of Chapter 3 is in part a reprint of materials to appear in the journal *Bioconjugate Chemistry*. Virginia M. Platt wrote the paper, F.C. Szoka revised the manuscript, Zhaohua Huang, Limin Cao and Kareen Riviere contributed invaluable experimental materials.

The text of Chapter 4 is co-authored by Douglas Watson, who assisted in designing experiments, preparing peptide-lipid conjugates and liposome formulations, performing animal immunization experiments and manuscript writing. F.C. Szoka formulated the results and revised the manuscript.

The contribution of Virginia Platt is comparable to that of a standard thesis.

Acknowledgements (II)

My sincerest appreciation is extended to Dr. Francis C. Szoka, Jr. for his resolute mentorship, guidance in pursuing experimental perfection and awe-inspiring dedication to intellectual curiosity.

I am deeply and sincerely grateful to those who contributed to the completion of this thesis:

Dr. Robert Stern who served on both my qualifying exam and dissertation committees, as well as provided honest, friendly guidance and support.

Dr. Tejal Desai who served on my dissertation committee and graciously acted as my academic advisor.

Dr. Chris Cullander who served on my qualifying exam committee, dissertation committee and who is an encouraging force for all students.

Dr. Jeff Lotz, Dr. David Schaffer and Dr. Kathleen Giacomini for kindly serving on my qualifying exam committee.

Current and Past Szoka Laboratory Members who are both friends and colleagues:

Dr. Zhaohua Huang for his expert tutelage in chemical conjugation techniques, his eagerness for scientific discussion and his numerous experimental contributions.

Dr. Dipali Ruhela for patient mentorship in all things, including carbohydrate chemistry, as well as her experimental involvement.

Dr. Douglas Watson for collaborating on the NTA adjuvant project and for the sense of peace he brought to the laboratory environment.

Katherine Jerger for expert assistance with animal work and cell culture as well as her graceful, comforting manner and immeasurable patience.

Dr. Joshua Park, Dr. Kareen Riviere and Dr. Limin Cao for experimental assistance and friendly discussions regarding science and life.

Nichole Macareg, Ed Dy and Leanna Lagpacan for laboratory guidance, cell culture and protein production.

Dr. Juliane Nguyen for her fruitful intellectual dialogues.

With the greatest warmth I extend appreciation for the contributions made to both my scientific and personal endeavors by Dr. Andrew Mackay, Dr. Rich Cohen, Dr. Marieke van der Aa, Dr. Oana Martin, Dr. Mahmoud Jaafari, Dr. Lisa Ueychi-O'Brien, Dr. Weijun Li, Dr. Bo Chen, Dr. Mark Rashkin, Dr. Norased Nasongkla, Dr. Grace Huynh, Ms. Emily Perttu, Mr. Matthew Tiffany, Mr. Colin Walsh, Mr. Michael Motion, Mrs. Aiping Lee, Ms. Laura Serwer, Ms. Becky Cebula and Mr. Steve Ha.

Ms. SarahJane Taylor for her endearingly positive outlook on the bureaucratic process.

The family and friends who have supported me on this journey without hesitation:

My mother, Elizabeth Dunn who showed me true bravery, love and compassion throughout my life and who is the epitome of strength in womanhood.

My stepfather, Edward Dunn who taught me how to sleep anywhere and from whom I continually learn about peace and grace.

My brother, Alanson Platt who is the greatest older brother on the planet.

Dr. Eric Johansen who was unflinchingly helpful and was always there for a hug, a laugh, a smile or a diabolical scheme.

Mr. Jesse Engelberg who is the best advocate a devil could want and the only neighbor I will ever need.

My partner, Jack Maclean who has been an unrelenting force for balance, serenity and hope.

This work was funded by NIH R01-GM061851.

Abstract

Surface Functionalization of Liposomes with Proteins and Carbohydrates for Use in Anti-Cancer Applications

Virginia M. Platt

Liposomes can be used to exploit the altered biology of cancer thereby increasing delivery of liposome-associated anti-cancer drugs. In this dissertation, I explore methods that utilize the unique cancer expression of the polymeric glycosaminoglycan hyaluronan (HA) and the HA receptor CD44 to target liposomes to tumors, using liposomes functionalized with proteins or oligosaccharides on their surface. To make it easier to prepare protein-functionalized liposomes, a non-covalent protein/liposome association method based upon metal chelation/his_6 interaction was devised and characterized. I evaluated non-covalent attachment of the prodrug converting enzyme yeast cytosine deaminase, the far-red fluorescent protein mKate, two antigens ovalbumin and the membrane proximal region of an HIV GAG and hyaluronidase, a HA-degrading enzyme.

In **Chapter 2,** I describe the synthesis of hyaluronan-oligosaccharide (HA-O) lipid conjugates and their incorporation into liposomes to target CD44-overexpressing cancer cells. HA-O ligands of defined-length, up to 10 monosaccharides, were attached to lipids via various linkers by reductive amination. The HA-lipids were easily incorporated into liposomes but did not mediate binding of liposomes to CD44 overexpressing cells.

In **Chapter 3**, I evaluate the capacity of tris-NTA-Ni-lipids incorporated within a liposome bilayer to associate with his_6-tagged proteins. Tris-NTA-lipids of differing structures and avidities were used to associate yeast cytosine deaminase and mKate to the surface of liposomes. Two tris-NTA-lipids and a mono-NTA lipid associated his-tagged proteins to a 1:1 molar ratio in solution. The proteins remained active while associated with the liposome surface. When challenged *in vitro* with fetal calf serum, tris-NTA-containing liposomes retained his-tagged proteins longer than mono-NTA. However, the tris-NTA/his_6 interaction was found to be in a dynamic state; free yeast cytosine deaminase rapidly competed with pre-bound mKate for NTA occupancy. In the circulation of mice, his-tagged proteins associated with NTA-liposomes were cleared as rapidly as free protein.

In **Chapter 4**, I study the effect of NTA/his-tag avidity on immune response when NTA-containing liposomes are used as non-covalent, particulate adjuvants. Two his-tagged antigens, ovalbumin and the membrane proximal portion of HIV Gag, were associated with NTA-liposomes containing either mono-NTA or tris-NTA lipids. The immune response to each antigen was compared to control adjuvant formulations in which antigens were admixed with or covalently-conjugated to liposomes. The weaker antigen, the HIV Gag peptide, induced a stronger immune response when associated with NTA-containing liposomes than when admixed with liposomes. Ovalbumin preparations in which the protein was admixed with particles or non-covalently associated with NTA-liposomes elicited a higher immune response than free ovalbumin or ovalbumin admixed

with the control adjuvant alum. For both antigens, NTA-liposome responses were less than the response to antigens covalently linked to the liposome.

In **Chapter 5**, I evaluate the potential for hyaluronidase to target conjugated liposomes to tumors or improve liposome motility within hyaluronan-rich tumors. Ovine hyaluronidase was modified using iminothiolane to introduce sulfhydryl groups into the enzyme. The enzyme was attached to liposomes via maleimide lipids or to maleimide-his_{10} in order to engineer non-covalent NTA-liposome association. Enzyme activity was retained after sulfhydryl addition and after attachment to liposomes. Liposome-conjugated hyaluronidase degraded an HA-gel at the same rate as admixed liposomes. When hyaluronidase-liposomes were injected intravenously in mice, the hyaluronidase conjugated-liposomes experienced faster clearance than control liposomes but slower clearance than free hyaluronidase.

As a whole, these studies may help develop universal methods for a range of protein therapeutics and anti-cancer targeting agents.

Table of Contents

Preliminary Pages

Abstract vi
List of Tables xii
List of Figures and Schemes xiii

Chapter 1: Surface Functionalization of Liposomes for Anti-Cancer Applications

1.1 Overview 1
1.2 Exploiting Hyaluronan Biology for Anti-Cancer Therapeutics
1.2.1 The Biology of Hyaluronan 4
1.2.2 Hyaluronan as a Drug Carrier 5
1.2.3 Hyaluronan Drug Conjugates 9
1.2.4 Hyaluronan as a Targeting Agent 10
1.2.5 Targeting to the Hyaluronan Extracellular Matrix with Proteins 13
1.2.6 Disrupting the Hyaluronan Extracellular Matrix 15
1.3 Nitrilotriacetic Acids for Non-Covalent Liposome-Protein Association
1.3.1 Multivalent-Nitrilotriacetic Acids Increase Particle/Protein Avidity 16
1.3.2 Monovalent and Multivalent Nitrilotriacetic Acids on Liposomes 19
1.4 Therapeutic Proteins on the Surface of Liposomes 23
1.4.1 Recombinant Factor VIII 25
1.4.2 Superoxide Dismutase 26
1.4.3 Anti-HER2 Antibodies 27
1.5 Conclusion 29
1.6 Literature Cited 30

Chapter 2: Synthesis, Formulation and Cell Binding of Hyaluronan Oligosaccharide-Targeted Liposomes

2.1 Abstract 37
2.2 Introduction 38
2.3 Experimental Procedures
2.3.1 Materials 42
2.3.2 Digestion of HA 42
2.3.3 Separation of HA Oligomers by Size Exclusion Chromatography 43
2.3.4 MALDI-TOF MS Analysis of HA Oligomers and HA_n-DPPE Conjugates 43
2.3.5 Coupling HA_4 to DPPE via Reductive Amination 44
2.3.6 Coupling HA_n to DPPE with Alternate Solvents 45
2.3.7 Coupling HA_n with Alternative Lipids and Linkers 47
2.3.8 HA_n-DPPE Conjugate Purification 49
2.3.9 Conjugating HMW-HA to Fluorescein Amine 49
2.3.10 Liposome Preparation 50
2.3.11 Liposome Binding to Cells 50
2.3.12 CD44 Analysis and Manipulation using FACS 51
2.4 Results
2.4.1 Digestion and Separation of HA Oligomers 52
2.4.2 Synthesis of Lipooligosaccharides 53
2.4.3 Coupling HA_n to DPPE with Alternate Solvents 54
2.4.4 Purification of Lipooligosaccharides 55

2.4.5 Analysis of Lipooligosaccharides 55
2.4.6 Binding of HA-Modified Liposomes to Cultured CD44-Expressing Cells 58
2.4.7 Binding of Fluorescent HMW-HA-FA to Cultured CD44-Expressing Cells 60
2.5 Discussion 61
2.6 Acknowledgements and Author Contributions 64
2.7 Literature Cited 64

Chapter 3: Influence of Multivalent Nitrilotriacetic Acid Lipid-Ligand Affinity on the Circulation Half-Life in Mice of a Liposome-Attached His_6-Protein

3.1 Abstract 67
3.2 Introduction 68
3.3 Experimental Procedures
3.3.1 Materials 71
3.3.2 Synthesis of tris-NTA-LYS-DOD and tris-NTA-DAP-DOD 72
3.3.3 Synthesis of FITC-DSPE 72
3.3.4 Formation of Liposomes 73
3.3.5 Protein Production 74
3.3.6 Liposome-Protein Association 75
3.3.7 Protein Activity 75
3.3.8 Protein Dissociation in Fetal Calf Serum 76
3.3.9 His-Tagged Protein Competition 77
3.3.10 Protein Half-Life *in vivo* 77
3.4 Results
3.4.1 Liposome Formulation and Construction 79
3.4.2 His-Tagged Protein Association with Surface Displayed NTA on Liposomes 80
3.4.3 Activity Retention of Surface Associated Proteins 83
3.4.4 Protein Dissociation in the Presence of Refiltered FCS 85
3.4.5 Competition between NTA-Liposome Bound His_6-Proteins and Subsequently Added His_6-Proteins 87
3.4.6 Serum Half-Life of NTA-Liposome Associated Proteins Upon Intravenous Administration 88
3.5 Discussion 88
3.6 Acknowledgements and Author Contributions 94
3.7 Literature Cited 94

Chapter 4: Antibody Response in Mice to Polyhistidine-Tagged Peptide and Protein Antigens Attached to Liposomes via Lipid-Linked Nitrilotriacetic Acid

4.1 Abstract 97
4.2 Introduction 98
4.3 Experimental Procedures
4.3.1 Materials 102
4.3.2 Synthesis of Peptides and Lipids 102
4.3.3 Preparation of Polyhistidinylated Ovalbumin 106
4.3.4 Preparation of Fluorescent Proteins 107
4.3.5 Liposome Preparation 108
4.3.6 Liposome-Antigen Association *in vitro* 109
4.3.7 Animal Immunizations 110
4.3.8 ELISA 111
4.3.9 Statistical Analysis 112
4.4 Results
4.4.1 Preparation of Antigens and Liposomes 112

4.4.2 Liposome-Antigen Association 116
4.4.3 Humoral Immune Responses in Mice 117
4.5 Discussion 122
4.6 Acknowledgements and Author Contributions 126
4.7 Literature Cited 127

Chapter 5: Evaluating the Potential for Hyaluronidase-Liposome Targeting to Tumors and Intratumoral Translocation

5.1 Abstract 130
5.2 Introduction 131
5.3 Experimental Procedures
5.3.1 Materials 134
5.3.2 Modification of Hyaluronidase for Covalent Attachment 134
5.3.3 Formation of Liposomes 135
5.3.4 Association of Hyaluronidase-His_{10} with NTA-Containing Liposomes 136
5.3.5 Covalent Attachment of Modified Hyaluronidase to Liposomes 137
5.3.6 Quantitation of Liposome-Protein Association or Attachment 138
5.3.7 Hyaluronidase Activity Assay 138
5.3.8 Liposome Diffusion Through a Hyaluronan Gel 139
5.3.9 Hyaluronidase-Liposome Interactions with HA-Expressing Cells 140
5.3.10 Hyaluronidase-Liposome Half-Life and Biodistribution in Tumored Mice 141
5.4 Results
5.4.1 Non-Covalent Association of Hyaluronidase with NTA-Liposomes 142
5.4.2 Covalent Attachment of Hyaluronidase to Liposomes 144
5.4.3 Enzymatic Activity of Hyaluronidase-Liposomes 145
5.4.4 Hyaluronidase Diffusion Through an Hyaluronan Gel 146
5.4.5 Hyaluronidase-Liposome Binding to HA-Expressing Cells 148
5.4.6 Hyaluronidase-Liposome Half-Life and Biodistribution in Tumored Mice 150
5.5 Discussion 154
5.6 Acknowledgements and Author Contributions 159
5.7 Literature Cited 159

Chapter 6: Conclusions and Future Outlook

6.1 Summary of Findings 161
6.2 Future Directions 164
6.3 Literature Cited 167

List of Tables

Chapter 1

Table 1-1	Hallmarks of the Enhanced Permeability and Retention (EPR) Effect	6

Chapter 2

Table 2-1	Reaction Conditions for Various Length Oligomers	44
Table 2-2	MALDI-TOF MS Results for HA Oligosaccharides	53
Table 2-3	MALDI-TOF MS Results for HA_n-DPPE Conjugates	56

Chapter 3

Table 3-1	Liposome Diameter and Zeta-Potential of NTA-Containing Liposomes	79
Table 3-2	Measurement of yCD Association with NTA-Containing Liposomes	82

Chapter 4

Table 4-1	Sequences and Molecular Weights of Peptide Antigens	105
Table 4-2	Vesicle Sizes of Ovalbumin-Containing Liposome Preparations	115
Table 4-3	Association of Ovalbumin with Liposomes Containing NTA-Lipids	118
Table 4-4	Statistical Significance of Differences in Anti-Ovalbumin IgG Titer	121

Chapter 5

Table 5-1	Hyaluronidase Association with Liposomes and Retained Enzymatic Activity	145
Table 5-2	Diameter and Zeta-Potential of Hyaluronidase-Liposomes	146
Table 5-3	Half-Life of Hyaluronidase-Liposomes	151
Table 5-4	Amount of Tritiated Hyaluronidase-Liposome Per Organ	153

List of Figures and Schemes

Chapter 1

Figure 1-1	The Potential Ways the CD44-HA System may be Targeted for Cancer Therapies	3
Figure 1-2	The Polymeric Repeat Structure of Hyaluronic Acid	7
Figure 1-3	The HA/CD44 Binding Interaction	8
Figure 1-4	Matrix Attachment Therapy	14
Figure 1-5	The Structure of the Nitrilotriacetic Acid (NTA)/Histidine Interaction	17
Figure 1-6	Potential Uses of Nitrilotriacetic Acid Lipids	18
Figure 1-7	The Multiple Types of Liposome/Protein Interactions	24

Chapter 2

Figure 2-1	The Polymeric Repeat of Hyaluronic Acid	39
Figure 2-2	Amine-Containing Lipids Conjugated to HA via Reductive Amination	48
Figure 2-3	Example Size Exclusion Column Profile of HA Oligomers	52
Figure 2-4	Illustrated TLC of HA_4-DPPE	55
Figure 2-5	Example MALDI-TOF MS Spectrum of an HA_4-DPPE Conjugate	56
Figure 2-6	Example NMR Spectrum of an HA_4-DPPE Conjugate	57
Figure 2-7	Cell Binding of HA_4-Liposomes	58
Figure 2-8	Cell Binding of HA-Linker-Liposomes	59
Figure 2-9	FACS Competition Assay of Unlabeled and Fluorescein Labeled HMW-HA	60
Scheme 2-1	Synthesis of HA_n-DPPE	45
Scheme 2-2	Example Formation of a Room Temperature Ionic Liquid (RTIL)	46

Chapter 3

Figure 3-1	Illustration of Nitrilotriacetic Acid (NTA)-Containing PEGylated Liposomes with an Associated His-Tagged Protein	71
Figure 3-2	Representative Association of Proteins with the Surface of NTA-Liposomes	80
Figure 3-3	Association of mKate with the Surface of NTA-Liposomes	83
Figure 3-4	Retained Protein Activity of yCD or mKate on the Surface of NTA-Liposomes	84
Figure 3-5	Dissociation of yCD or mKate from NTA-Liposomes in Refiltered FCS	86
Figure 3-6	Competition of Proteins with Pre-Associated mKate	87
Figure 3-7	Half-Life of Iodinated yCD or mKate *in vivo*	89
Figure 3-8	The Interaction of His-Tagged Proteins with NTA-Containing PEGylated Liposomes	93

Chapter 4

Figure 4-1	Structures of NTA-Lipids and Polyhistidine-Tagged Antigens	101
Figure 4-2	SDS-PAGE of Polyhistidinylated Ovalbumin	115
Figure 4-3	Effect of Serum on Association of a Fluorescent Hexahistidine-Tagged Protein with Liposomes Containing NTA-Lipids	116
Figure 4-4	Association of Ovalbumin with Liposomes Containing NTA-Lipids	118
Figure 4-5	Effect of N-MPR-Liposome Linkage on Anti-N-MPR IgG Response in Mice	119
Figure 4-6	Effect of Ovalbumin-Liposome Linkage on Anti-Ovalbumin IgG Response in Mice	121

Chapter 5

Figure 5-1	Hyaluronidase-Liposomes	134
Figure 5-2	Effect of Covalent Modification on Hyaluronidase	143
Figure 5-3	Hyaluronidase-Assisted Liposome Diffusion through a Hyaluronan-Gel	147
Figure 5-4	Cell Binding of Hyaluronidase-Liposomes	149
Figure 5-5	*In vivo* Fraction of Injected Liposome Dose in Blood as a Function of Time	151
Figure 5-6	Biodistribution of Hyaluronidase-Liposomes	152

Chapter 1

Surface Functionalization of Liposomes for Anti-Cancer Applications

Portions of this work are published as (*1, 2*)

1.1 Overview

This dissertation devised and characterized methods to functionalize liposomes with hyaluronan or proteins that might be used in cancer therapeutics. I examine liposomes functionalized with either hyaluronan oligosaccharides to target to HA receptors overexpressed on cancer cells or the HA degrading enzyme hyaluronidase to target the blood-accessible, HA-rich tumor extracellular matrix. In addition, to improve protein/liposome conjugation techniques, such as those used with hyaluronidase, I investigate the effect of increased avidity between his-tagged proteins and multivalent-nitrilotriacetic acid (NTA)-lipids on protein/liposome association *in vitro* and *in vivo*. A robust method to non-covalently associate ligands with the liposome could find uses in protein therapies as well as other applications.

The complex system involved in the synthesis, degradation and binding of the high molecular weight glycosaminoglycan hyaluronic acid (hyaluronan or HA) provides a variety of structures that can be exploited for targeted cancer therapy. In many cancers of epithelial origin, there is an upregulation of CD44. In other cancers, HA in the tumor matrix is overexpressed. Although CD44 is expressed in normal epithelial cells and HA is part of the matrix of normal tissues, selective targeting to cancer is possible. Macromolecular carriers can be designed to predominantly extravasate into the tumor and not normal tissue; CD44-HA targeted carriers administered intravenously localize

preferentially into tumors. HA has been used as a drug carrier and a ligand on nanoparticles to target drugs to CD44 overexpressing cells. Drugs delivered in HA-modified liposomes exhibited excellent antitumor activity both *in vitro* and in murine tumor models. The HA matrix is also a potential target for anticancer therapies. In this chapter, the options for anticancer therapeutics that target either CD44 or the HA extracellular matrix are described.

Methods to attach proteins onto the carriers' surfaces are limited by protein sensitivity to chemical conjugation techniques. Proteins that are modified to include a histidine-tag (his-tag) can associate with particles that display a nitrilotriacetic acid (NTA)-nickel ligand. This non-covalent association procedure is mild and results in a site specific attachment of the protein to the particle. NTA-lipid conjugates are used to functionalize liposomes with the activity of associated proteins. Monovalent-NTA liposomes functionalized with his-tagged proteins can bind to cells *in vitro* and act as particulate adjuvants *in vivo*. However, the mono-NTA-liposome/his-tagged protein interaction is not strong enough to retain proteins when the liposomes are in contact with plasma. The strength of association of his-tagged proteins with NTA is increased by placing multiple NTA headgroups within close proximity. This multivalent NTA display can increase avidity into the picomolar range for some proteins.

This introductory chapter reviews HA biology in cancer and suggests methods to exploit abnormal cancer biology for anti-cancer applications (Figure **1-1**). The uses of monovalent- and multivalent- NTA-containing liposomes and therapeutics are

summarized. Finally, three examples of successful protein/liposome therapeutics, and the mechanisms by which the therapies are made more effective, are presented.

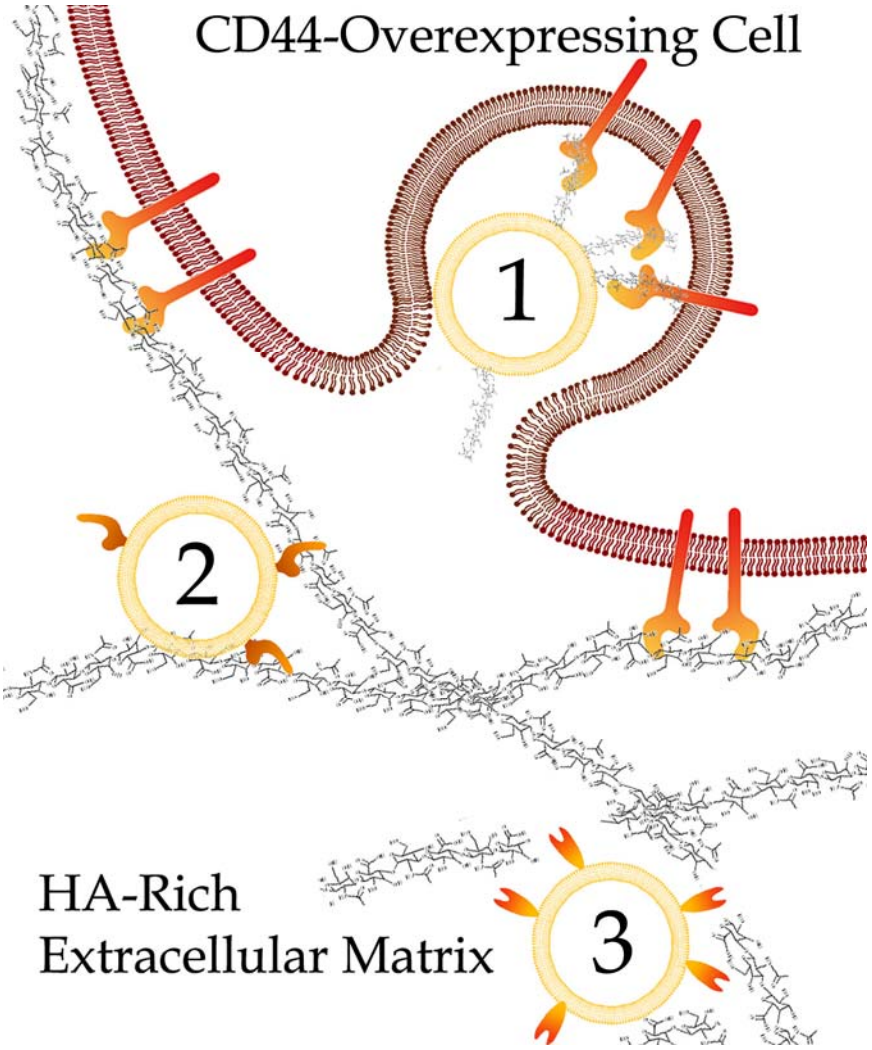


Figure 1-1. The Potential Ways the CD44-HA System may be Targeted for Cancer Therapies. Intracellular delivery of HA-conjugated drugs and drug carriers (**1**), extracellular localization of HA binding protein carriers and conjugates (**2**) or disruption of the extracellular matrix by enzymatic degradation (**3**).

1.2 Exploiting Hyaluronan Biology for Anti-Cancer Therapeutics

1.2.1 The Biology of Hyaluronan

Hyaluronan (HA) mediates the connection between a cell and its local environment by acting as a structural component of the extracellular matrix and by signaling through cell surface receptors. CD44, interacting with extracellular matrix HA, regulates cell motility and survival during tissue growth and maintenance (*3*). Malfunctions in tissue development caused by aberrant interactions between CD44 and HA (CD44-HA) contribute to cancer growth and progression (*4*). In many types of cancer, CD44 expression differs substantially from the expression normally seen in healthy tissue; CD44 expression is upregulated or CD44 is alternately spliced to produce non-native variants (*4*). When deregulated, signaling pathways downstream of CD44 activation lead to tumor growth, progression and metastasis (*5-7*). The composition of the extracellular matrix is also directly modulated during progression of some cancers; HA levels change within the tumor extracellular matrix (*8*).

The amount of HA in a tissue depends upon a complex interplay among HA synthesis by HA synthases (*9*), HA internalization by cell surface receptors (*10*) and extracellular degradation by hyaluronidases (*11*). HA turnover is due to local cellular catabolism, removal by an HA endocytosing receptor (LYVE-1) on cells located in the lymphatics (*12*) and systemic clearance from the blood by the HARE receptor on liver sinusoidal endothelial cells (*13*). In skin, HA has a half-life of over a day (*14*). In contrast, circulating high molecular weight HA (HMW-HA) has a half-life of two to five minutes (*15*). The net outcome of the various HA clearance processes results in a total turnover of about five grams of HA per day in humans (*16*).

1.2.2 Hyaluronan as a Drug Carrier

Although the ideal anticancer drug would have high specificity and activity against cancers, most drugs distribute throughout the body and are toxic to healthy as well as neoplastic cells. To minimize adverse effects, drugs can be formulated to increase the concentration at the target site and decrease concentrations elsewhere in the body. Targeted therapies are effective in cancer treatments for three principal reasons: 1) The ligand recognized by the targeting moiety is overexpressed on the tumor cell. 2) The carrier has better access to the tumor than to normal tissues that also express the targeted ligand. 3) The carrier circulates for a long enough period that a high fraction of the injected dose passes through the tumor.

In the CD44-HA system, mechanism one occurs because CD44 is often overexpressed on the surface of tumor cells (*4*). Targeting cytotoxic drugs to CD44 can localize therapies to areas where CD44 is highly expressed. Several reviews have previously discussed the advantages of HA as a drug carrier and a targeting ligand for cancer, as well as other pathologies (*1, 17-22*).

Mechanism two arises because tumors often exhibit a phenomenon known as the enhanced permeability and retention (EPR) effect (*23*). The properties of the EPR effect are summarized in Table **1-1**. This phenomenon is thought to occur because solid tumors have a much leakier blood supply than healthy capillary beds; particles of up to approximately 0.5 μm can extravasate into the tumor from the blood (*23*). Additionally, tumors lack a well-developed lymphatic system. This combination allows

macromolecules or nanoparticles to passively accumulate within tumors due to leakage from the improperly formed tumor vasculature and remain within the tumor due to limited lymphatic clearance (*23*). Administering a drug within a carrier alters the drug's distribution profile by directing the drug away from sites of toxicity and (by exploiting the EPR effect) into the tumor.

Healthy Tissue	Cancerous Tissue
Small molecules diffuse across capillary walls	Small molecules diffuse across capillary walls and enter through large gaps in the capillary walls
Large molecules can not diffuse due to tight capillary cell junctions	Large molecules enter through large gaps in capillary walls
Small molecules are cleared by a well-formed lymphatic system	No lymphatic clearance is present

Table 1-1. Hallmarks of the Enhanced Permeability and Retention (EPR) Effect.

In mechanism three, carriers alter drug stability or solubility and improve drug circulation time (*24*). Studies in which HA was covalently attached to the surface of liposomes showed that these modified liposomes exhibited reduced clearance *in vivo* (*25, 26*). Successfully targeted anticancer therapies utilize a specific drug target and also exploit the altered biology of cancerous tissue to achieve a therapeutic effect.

The polymeric nature of HA yields multiple functional groups for chemical conjugation (Figure **1-2**) (*17-19*). HA can be modified on the carboxyl moiety of the glucuronic acid residue, the hydroxyl of the *N*-acetylglucosamine or the single, terminal reducing end. HA-drug conjugates increase drug cytotoxicity for CD44 overexpressing cancer cells and

decrease toxicity for healthy cells. CD44-associated HA can be endocytosed (*27, 28*) carrying conjugated cargo, such as drugs or drug carriers, into the cell. Cellular uptake increases therapeutic efficiency of HA conjugated drugs (*29-31*).

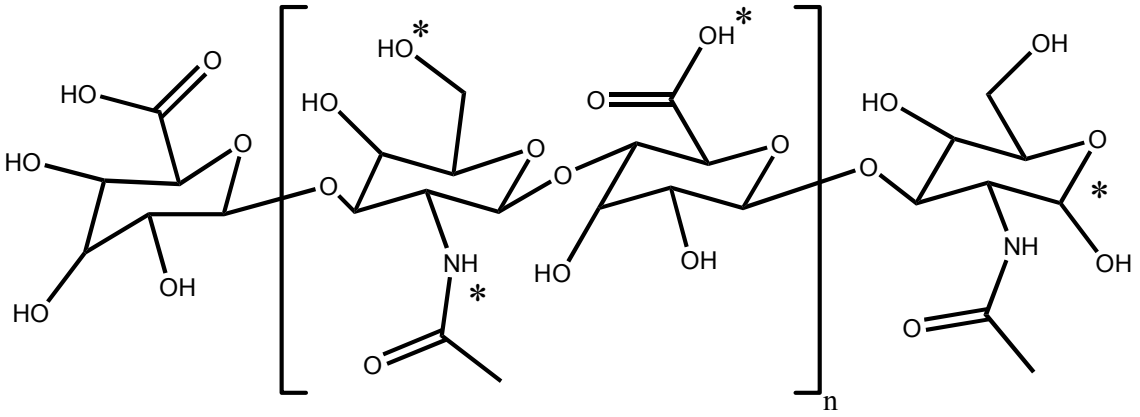


Figure 1-2. The Polymeric Repeat Structure of Hyaluronic Acid showing D-glucuronic acid and N-acetylglucosamine. The asterisk (*) shows potential sites of chemical conjugation.

HA has additional benefits as a drug carrier. Once it reaches the cell surface HA can cross-link multiple receptors, potentially inducing binding and endocytosis (*27, 32, 33*). Drug potency is improved by increased cellular uptake of the drug-carrier complex and, for certain drugs, by circumvention of multidrug resistance efflux pumps (*34*). Potency may also be improved by altering the drug's location inside the cell so that the intrinsic activity of the drug in the carrier is higher than the intrinsic activity of the free drug (*31, 35*).

A challenge for using HMW-HA as a targeting carrier is that HA is cleared from circulation by the liver (*36*). For HMW-HA to be a useful intravenous targeting carrier, strategies must be devised to reduce HA clearance from the blood.

Drug carrier-target cell interactions can be tuned to be effective only at sites of high receptor density by taking advantage of multiple ligands with moderate affinity but high specificity (*37*). In the case of CD44, we hypothesize that specific targeting can be achieved by employing short HA oligosaccharides on a larger carrier (*31, 38*). CD44 is reported to interact with a minimum HA length of 6 to 8 saccharides (*39*). The extracellular portion of CD44 with an octasaccharide HA positioned in the binding groove is illustrated in Figure **1-3** (*40*). Selecting HA oligosaccharides long enough to bind to CD44 but too short to bind to the HARE receptor may permit an HA-targeted carrier to avoid elimination by the liver while maintaining targeting to cells that overexpress CD44. Short oligosaccharides may maintain a high enough affinity with individual CD44 that binding to multiple CD44 by different HA on the same carrier creates an avidity strong enough for effective targeting.

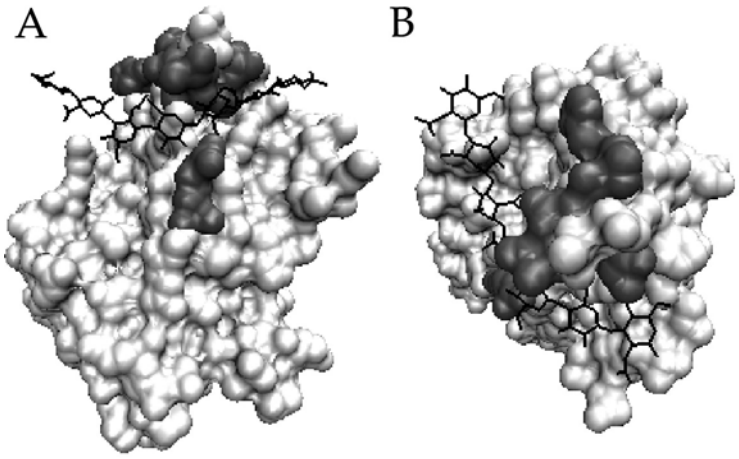


Figure 1-3. The HA/CD44 Binding Interaction. The structure of the extracellular portion of CD44 is shown with residues important for binding in gray (**A:** front view, **B:** top view). Saccharides 2-8 of a co-crystallized HA_8 are shown in the binding groove. (Reproduced from the Protein Data Bank structure from *(40)*.)

1.2.3 Hyaluronan Drug Conjugates

A number of cytotoxic anti-cancer drugs exhibited CD44-specific internalization and cell cytotoxicity when conjugated to HA: including paclitaxel (*27, 28, 41*), doxorubicin (*42*), sodium butyrate (*29, 30, 32*), mitomycin c (*33*) and epirubicin (*33*).

HA-paclitaxel increased cytotoxic delivery to CD44 overexpressing cancer cell lines including breast, colon and ovarian carcinoma (*27, 28*). HA-conjugated paclitaxel was taken up in a dose-dependent manner that could be blocked by competition with anti-CD44 antibodies or HMW-HA but not chondroitin sulfate (*28*), a sulfated polymeric sugar composed of the same two saccharides as HA.

HA-drug conjugates improve efficacy *in vivo*. Studies performed by Akima *et. al.* showed potent anti-metastatic effects of HA-mitomycin c injected subcutaneously in a murine model of Lewis lung adenocarcinoma (*33*). HA-paclitaxel conjugates injected locally to the tumor increased the mean survival time in a human ovarian carcinoma xenograft mouse model (*41*). Sodium butyrate-HA conjugates injected intratumorally or subcutaneously reduced primary tumor growth and lung metastasis in a murine Lewis lung carcinoma model (*29, 30*) and a murine melanoma model (*30*). However, HMW-HA conjugates injected intravenously exhibited a short half-life due to HA specific clearance mechanisms; conjugates collected in the liver and spleen (*30*).

HA-drug conjugate studies performed *in vivo* often did not employ intravenous dosing, opting for intratumoral, subcutaneous or intraperitoneal injection, thus avoided many HA

clearance mechanisms. The short half-life of HMW-HA conjugates (*30, 43, 44*) is most likely due to HA clearance from the blood by the HARE receptor present in the liver and spleen (*13*).

Improvement in the distribution of HA conjugated drugs *in vivo* may be achieved by reducing endogenous HA blood clearance mechanisms. Luo *et al.* suggested that systemic HA clearance can be reduced by pretreatment with a high molecular weight saccharide that competes with HA for binding during clearance but not during target cell drug internalization (*28*). HARE binds chondroitin sulfate and HA; CD44 binds only to HA (*36*). In rats with hepatic metastases of colon adenocarcinoma cells, pretreatment by intravenous injection of either chondroitin sulfate or HA resulted in higher tumor accumulation of a subsequent intravenous HA dose (*45*). In perfused liver, pre-blocking with an anti-HARE antibody or immediate pre-dosing with free HA decreased HA clearance of the second dose (*46*). These results parallel the *in vitro* observations of Luo *et al.*, strongly suggesting that cancer treatments utilizing HA targeting to CD44-overexpressing tumor types may benefit from pretreatment with a HARE blocking moiety such as free chondroitin sulfate, unconjugated HA or antibodies (*28, 45, 46*).

1.2.4 Hyaluronan as a Targeting Agent

Combining the tumor targeting characteristics of HA with the pharmacokinetic benefits of drug carriers appeared to efficiently treat tumors. HA targeted liposomes increased tumor toxicity due to advantageous *in vivo* characteristics, such as prolonged circulation time, increased tumor accumulation and sustained release parameters (*25, 26, 47*).

Liposomes coated with HMW-HA (*25, 26*) or HA-O (*31, 35*) showed specific uptake into CD44 expressing cells.

HA targeted liposomes increased potency of doxorubicin (*31*) and mitomycin c (*26*) by improving *in vitro* drug uptake (*25, 31, 35, 38*) in CD44 expressing cells. HMW-HA liposomes acted as a drug depot; these liposomes released mitomycin c more slowly than uncoated liposomes (*26, 47*).

In the earliest report, HMW-HA was coupled via the glucuronic carboxylate to phosphatidylethanolamine in preformed liposomes (*48*). This coupling method results in multipoint attachment of HA to a liposome. The number and distribution of the resulting attachment points was difficult to characterize. HMW-HA liposomes decreased tumor burden in several different tumor models. HA-coated liposomes carrying either doxorubicin or mitomycin c also showed an increased circulation time over traditional, non-targeted liposomes (*25, 26*) with a half-life slightly less than that of PEGylated "stealth" liposomes. Liposomes in which HMW-HA was attached to the liposome surface at multiple sites avoided immediate clearance by the liver HA receptor.

Drug-loaded HA-coated liposomes increased drug accumulation in CD44 expressing tumors, decreased systemic toxicity and increased survival time in multiple cancer models (*25, 26*). Treatment with mitomycin c or doxorubicin containing targeting liposomes significantly decreased solid tumor growth and reduced metastatic lung tumor

burden in colon cancer models, increased survival in models of intraperitoneal ascites tumors and reduced tumor burden in a solid pancreatic tumor model (*25, 26*).

The second conjugation method consisted of oligosaccharide HA attached via the reducing end of a phosphatidylethanolamine by reductive amination (*38*). A mixture of oligosaccharides of increasing disaccharide number was coupled to phosphatidylethanolamine (*38*). The precise composition of the oligosaccharide mixture was not completely specified. This lipid-HA was incorporated at a defined surface density in the liposome and the binding of radiolabeled and fluorescent liposomes to cells that expressed different levels of CD44 was examined.

Liposome uptake was dependent on the expression of CD44. The uptake was CD44 specific and could be blocked by both free HA and anti-CD44 antibodies (*38*). Liposome uptake was also dependent on the density of the HA-O targeting ligand (*31, 35*), suggesting that receptor clustering might occur because of multivalent ligand presentation on the liposomal surface. Targeting was observed with as little as 0.1 mol % HA-ligand on the liposome. Encapsulated doxorubicin was significantly more cytotoxic to CD44 overexpressing cell types in culture than was free drug. Uptake of targeted liposomes was modeled and provided a quantitative confirmation of the hypothesis that the increased cytotoxicity of the HA-targeted liposome stemmed specifically from the internalization of the doxorubicin containing liposomes (*31*).

1.2.5 Targeting to the Hyaluronan Extracellular Matrix with Proteins

The tumor matrix is a multivalent ligand accessible from the blood. As a target for drug delivery, the matrix has a number of advantages over targeting the tumor itself: 1) The number of binding sites is very large so that a high concentration of a matrix targeted system can accumulate at the site. 2) The tumor cannot shed the matrix as it can shed a surface antigen. 3) The tumor cannot directly internalize the delivery system, as it could a system targeted to the cell surface. 4) Targeting the matrix may kill matrix-associated fibroblasts that supply growth factors that promote tumor growth. 5) Targeting the matrix may also kill local endothelial cells that provide a blood supply to the growing tumor. The combination of these mechanisms could have a synergistic effect to slow or stop tumor progression.

To implement matrix attachment therapy, Park and coworkers (*49*) prepared a recombinant fusion protein consisting of TSG6-Link, a soluble HA binding domain, and yeast cytosine deaminase. The fusion protein could convert the prodrug 5-fluorocytosine into cytotoxic 5-fluorouracil. When the fusion protein was injected intratumorally into a C26 colon carcinoma tumor model and the animals were supplied with 5-fluorocytosine in their drinking water, tumor progression was slowed and long-term survival observed. The presence of the drug, active enzyme and an HA binding component were all required to observe an antitumor effect (*49*), as illustrated in Figure **1-4**.

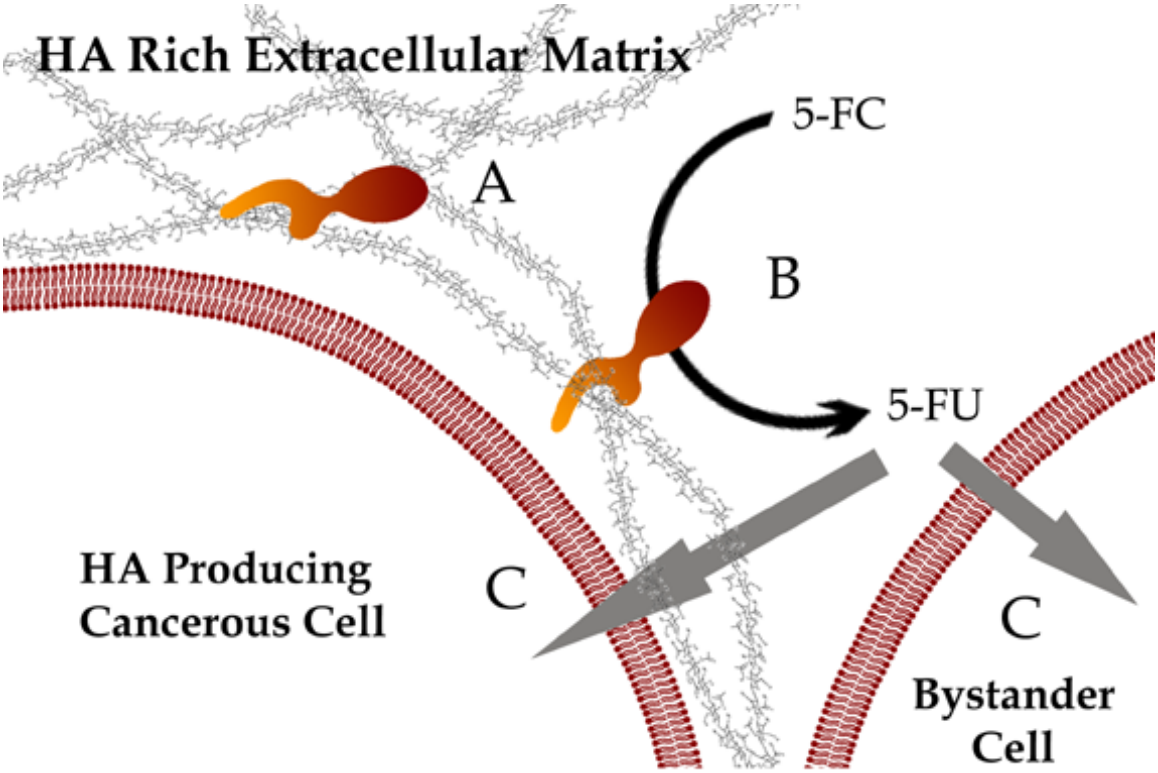


Figure 1-4. Matrix Attachment Therapy. A fusion protein between TSG6-Link and a prodrug converting enzyme binds to the HA rich extracellular matrix of cancerous cells (**A**) and converts prodrug to a drug (**B**) which is cytotoxic to HA-expressing neoplastic cells, HA-poor cancer cells, vasculature and other local cells in a phenomenon call the "Bystander Effect" (**C**).

Other groups have shown that the soluble portion of HA binding receptors (either as individual molecules or as immunoglobulin fusion constructs) decreased tumor growth in several cell lines and animal tumor models. Soluble CD44-immunoglobin constructs, injected intravenously (*50*) or delivered by a slow release infusion pump implanted subcutaneously near the tumor (*51*), decreased tumor growth and inhibited invasion.

Addition of exogenous soluble RHAMM (receptor for HA mediated motility) (*52, 53*) and a peptide mimetic of RHAMM consisting of three repeats of an HA binding motif (*54*) inhibited tumor growth. *In vivo*, pretreatment of fibrosarcoma cells with soluble

RHAMM prior to either subcutaneous or intravenous injection decreased primary tumor formation, limited metastasis and decreased lung nodule formation (*52*). *In vitro* studies using the RHAMM peptide mimetic suggested that soluble RHAMM may cause apoptosis (*55*).

1.2.6 Disrupting the Hyaluronan Extracellular Matrix

The intimate relationship between tumor survival and the extracellular matrix is a viable target for anticancer treatments. Manipulating the interaction between cancer cells and HA by disrupting HA binding to cell surface receptors can lead to disease regression. Degradation of the HA matrix by adding hyaluronidase decreases tumor growth (*56*). Intravenous injection of hyaluronidase into mice bearing human breast carcinoma tumors resulted in substantial tumor regression. Although the tumors were grown initially in the presence of an HA gel, and grew more slowly without an HA matrix (*56*), this study illustrated the combinatorial effect of targeted treatment (hyaluronidase disruption of the HA matrix) and utilization of cancer biology (access of the hyaluronidase to the tumor, potentially via the EPR phenomenon).

Bovine testicular hyaluronidase decreased the fluid pressure in solid tumors (*57, 58*) and increased the permeation of macromolecular carriers (*59*) into osteogenic human sarcoma xenografts. In these studies, hyaluronidase was injected prior to the macromolecule. Localized coinjection of recombinant human hyaluronidase improved the spread of a traceable dye (*60*) and increased transfection potency of an oncolytic virus (*61*). The disruption of the HA tumor matrix by direct hyaluronidase injection increased delivery of

intravenously injected, untargeted liposomes containing doxorubicin in a human osteosarcoma solid tumor model (*62*).

We hypothesize that attaching hyaluronidase to liposomes may increase liposome delivery through three mechanisms. First, hyaluronidase may target liposomes to the tumor extracellular matrix by binding to hyaluronan. Second, it may act as an anti-cancer agent upon initial entrance into the tumor by degrading the tumor matrix and dislodging cancerous cells. Third, hyaluronidase may alter the way conjugate liposomes enter the tumor and improve motility within the tumor mass.

1.3 Nitrilotriacetic Acids for Non-Covalent Liposome-Protein Association

1.3.1 Multivalent-Nitrilotriacetic Acids Increase Particle/Protein Avidity

A technique to attach proteins to the liposome surface, that is applicable to a wide range of proteins and requires no substantial alteration of the protein structure or activity, would be desirable to improve protein and liposome therapies. However, a universal method for particulate-protein association is difficult to achieve as proteins have diverse particle association behaviors and conjugation requirements (*63-67*). Any conjugation method would have to retain the protein's nascent activity under a wide range of physiological conditions, including those experienced during circulation.

Nitrilotriacetic acids interact, through a chelated metal ion, to the histidine tag (his-tag) of recombinant proteins (Figure **1-5A**). Each NTA chelates a single nickel ion, which interacts with two histidines. The association between the protein and the NTA is

reversible; proteins can be released by competitive chelation for the metal ion or another histidine containing protein (*68*). Multivalent NTAs have an increased avidity for his-tagged proteins because they align multiple NTA headgroups to interact with a single his-tag (Figure **1-5B**) (*69*). Spacing of the NTA headgroups in multivalent display affects the strength of protein interactions. Huang *et. al*. determined that incrementally decreasing the carbon linkage length between the tris-NTA headgroups (Figure **1-5B**) increases his-tag/NTA avidity (*70*).

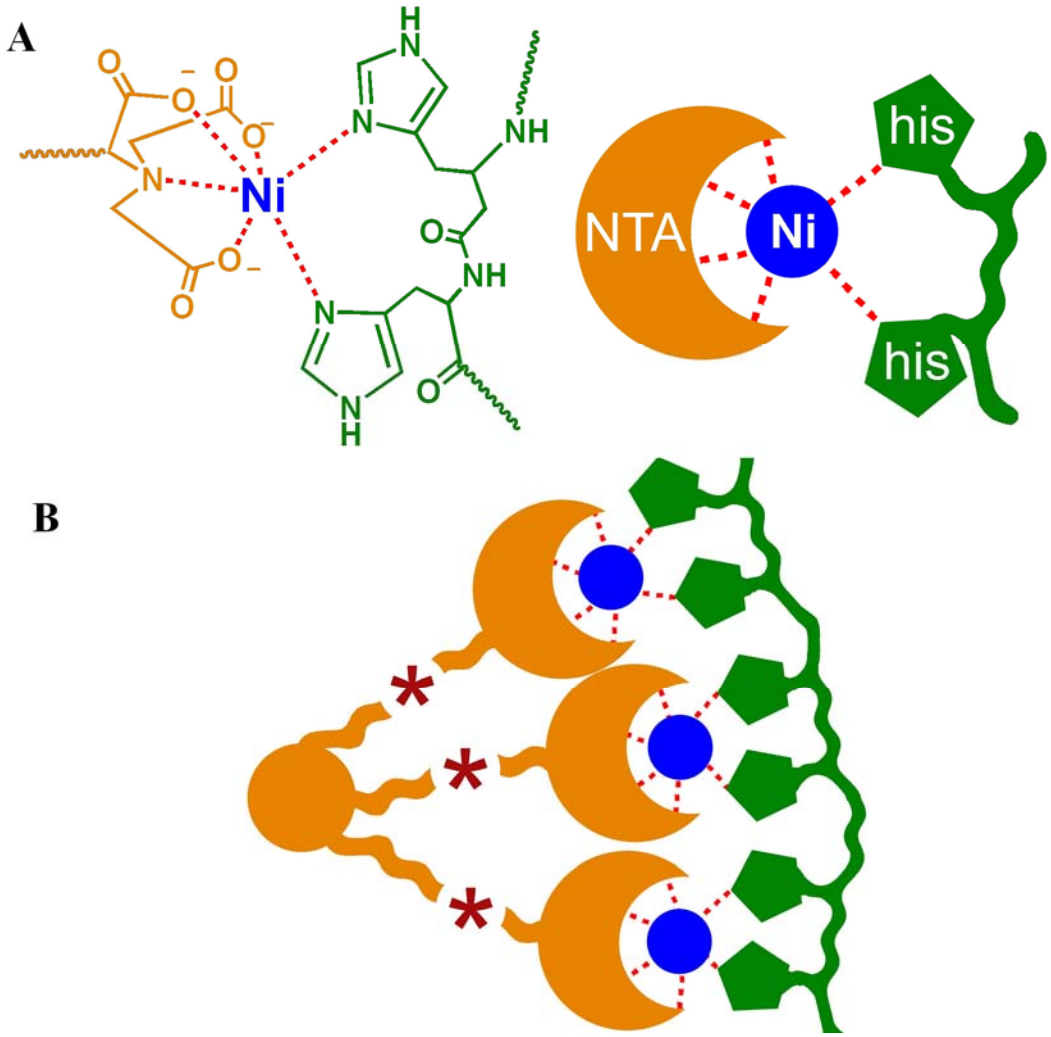


Figure 1-5. The Structure of the Nitrilotriacetic Acid (NTA)/Histidine Interaction (**A**) and the trivalent nitrilotriacetic acid (tris-NTA) interaction with a his_6-tag (**B**). Asterisk (*) denotes carbon chain decreased during avidity studies *(72)*.

The NTA/his-tag system is frequently used to functionalize surfaces in order to explore protein properties or exploit protein activity (Figure **1-6**) (*71-77*).

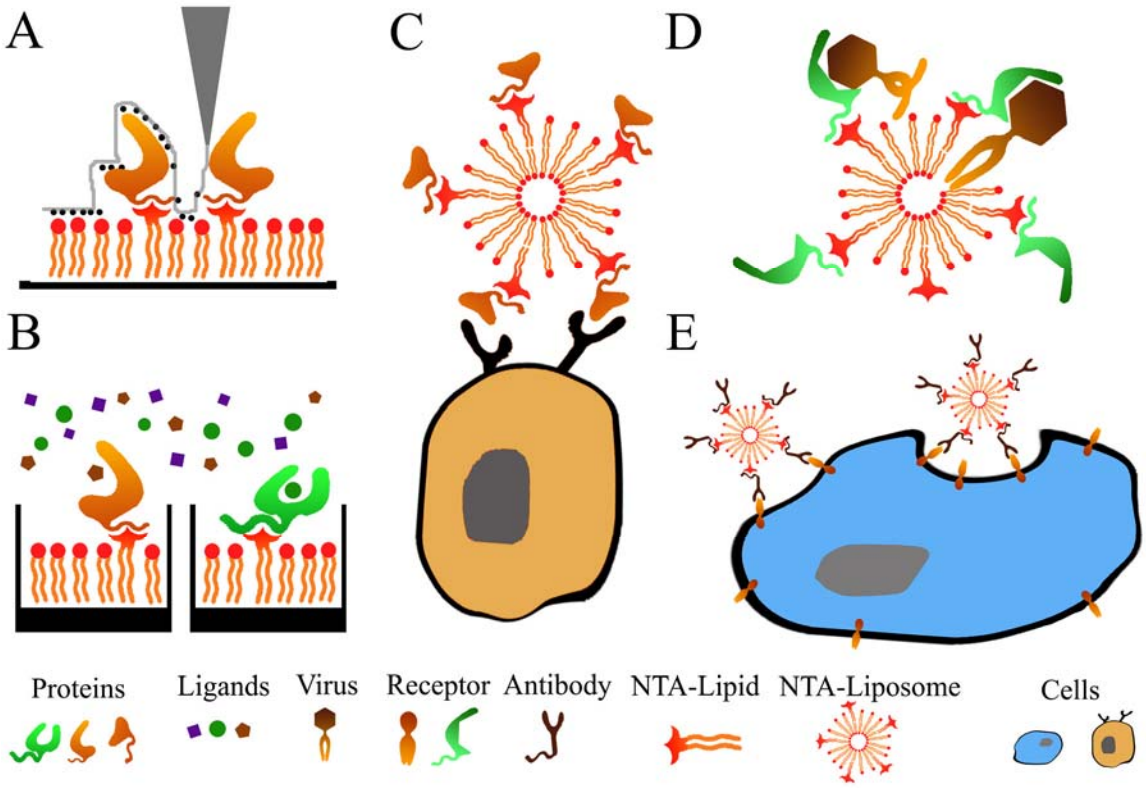


Figure 1-6. Potential Uses of Nitrilotriacetic Acid Lipids on protein functionalized chips for *in silico* structural determination (such as by atomic force microscopy) (**A**) or ligand association studies (**B**), in liposomes as *in vivo* particulate adjuvants (**C**), for modeling bilayer interactions (such as during viral insertion) (**D**) or *in vitro* for antibody-mediated cell binding (**E**).

NTAs interact with the single multihistidine sequence within a protein and induce a unidirectional, monolayer orientation of the protein (*72, 78*). Protein association with NTAs retains the native protein structure and activity (*71, 72, 78*). Mica surfaces coated with monovalent-NTA containing lipid vesicles form a thin, uniform lipid sheet which associates protein in a his-tag dependent orientation. Lateral orientation of his-tagged 20S proteosomes was determined by scanning atomic force microscopy using an oxide-sharpened silicon nitride tip to tap the lipid-mica surface (Figure **1-6A**). A side-view

profile of the 4 proteosome rings was obtained (*71*). No top-view profiles were observed because the positioning of the his-tag orients the protein specifically in the side-view direction. While immobilized, the 20S proteosome bound and degraded β-chain insulin. Proteosome activity was observed on the NTA-lipid coated chip using surface plasmon resonance (Figure **1-6B**). As the insulin bound and degraded, the mass change at the chip surface was measured to determine proteosome activity over time (*71*).

1.3.2 Monovalent and Multivalent Nitrilotriacetic Acids on Liposomes

NTA-lipids have been synthesized, incorporated into liposomes and used to associate his_6-containing proteins with the liposome bilayer. Liposomes are nanometer-sized vesicles composed of a phospholipid bilayer surrounding an aqueous core. NTA-liposome/protein-his_6 complexes have been used in animals as adjuvants (*69, 79*), as models for protein/bilayer interactions (*74, 75, 80*) and on cells to screen for antibodies suitable for liposome targeting (*63, 77, 81, 82*).

Particles containing monovalent-NTA (mono-NTA) have been used as immunogenic adjuvants in animals (Figure **1-6C**). The protein AntpHD-CW3 crosses cell membranes and delivers an epitope, CW3, which primes cytotoxic T-cells. The AntpHD-CW3 fusion peptide associated with liposomes nonspecifically. When the peptide contained an additional his-tag, NTA-liposome incorporation increased from 35% to nearly 100% of admixed peptide (*73*). PEGylation of the liposomes prevented multi-histidine mediated liposome crosslinking. Subcutaneous immunization of mice with NTA associated AntpHD-CW3 increased splenocyte stimulation. However, this stimulation was not

significantly greater than induced by AntpHD-CW3 liposomes prepared without NTA (*73*) so the advantage of protein association by NTA within the liposome was not evident.

Composite vesicles were formed from the membrane of mastocytoma cells and included either a mono-NTA or a trivalent NTA (tris-NTA). His-tagged costimulatory molecules (B7.1, CD40 and the extracellular region of the human erythropoietin receptor, EPOR) were associated with the surface of NTA-liposome. Additional immunostimulatory molecules, interleukin 2 or interleukin 12, were encapsulated within the vesicle. When on the surface of liposomes, tris-NTA increased B7.1 or CD40-mediated liposome binding to T-cells; fluorescence increased from 17.5 times above background (for mono-NTA) to 35 times in cell sorting studies (*69*). The control vesicles, with tris-NTA associated EPOR-his_6, increased fluorescence 3-fold above baseline.

Both mono- and tris-NTA liposomes immunized mice against tumor formation *in vivo*. Tris-NTA, at concentrations 10-fold lower than mono-NTA, exhibited similar immunization response in mice (*69, 79*). Syngenic mice immunized with mono-NTA composite liposomes had decreased tumor burden when challenged with native mastocytoma cells as compared to mice immunized with admixed vesicles, costimulatory molecules and interleukin 2. Mice exhibited similar survival when immunized with either composite liposomes or vesicles admixed with costimulatory molecules and interleukin 2 (*79*). Mice immunized with composite membrane vesicles containing tris-NTA lipid and CD40-his_6 had decreased tumor burden and increased survival as compared to control liposomes, which contained EPOR-his_6. Addition of interleukin 2,

12 or a combination of both proteins further decreased survival and increased tumor growth (*69*) However, the effect of the mono-NTA containing liposomes was not directly compared to tris-NTA containing liposomes for *in vivo* therapeutic effect so the advantage of increased avidity from tris-NTA association, compared to mono-NTA, is not clear (*69, 79*).

Mono-NTA on the surface of lipid vesicles has also been used to investigate the properties of bilayer-interacting proteins, such as those that induce pore formation (Figure **1-6D**) (*74, 75, 80*). The protective antigen (PA) of anthrax toxin forms a heptameric pore complex within a lipid membrane to access the intracellular compartment. Initial interaction with the lipid membrane occurs when PA associates with the cell receptor ANTXR2 (*74*). Incorporating a his-tag into either the ANTXR2 receptor or into a subunit of PA induced pore formation in vesicles containing mono-NTA lipids. ANTXR2 containing a his-tag bound to NTA-lipid vesicles and mediated binding of PA, which did not contain a his-tag. Once membrane associated, the PA oligomerized, formed pores and released potassium from within the vesicle (*74*). Pore formation could be recreated by docking his-tagged PA to the NTA-lipid vesicle directly, suggesting the ANTXR2 receptor functioned primarily as a membrane anchor (*74*).

A poliovirus receptor ectodomain (PVR), comprised of the active virus docking site, was associated with liposomes to explore the insertion and conformation changes of the poliovirus proteins (*75*). His-tagged PVR associated with the surface of mono-NTA containing liposomes. Radiolabeled poliovirus bound to PVR and the viral particle

inserted proteins into the liposome to induce pore formation. Pore presence, based on changes in sucrose density gradient flotation, was NTA-independent; when the pore was extracted from the NTA-containing liposome, it inserted into an NTA free-bilayer and retained pore-structure (*75*). In both studies, the NTA/his-tag was sufficient to orient the proteins toward the lipid membrane in a manner which induced protein activation.

Protein presentation on NTA-liposomes can affect liposome behavior (*63, 77, 81, 82*). Liposomes containing mono-NTA lipids were used to observe the internalization of cell specific antibodies (Figure **1-6E**) (*77*). His-tagged anti-HER2 scFv antibodies caused internalization of associated-liposomes into HER2-overexpressing SKVR3 cells. The specific his-tag/NTA interaction allowed liposomes to associate antibodies directly from crude lysate. NTA-liposomes mixed with supernatant from anti-HER2 antibody-expressing bacteria internalized at similar concentrations to liposomes prepared with purified his-tagged antibody. Control antibodies did not cause liposome internalization when mixed from cell lysate or a pure antibody preparations (*77*). Immunoliposomes were loaded with the anticancer drugs vinorelbine and doxorubicin. NTA presence at the surface of the liposome decreased encapsulation of the drugs to 9 and 27% of the total loaded drug (for vinorelbine and doxorubicin respectively) compared to liposomes without NTA, which have 95 – 100% drug encapsulation efficiencies. When the NTA was spaced away from the liposome surface with a PEG spacer, loading efficiency returned to 90%. Doxorubicin containing, NTA immunoliposomes were 26 times more toxic than untargeted, drug containing liposomes in HER2-overexpressing mammary carcinoma cells (*77*).

Anti-endoglin NTA-immunoliposomes showed targeting specificity to human umbilical vein endothelial cells (HUVEC) (*82*). Analysis of cell fluorescence by fluorescence assisted cell sorting (FACS) showed immunoliposomes bound to HUVECs but not control endothelial cells. Antibodies were not retained by NTA-liposomes when mixed with human plasma. Incubation of antibodies-liposomes in human plasma for 5 minutes at 37 ºC eliminated binding to HUVECs in a plasma concentration dependent manner. Loss of binding was traced to increased plasma proteins present on the liposome surface and increased antibody displacement, suggesting the protein/NTA interaction is affected by serum proteins (*76*).

1.4 Therapeutic Proteins on the Surface of Liposomes

The behavior of proteins *in vivo* is affected by associating the protein with a liposome (*66, 83-85*). Proteins can be encapsulated within the liposome core (*86, 87*), inserted into the lipid bilayer (*88, 89*) or attached to the surface (*66, 87*) to alter protein pharmacokinetics (Figure **1-7**). Polyethylene glycol (PEG) shields the liposome from clearance and increases its circulation time *in vivo* (*90*). Long-circulating liposomes can increase the half-life of associated proteins in circulation (*91-93*) and cause accumulation within disease tissue (*93*). Associating proteins with liposomes can reduce enzymatic degradation of the protein, reduce product inhibition if the protein is an enzyme and decrease the attached protein's immunological reactivity (*83, 94-97*).

The protein-liposome complex can exhibit the pharmacokinetic parameters of the carrier and the functions of the associated protein. Several proteins, such as recombinant factor VIII and superoxide dismutase, show higher therapeutic efficacy when displayed on the liposome's surface because of multiple carrier-related changes to the protein's behavior in circulation. The protein may also act to target the liposome to the disease region, such as is seen with liposome targeting by attached anti-HER2 antibodies.

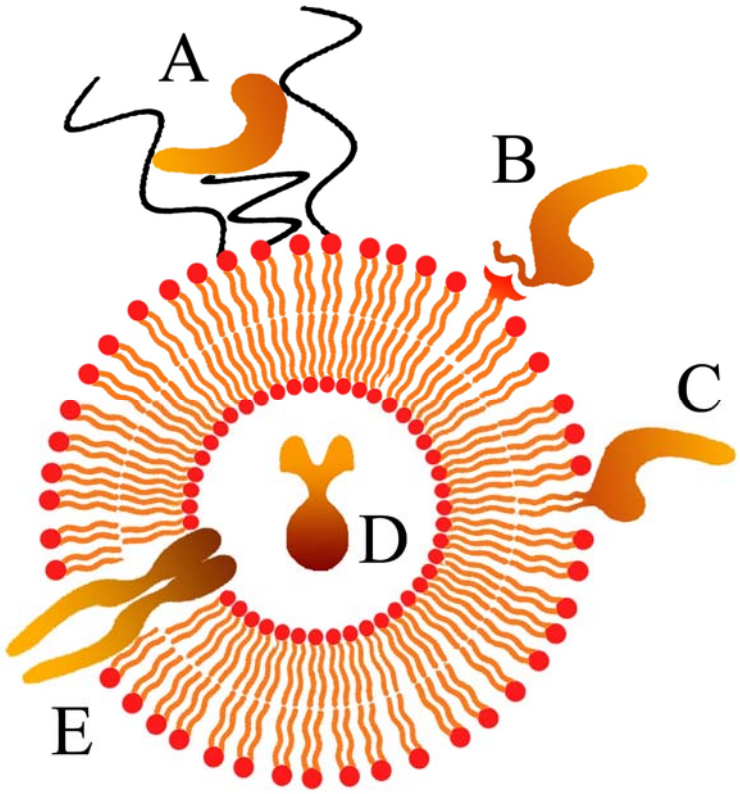


Figure 1-7. The Multiple Types of Liposome/Protein Interactions including non-specific, non-covalent surface association (**A**), specific non-covalent surface association (**B**), covalent surface attachment (**C**), encapsulation within the aqueous core (**D**) and insertion within the lipid bilayer (**E**).

1.4.1 Recombinant Factor VIII

The *in vivo* therapeutic efficacy of factor VIII (FVIII) improved when associated with liposomes. The blood clotting protein FVIII is used to reduce the frequency and duration of hemorrhagic events in patients with hemophilia A. Compared to episodic treatment, prophylactic infusion of free recombinant FVIII (rFVIII) every other day decreased the number of joint hemorrhages from 18 to 3 per year (*98*). When infused as a PEGylated liposome-associated protein, at a dose of 15 U/μmol lipid (or approximately 36 μg/μmol lipid), rFVIII nearly doubled the periods between hemorrhagic events compared to that experienced with infusions of free protein (*66, 67*). The mechanism by which liposomal rFVIII increases the bleed free period is unclear (*99*). In clinical trials, the circulation half-life of rFVIII was approximately 10 hours when the protein was injected with or without liposomes (*99*).

Other changes to the protein's *in vivo* interactions could be responsible for the observed clinical effects, such as decreased immunogenic inhibitors of FVIII activity or prolonged residence of rFVIII in locations prone to hemorrhage (*94, 97, 99*). In a murine model, liposomal-rFVIII containing the lipid phosphatidylserine (PS) exhibited reduced immunogenicity (*94*). In murine models, a small increase in retained rFVIII activity was observed after 24 hours in circulation; liposomal-rFVIII activity was higher than free protein (*96, 97*). rFVIII-liposomes associated with platelets *in vivo* (*97*). The mechanism for improved rFVIII *in vivo* efficacy may be a function of multiple drug-carrier effects, including reduced immunogenicity and increased association platelets, accumulation within tissue and increased rFVIII activity.

1.4.2 Superoxide Dismutase

Most proteins do not passively associate with carriers; covalent protein modifications can lead to stable liposome association. Superoxide dismutase (SOD) can alleviate the symptoms of arthritis and has anti-inflammatory effects. When injected intravenously, free SOD had a half-life of approximately 6 minutes (*100*). Liposome-encapsulated SOD had a plasma half-life of over 4 hours but the encapsulation efficiency was less than 25% of the formulated protein (*87*). To increase the amount of formulated protein associated with the liposome and increase SOD access to its substrate, the protein was covalently attached to the liposome surface. Addition of acyl chains, 16 carbons in length, to the protein anchored it to the liposomal bilayer (*65*). Acylation of some proteins can lead to protein inactivation or instability (*65*); however, SOD retained approximately 90% activity with 30% of the potential sites of modification acylated (*64*). Liposome-associated SOD accounted for between 35 and 60% of the formulated protein, approximately 7 to 14 µg/µmol lipid, depending on the initial protein concentration used during liposome incubation. The surface exposed protein accounted for 30 - 50% total expected activity per unit of associated protein (*65*). In an adjuvant-induced rat arthritis model, intravenous injection of PEGylated liposome-SOD at a dose of approximately 13 µg/µmol lipid, regressed ankle edema while formulations containing non-acylated, liposome admixed SOD did not significantly induce regression (*93*). At 24 hours post injection, approximately 15% of the total acylated-SOD liposomes had accumulated in the arthritis-inflamed area. Rat ankle inflammation 18 days after arthritis induction regressed by 25% when treated with SOD liposome formulations, compared to untreated

animals. Inflammation increased by 60% when the animals were treated with an equivalent dose of free SOD (*93*).

Association of SOD with the surface of the liposome reduced enzyme degradation by peroxide, a product of SOD enzymatic activity. The activity of SOD incubated with peroxide decreased over time, corresponding to a loss of α-helical secondary structure determined by circular dichroism. In the presence of liposomes, peroxide did not induce a structural change and the protein retained full activity (*83*). Previously inactivated peptide fragments of oxidize SOD regained 20 – 30% activity when mixed with liposomes (*95*). Like rFVIII efficacy, the mechanism which improved SOD mediated inflammation reduction may be a function of multiple drug-carrier effects including protein protection from product initiated degradation, increased circulation half-life and accumulation in inflamed tissue.

1.4.3 Anti-HER2 Antibodies

Proteins displayed on the liposome surface can be used to target the liposome. Targeting requires that the protein have access to the extra-liposomal environment. Antibody-liposome conjugates, called immunoliposomes, exploit the high affinity of antibodies for their antigens to actively target the liposomes to tissues with high antigen density (*81, 101*). Antibodies were designed that targeted and internalized into HER2 overexpressing cells, a receptor commonly overexpressed in breast cancer (*63*). The antibodies had an additional cysteine incorporated into the amino acid structure prior to production to allow for covalent conjugation (*102*). Anti-HER2 short chain antibody fragments (scFv) with a

c-terminal cysteine were covalently conjugated to the distal end of PEG with 75 – 95% conjugation efficiency and 70 – 90% incorporation efficiency into preformed liposomes (*103*). Targeting to anti-HER2 expressing cells could be achieved with antibody surface densities of 25 – 100 scFv antibodies per liposome, approximately 8 - 50 μg/μmol lipid (*103, 104*).

Targeted anti-HER2 immunoliposomes were formulated to include the anticancer drugs doxorubicin (*102-104*), vincristine or vinblastine (*92*) within the aqueous core. Anti-HER2 immunoliposomes had a half-life of over 16 hours in rats after multiple injections (*102*). Treatment with 3 doses of anti-HER2 immunoliposomes, containing doxorubicin, decreased tumor volume and cured 5 of 10 mice with HER-2 overexpressing subcutaneous BT-474/SF mammary carcinoma (*102*). In a subcutaneous BT-474-M2 murine model of human mammary adenocarcinoma, vincristine loaded immunoliposomes, with 13 μg antibody/μmol lipid, eliminated measurable tumor burden in 5 of 9 mice compared to 1 of 9 mice for untargeted liposomes (*92*). These liposomes exploited the long circulating effects of PEGylated liposomes along with antibody targeting to deliver anticancer drugs.

The improved therapeutic efficacy of rFVIII, SOD and anti-HER2 antibodies is attributable to a combination of multiple property changes related to liposome association. These changes improve the protein's clinical effectiveness by influencing the way the protein or the liposome acts within the body. Proteins attached to the liposome surface can interact with the extra-liposomal environment; the protein has

access to this environment while circulating and after accumulating in target tissue (*92, 93, 102*). Association with the liposome can reduce protein degradation, increase protein activity, decrease product inhibition if the protein has enzymatic activity, prevent immunological reactivity of the liposome attached protein or target the liposome to a site of therapeutic action (*83, 94-97*).

1.5 Conclusion

In the following chapters, I will discuss two methods that use functionalized liposomes to exploit the altered CD44-HA biology of cancerous tissues: liposomes targeted to CD44-overexpressing cells using HA oligosaccharides or using hyaluronidase. In Chapter 2, I synthesize HA-O/lipid conjugates and investigate the binding of HA-O bearing liposomes to CD44 overexpressing tumor cells.

How the increased avidity of the NTA/protein interaction caused by headgroup multivalency affects particle/protein interaction *in vivo* is still unclear. In the following chapters, I study covalent and non-covalent protein association with NTA functionalized liposomes under a variety of conditions. I compare the protein/particle association using liposomes formulated with mono-NTA or tris-NTA lipids. In Chapter 3, I characterize the retention of proteins on NTA-liposomes *in vitro* under surrogate biological conditions and *in vivo* during circulation in blood using two proteins, yCD and mKate. In Chapter 4, I examine the relationship between NTA avidity and immune response to a strong and weak antigen, ovalbumin and a peptide membrane proximal portion of HIV Gag.

Finally, in Chapter 5, I use both covalent and non-covalent techniques to produce a hyaluronidase/liposome complex. I examine the activity of hyaluronidase-liposomes as a means to exploit the blood-accessible, HA-rich tumor extracellular matrix.

1.6 Literature Cited

(1) Platt, V. M., and Szoka, F. C., Jr. (2008) Anticancer therapeutics: targeting macromolecules and nanocarriers to hyaluronan or CD44, a hyaluronan receptor. *Mol Pharm 5*, 474-86.

(2) Platt, V. M., and Szoka, F. (2009) Exploiting the Hyaluronan-CD44 Interaction for Cancer Therapy, in *Hyaluronan in Cancer Biology* (Stern, R., Ed.) pp 379-403, Elsevier, San Francisco.

(3) McKee, C. M., Penno, M. B., Cowman, M., Burdick, M. D., Strieter, R. M., Bao, C., and Noble, P. W. (1996) Hyaluronan (HA) fragments induce chemokine gene expression in alveolar macrophages. The role of HA size and CD44. *J Clin Invest 98*, 2403-13.

(4) Naor, D., Nedvetzki, S., Golan, I., Melnik, L., and Faitelson, Y. (2002) CD44 in cancer. *Crit Rev Clin Lab Sci 39*, 527-79.

(5) Bourguignon, L. Y., Zhu, H., Shao, L., and Chen, Y. W. (2000) CD44 interaction with tiam1 promotes Rac1 signaling and hyaluronic acid-mediated breast tumor cell migration. *J Biol Chem 275*, 1829-38.

(6) Bourguignon, L. Y., Singleton, P. A., Zhu, H., and Diedrich, F. (2003) Hyaluronan-mediated CD44 interaction with RhoGEF and Rho kinase promotes Grb2-associated binder-1 phosphorylation and phosphatidylinositol 3-kinase signaling leading to cytokine (macrophage-colony stimulating factor) production and breast tumor progression. *J Biol Chem 278*, 29420-34.

(7) Bourguignon, L. Y., Peyrollier, K., Gilad, E., and Brightman, A. (2007) Hyaluronan-CD44 interaction with neural Wiskott-Aldrich syndrome protein (N-WASP) promotes actin polymerization and ErbB2 activation leading to beta-catenin nuclear translocation, transcriptional up-regulation, and cell migration in ovarian tumor cells. *J Biol Chem 282*, 1265-80.

(8) Toole, B. P. (2004) Hyaluronan: from extracellular glue to pericellular cue. *Nat Rev Cancer 4*, 528-39.

(9) Weigel, P. H., and DeAngelis, P. L. (2007) Hyaluronan synthases: a decade-plus of novel glycosyltransferases. *J Biol Chem 282*, 36777-81.

(10) Hua, Q., Knudson, C. B., and Knudson, W. (1993) Internalization of hyaluronan by chondrocytes occurs via receptor-mediated endocytosis. *J Cell Sci 106 (Pt 1)*, 365-75.

(11) Stern, R., and Jedrzejas, M. J. (2006) Hyaluronidases: their genomics, structures, and mechanisms of action. *Chem Rev 106*, 818-39.

(12) Banerji, S., Ni, J., Wang, S. X., Clasper, S., Su, J., Tammi, R., Jones, M., and Jackson, D. G. (1999) LYVE-1, a new homologue of the CD44 glycoprotein, is a lymph-specific receptor for hyaluronan. *J Cell Biol 144*, 789-801.

(13) Zhou, B., Weigel, J. A., Fauss, L., and Weigel, P. H. (2000) Identification of the hyaluronan receptor for endocytosis (HARE). *J Biol Chem 275*, 37733-41.

(14) Tammi, R., Saamanen, A. M., Maibach, H. I., and Tammi, M. (1991) Degradation of newly synthesized high molecular mass hyaluronan in the epidermal and dermal compartments of human skin in organ culture. *J Invest Dermatol 97*, 126-30.

(15) Fraser, J. R., Laurent, T. C., and Laurent, U. B. (1997) Hyaluronan: its nature, distribution, functions and turnover. *J Intern Med 242*, 27-33.

(16) Laurent, T. C. a. F., J.R. (1991) Catabolism of Hyaluronan, in *Degradation of Bioactive Substances; Physiology and Pathophysiology* (Henriksen, J. H., Ed.) pp 249-88, CRC Press, Boston.

(17) Pouyani, T., and Prestwich, G. D. (1994) Functionalized derivatives of hyaluronic acid oligosaccharides: drug carriers and novel biomaterials. *Bioconjug Chem 5*, 339-47.

(18) Prestwich, G. D., Marecak, D. M., Marecek, J. F., Vercruysse, K. P., and Ziebell, M. R. (1998) Controlled chemical modification of hyaluronic acid: synthesis, applications, and biodegradation of hydrazide derivatives. *J Control Release 53*, 93-103.

(19) Vercruysse, K. P., and Prestwich, G. D. (1998) Hyaluronate derivatives in drug delivery. *Crit Rev Ther Drug Carrier Syst 15*, 513-55.

(20) Jaracz, S., Chen, J., Kuznetsova, L. V., and Ojima, I. (2005) Recent advances in tumor-targeting anticancer drug conjugates. *Bioorg Med Chem 13*, 5043-54.

(21) Liao, Y. H., Jones, S. A., Forbes, B., Martin, G. P., and Brown, M. B. (2005) Hyaluronan: pharmaceutical characterization and drug delivery. *Drug Deliv 12*, 327-42.

(22) Yadav, A. K., Mishra, P., and Agrawal, G. P. (2008) An insight on hyaluronic acid in drug targeting and drug delivery. *J Drug Target 16*, 91-107.

(23) Maeda, H., Seymour, L. W., and Miyamoto, Y. (1992) Conjugates of anticancer agents and polymers: advantages of macromolecular therapeutics in vivo. *Bioconjug Chem 3*, 351-62.

(24) Allen, T. M., and Cullis, P. R. (2004) Drug delivery systems: entering the mainstream. *Science 303*, 1818-22.

(25) Peer, D., and Margalit, R. (2004) Tumor-targeted hyaluronan nanoliposomes increase the antitumor activity of liposomal Doxorubicin in syngeneic and human xenograft mouse tumor models. *Neoplasia 6*, 343-53.

(26) Peer, D., and Margalit, R. (2004) Loading mitomycin C inside long circulating hyaluronan targeted nano-liposomes increases its antitumor activity in three mice tumor models. *Int J Cancer 108*, 780-9.

(27) Luo, Y., and Prestwich, G. D. (1999) Synthesis and selective cytotoxicity of a hyaluronic acid-antitumor bioconjugate. *Bioconjug Chem 10*, 755-63.

(28) Luo, Y., Ziebell, M. R., and Prestwich, G. D. (2000) A hyaluronic acid-taxol antitumor bioconjugate targeted to cancer cells. *Biomacromolecules 1*, 208-18.

(29) Coradini, D., Pellizzaro, C., Abolafio, G., Bosco, M., Scarlata, I., Cantoni, S., Stucchi, L., Zorzet, S., Turrin, C., Sava, G., Perbellini, A., and Daidone, M. G. (2004) Hyaluronic-acid butyric esters as promising antineoplastic agents in human lung carcinoma: a preclinical study. *Invest New Drugs 22*, 207-17.

(30) Coradini, D., Zorzet, S., Rossin, R., Scarlata, I., Pellizzaro, C., Turrin, C., Bello, M., Cantoni, S., Speranza, A., Sava, G., Mazzi, U., and Perbellini, A. (2004) Inhibition of hepatocellular carcinomas in vitro and hepatic metastases in vivo in mice by the histone deacetylase inhibitor HA-But. *Clin Cancer Res 10*, 4822-30.

(31) Eliaz, R. E., Nir, S., Marty, C., and Szoka, F. C., Jr. (2004) Determination and modeling of kinetics of cancer cell killing by doxorubicin and doxorubicin encapsulated in targeted liposomes. *Cancer Res 64*, 711-8.

(32) Coradini, D., Pellizzaro, C., Miglierini, G., Daidone, M. G., and Perbellini, A. (1999) Hyaluronic acid as drug delivery for sodium butyrate: improvement of the anti-proliferative activity on a breast-cancer cell line. *Int J Cancer 81*, 411-6.

(33) Akima, K., Ito, H., Iwata, Y., Matsuo, K., Watari, N., Yanagi, M., Hagi, H., Oshima, K., Yagita, A., Atomi, Y., and Tatekawa, I. (1996) Evaluation of antitumor activities of hyaluronate binding antitumor drugs: synthesis, characterization and antitumor activity. *J Drug Target 4*, 1-8.

(34) Brigger, I., Dubernet, C., and Couvreur, P. (2002) Nanoparticles in cancer therapy and diagnosis. *Adv Drug Deliv Rev 54*, 631-51.

(35) Eliaz, R. E., Nir, S., and Szoka, F. C., Jr. (2004) Interactions of hyaluronan-targeted liposomes with cultured cells: modeling of binding and endocytosis. *Methods Enzymol 387*, 16-33.

(36) Harris, E. N., Kyosseva, S. V., Weigel, J. A., and Weigel, P. H. (2007) Expression, processing, and glycosaminoglycan binding activity of the recombinant human 315-kDa hyaluronic acid receptor for endocytosis (HARE). *J Biol Chem 282*, 2785-97.

(37) Mammen, M., Choi, S., and Whitesides, G. M. (1998) Polyvalent Interactions in Biological Systems: Implications for Design and Use of Multivalent Ligands and Inhibitors. *Angew. Chem. International Ed. 37*, 2754-94.

(38) Eliaz, R. E., and Szoka, F. C., Jr. (2001) Liposome-encapsulated doxorubicin targeted to CD44: a strategy to kill CD44-overexpressing tumor cells. *Cancer Res 61*, 2592-601.

(39) Lesley, J., Hascall, V. C., Tammi, M., and Hyman, R. (2000) Hyaluronan binding by cell surface CD44. *J Biol Chem 275*, 26967-75.

(40) Banerji, S., Wright, A. J., Noble, M., Mahoney, D. J., Campbell, I. D., Day, A. J., and Jackson, D. G. (2007) Structures of the Cd44-hyaluronan complex provide insight into a fundamental carbohydrate-protein interaction. *Nat Struct Mol Biol 14*, 234-9.

(41) Auzenne, E., Ghosh, S. C., Khodadadian, M., Rivera, B., Farquhar, D., Price, R. E., Ravoori, M., Kundra, V., Freedman, R. S., and Klostergaard, J. (2007) Hyaluronic acid-paclitaxel: antitumor efficacy against CD44(+) human ovarian carcinoma xenografts. *Neoplasia 9*, 479-86.

(42) Luo, Y., Bernshaw, N. J., Lu, Z. R., Kopecek, J., and Prestwich, G. D. (2002) Targeted delivery of doxorubicin by HPMA copolymer-hyaluronan bioconjugates. *Pharm Res 19*, 396-402.

(43) Fraser, J. R., Dahl, L. B., Kimpton, W. G., Cahill, R. N., Brown, T. J., and Vakakis, N. (1989) Elimination and subsequent metabolism of circulating hyaluronic acid in the fetus. *J Dev Physiol 11*, 235-42.

(44) Sugahara, S., Okuno, S., Yano, T., Hamana, H., and Inoue, K. (2001) Characteristics of tissue distribution of various polysaccharides as drug carriers: influences of molecular weight and anionic charge on tumor targeting. *Biol Pharm Bull 24*, 535-43.

(45) Mahteme, H., Graf, W., Larsson, B. S., and Gustafson, S. (1998) Uptake of hyaluronan in hepatic metastases after blocking of liver endothelial cell receptors. *Glycoconj J 15*, 935-9.

(46) Weigel, J. A., Raymond, R. C., McGary, C., Singh, A., and Weigel, P. H. (2003) A blocking antibody to the hyaluronan receptor for endocytosis (HARE) inhibits hyaluronan clearance by perfused liver. *J Biol Chem 278*, 9808-12.

(47) Peer, D., and Margalit, R. (2000) Physicochemical evaluation of a stability-driven approach to drug entrapment in regular and in surface-modified liposomes. *Arch Biochem Biophys 383*, 185-90.

(48) Yerushalmi, N., Arad, A., and Margalit, R. (1994) Molecular and cellular studies of hyaluronic acid-modified liposomes as bioadhesive carriers for topical drug delivery in wound healing. *Arch Biochem Biophys 313*, 267-73.

(49) Park, J. I., Cao, L., Platt, V. M., Huang, Z., Stull, R. A., Dy, E. E., Sperinde, J. J., Yokoyama, J. S., and Szoka, F. C. (2009) Antitumor therapy mediated by 5-fluorocytosine and a recombinant fusion protein containing TSG-6 hyaluronan binding domain and yeast cytosine deaminase. *Mol Pharm 6*, 801-12.

(50) Sy, M. S., Guo, Y. J., and Stamenkovic, I. (1992) Inhibition of tumor growth in vivo with a soluble CD44-immunoglobulin fusion protein. *J Exp Med 176*, 623-7.

(51) Bartolazzi, A., Peach, R., Aruffo, A., and Stamenkovic, I. (1994) Interaction between CD44 and hyaluronate is directly implicated in the regulation of tumor development. *J Exp Med 180*, 53-66.

(52) Mohapatra, S., Yang, X., Wright, J. A., Turley, E. A., and Greenberg, A. H. (1996) Soluble hyaluronan receptor RHAMM induces mitotic arrest by suppressing Cdc2 and cyclin B1 expression. *J Exp Med 183*, 1663-8.

(53) Akiyama, Y., Jung, S., Salhia, B., Lee, S., Hubbard, S., Taylor, M., Mainprize, T., Akaishi, K., van Furth, W., and Rutka, J. T. (2001) Hyaluronate receptors mediating glioma cell migration and proliferation. *J Neurooncol 53*, 115-27.

(54) Xu, X. M., Chen, Y., Chen, J., Yang, S., Gao, F., Underhill, C. B., Creswell, K., and Zhang, L. (2003) A peptide with three hyaluronan binding motifs inhibits tumor growth and induces apoptosis. *Cancer Res 63*, 5685-90.

(55) Yu, Q., Toole, B. P., and Stamenkovic, I. (1997) Induction of apoptosis of metastatic mammary carcinoma cells in vivo by disruption of tumor cell surface CD44 function. *J Exp Med 186*, 1985-96.

(56) Shuster, S., Frost, G. I., Csoka, A. B., Formby, B., and Stern, R. (2002) Hyaluronidase reduces human breast cancer xenografts in SCID mice. *Int J Cancer 102*, 192-7.

(57) Brekken, C., and de Lange Davies, C. (1998) Hyaluronidase reduces the interstitial fluid pressure in solid tumours in a non-linear concentration-dependent manner. *Cancer Lett 131*, 65-70.

(58) Brekken, C., Hjelstuen, M. H., Bruland, O. S., and de Lange Davies, C. (2000) Hyaluronidase-induced periodic modulation of the interstitial fluid pressure increases selective antibody uptake in human osteosarcoma xenografts. *Anticancer Res 20*, 3513-9.

(59) Erikson, A., Tufto, I., Bjonnum, A. B., Bruland, O. S., and de Lange Davies , C. (2008) The impact of enzymatic degradation on the uptake of differently sized therapeutic molecules. *Anticancer Res 28*, 3557-66.

(60) Bookbinder, L. H., Hofer, A., Haller, M. F., Zepeda, M. L., Keller, G. A., Lim, J. E., Edgington, T. S., Shepard, H. M., Patton, J. S., and Frost, G. I. (2006) A recombinant human enzyme for enhanced interstitial transport of therapeutics. *J Control Release 114*, 230-41.

(61) Ganesh, S., Gonzalez-Edick, M., Gibbons, D., Van Roey, M., and Jooss, K. (2008) Intratumoral coadministration of hyaluronidase enzyme and oncolytic adenoviruses enhances virus potency in metastatic tumor models. *Clin Cancer Res 14*, 3933-41.

(62) Eikenes, L., Tari, M., Tufto, I., Bruland, O. S., and de Lange Davies, C. (2005) Hyaluronidase induces a transcapillary pressure gradient and improves the distribution and uptake of liposomal doxorubicin (Caelyx) in human osteosarcoma xenografts. *Br J Cancer 93*, 81-8.

(63) Poul, M. A., Becerril, B., Nielsen, U. B., Morisson, P., and Marks, J. D. (2000) Selection of tumor-specific internalizing human antibodies from phage libraries. *J Mol Biol 301*, 1149-61.

(64) Gaspar, M. M., Martins, M. B., Corvo, M. L., and Cruz, M. E. (2003) Design and characterization of enzymosomes with surface-exposed superoxide dismutase. *Biochim Biophys Acta 1609*, 211-7.

(65) Cruz, M. E., Manuela Gaspar, M., Barbara, M., Martins, F., and Luisa Corvo, M. (2005) Liposomal superoxide dismutases and their use in the treatment of experimental arthritis. *Methods Enzymol 391*, 395-413.

(66) Spira, J., Plyushch, O. P., Andreeva, T. A., and Andreev, Y. (2006) Prolonged bleeding-free period following prophylactic infusion of recombinant factor VIII reconstituted with pegylated liposomes. *Blood 108*, 3668-73.

(67) Powell, J. S. (2007) Liposomal approach towards the development of a longer-acting factor VIII. *Haemophilia 13 Suppl 2*, 23-8.

(68) Ueda, E. K., Gout, P. W., and Morganti, L. (2003) Current and prospective applications of metal ion-protein binding. *J Chromatogr A 988*, 1-23.

(69) van Broekhoven, C. L., and Altin, J. G. (2005) The novel chelator lipid 3(nitrilotriacetic acid)-ditetradecylamine (NTA(3)-DTDA) promotes stable binding of His-tagged proteins to liposomal membranes: potent anti-tumor responses induced by simultaneously targeting antigen, cytokine and costimulatory signals to T cells. *Biochim Biophys Acta 1716*, 104-16.

(70) Huang, Z., Hwang, P., Watson, D. S., Cao, L., and Szoka, F. C. (2009) Tris-Nitrilotriacetic Acids of Subnanomolar Affinity Toward Hexahistidine Tagged Molecules. *Bioconjug Chem 20*, 1667-72.

(71) Dorn, I. T., Eschrich, R., Seemuller, E., Guckenberger, R., and Tampe, R. (1999) High-resolution AFM-imaging and mechanistic analysis of the 20 S proteasome. *J Mol Biol 288*, 1027-36.

(72) Dietrich, C., Schmitt, L., and Tampe, R. (1995) Molecular organization of histidine-tagged biomolecules at self-assembled lipid interfaces using a novel class of chelator lipids. *Proc Natl Acad Sci U S A 92*, 9014-8.

(73) Chikh, G. G., Li, W. M., Schutze-Redelmeier, M. P., Meunier, J. C., and Bally, M. B. (2002) Attaching histidine-tagged peptides and proteins to lipid-based carriers through use of metal-ion-chelating lipids. *Biochim Biophys Acta 1567*, 204-12.

(74) Sun, J., Vernier, G., Wigelsworth, D. J., and Collier, R. J. (2007) Insertion of anthrax protective antigen into liposomal membranes: effects of a receptor. *J Biol Chem 282*, 1059-65.

(75) Tuthill, T. J., Bubeck, D., Rowlands, D. J., and Hogle, J. M. (2006) Characterization of early steps in the poliovirus infection process: receptor-decorated liposomes induce conversion of the virus to membrane-anchored entry-intermediate particles. *J Virol 80*, 172-80.

(76) Ruger, R., Muller, D., Fahr, A., and Kontermann, R. E. (2006) In vitro characterization of binding and stability of single-chain Fv Ni-NTA-liposomes. *J Drug Target 14*, 576-82.

(77) Nielsen, U. B., Kirpotin, D. B., Pickering, E. M., Drummond, D. C., and Marks, J. D. (2006) A novel assay for monitoring internalization of nanocarrier coupled antibodies. *BMC Immunol 7*, 24.

(78) Dorn, I. T., Pawlitschko, K., Pettinger, S. C., and Tampe, R. (1998) Orientation and two-dimensional organization of proteins at chelator lipid interfaces. *Biol Chem 379*, 1151-9.

(79) van Broekhoven, C. L., and Altin, J. G. (2002) A novel approach for modifying tumor cell-derived plasma membrane vesicles to contain encapsulated IL-2 and engrafted costimulatory molecules for use in tumor immunotherapy. *Int J Cancer 98*, 63-72.

(80) Bilek, G., Kremser, L., Wruss, J., Blaas, D., and Kenndler, E. (2007) Mimicking early events of virus infection: capillary electrophoretic analysis of virus attachment to receptor-decorated liposomes. *Anal Chem 79*, 1620-5.

(81) Park, J. W., Benz, C. C., and Martin, F. J. (2004) Future directions of liposome- and immunoliposome-based cancer therapeutics. *Semin Oncol 31*, 196-205.

(82) Ruger, R., Muller, D., Fahr, A., and Kontermann, R. E. (2005) Generation of immunoliposomes using recombinant single-chain Fv fragments bound to Ni-NTA-liposomes. *J Drug Target 13*, 399-406.

(83) Nagami, H., Yoshimoto, N., Umakoshi, H., Shimanouchi, T., and Kuboi, R. (2005) Liposome-assisted activity of superoxide dismutase under oxidative stress. *J Biosci Bioeng 99*, 423-8.

(84) Yatuv, R., Dayan, I., Carmel-Goren, L., Robinson, M., Aviv, I., Goldenberg-Furmanov, M., and Baru, M. (2008) Enhancement of factor VIIa haemostatic efficacy by formulation with PEGylated liposomes. *Haemophilia 14*, 476-83.

(85) Torchilin, V. P. (2006) Multifunctional nanocarriers. *Adv Drug Deliv Rev 58*, 1532-55.

(86) Pape, A., Kertscho, H., Meier, J., Horn, O., Laout, M., Steche, M., Lossen, M., Theisen, A., Zwissler, B., and Habler, O. (2008) Improved short-term survival with polyethylene glycol modified hemoglobin liposomes in critical normovolemic anemia. *Intensive Care Med 34*, 1534-43.

(87) Corvo, M. L., Boerman, O. C., Oyen, W. J., Van Bloois, L., Cruz, M. E., Crommelin, D. J., and Storm, G. (1999) Intravenous administration of superoxide dismutase entrapped in long circulating liposomes. II. In vivo fate in a rat model of adjuvant arthritis. *Biochim Biophys Acta 1419*, 325-34.

(88) Liguori, L., Marques, B., Villegas-Mendez, A., Rothe, R., and Lenormand, J. L. (2008) Liposomes-mediated delivery of pro-apoptotic therapeutic membrane proteins. *J Control Release 126*, 217-27.

(89) Haller, C. A., Cui, W., Wen, J., Robson, S. C., and Chaikof, E. L. (2006) Reconstitution of CD39 in liposomes amplifies nucleoside triphosphate diphosphohydrolase activity and restores thromboregulatory properties. *J Vasc Surg 43*, 816-23.

(90) Papahadjopoulos, D., Allen, T. M., Gabizon, A., Mayhew, E., Matthay, K., Huang, S. K., Lee, K. D., Woodle, M. C., Lasic, D. D., Redemann, C., and et al. (1991) Sterically stabilized liposomes: improvements in pharmacokinetics and antitumor therapeutic efficacy. *Proc Natl Acad Sci U S A 88*, 11460-4.

(91) Drummond, D. C., Meyer, O., Hong, K., Kirpotin, D. B., and Papahadjopoulos, D. (1999) Optimizing liposomes for delivery of chemotherapeutic agents to solid tumors. *Pharmacol Rev 51*, 691-743.

(92) Noble, C. O., Guo, Z., Hayes, M. E., Marks, J. D., Park, J. W., Benz, C. C., Kirpotin, D. B., and Drummond, D. C. (2009) Characterization of highly stable liposomal and immunoliposomal formulations of vincristine and vinblastine. *Cancer Chemother Pharmacol 64*, 741-51.

(93) Gaspar, M. M., Boerman, O. C., Laverman, P., Corvo, M. L., Storm, G., and Cruz, M. E. (2007) Enzymosomes with surface-exposed superoxide dismutase: in vivo behaviour and therapeutic activity in a model of adjuvant arthritis. *J Control Release 117*, 186-95.

(94) Ramani, K., Purohit, V., Miclea, R., Gaitonde, P., Straubinger, R. M., and Balu-Iyer, S. V. (2008) Passive transfer of polyethylene glycol to liposomal-recombinant human FVIII enhances its efficacy in a murine model for hemophilia A. *J Pharm Sci 97*, 3753-64.

(95) Tuan le, Q., Umakoshi, H., Shimanouchi, T., and Kuboi, R. (2008) Liposome-recruited activity of oxidized and fragmented superoxide dismutase. *Langmuir 24*, 350-4.

(96) Dayan, I., Robinson, M., and Baru, M. (2009) Enhancement of haemostatic efficacy of plasma-derived FVIII by formulation with PEGylated liposomes. *Haemophilia 15*, 1006-13.

(97) Pan, J., Liu, T., Kim, J. Y., Zhu, D., Patel, C., Cui, Z. H., Zhang, X., Newgren, J. O., Reames, A., Canivel, D., Jesmok, G., Pierce, G. F., Sommer, J. M., and Jiang, H. (2009) Enhanced efficacy of recombinant FVIII in noncovalent complex with PEGylated liposome in hemophilia A mice. *Blood 114*, 2802-11.

(98) Manco-Johnson, M. J., Abshire, T. C., Shapiro, A. D., Riske, B., Hacker, M. R., Kilcoyne, R., Ingram, J. D., Manco-Johnson, M. L., Funk, S., Jacobson, L., Valentino, L. A., Hoots, W. K., Buchanan, G. R., DiMichele, D., Recht, M., Brown, D., Leissinger, C., Bleak, S., Cohen, A., Mathew, P., Matsunaga, A., Medeiros, D., Nugent, D., Thomas, G. A., Thompson, A. A., McRedmond, K., Soucie, J. M., Austin, H., and Evatt, B. L. (2007) Prophylaxis versus episodic treatment to prevent joint disease in boys with severe hemophilia. *N Engl J Med 357*, 535-44.

(99) Powell, J. (2008) The next generation of anti-haemophilia factor, factor VIII. Long-lasting protection from spontaneous bleeding, are we there yet? *Thromb Haemost 100*, 365-6.

(100) Turrens, J. F., Crapo, J. D., and Freeman, B. A. (1984) Protection against oxygen toxicity by intravenous injection of liposome-entrapped catalase and superoxide dismutase. *J Clin Invest 73*, 87-95.

(101) Heath, T. D., Macher, B. A., and Papahadjopoulos, D. (1981) Covalent attachment of immunoglobulins to liposomes via glycosphingolipids. *Biochim Biophys Acta 640*, 66-81.

(102) Park, J. W., Hong, K., Kirpotin, D. B., Colbern, G., Shalaby, R., Baselga, J., Shao, Y., Nielsen, U. B., Marks, J. D., Moore, D., Papahadjopoulos, D., and Benz, C. C. (2002) Anti-HER2 immunoliposomes: enhanced efficacy attributable to targeted delivery. *Clin Cancer Res 8*, 1172-81.

(103) Nielsen, U. B., Kirpotin, D. B., Pickering, E. M., Hong, K., Park, J. W., Refaat Shalaby, M., Shao, Y., Benz, C. C., and Marks, J. D. (2002) Therapeutic efficacy of anti-ErbB2 immunoliposomes targeted by a phage antibody selected for cellular endocytosis. *Biochim Biophys Acta 1591*, 109-118.

(104) Park, J. W., Hong, K., Kirpotin, D. B., Meyer, O., Papahadjopoulos, D., and Benz, C. C. (1997) Anti-HER2 immunoliposomes for targeted therapy of human tumors. *Cancer Lett 118*, 153-60.

Chapter 2

Synthesis, Formulation and Cell Binding of Hyaluronan Oligosaccharide-Targeted Liposomes

2.1 Abstract

Hyaluronan (HA) conjugated to liposomes can increase liposome internalization through CD44 mediated interactions in a manner which increases encapsulated drug cytotoxicity. Liposomes with high molecular weight HA accumulate in tumors that overexpress CD44. We sought to determine if oligosaccharide HA (HA-O) could cause preferential liposome accumulation in tumors and avoid clearance by other HA-receptor displaying tissues, such as the liver. Discrete HA ligands are required to study the effect of modulating HA saccharide length on tumor targeting. Short HA fragments, 4 to 12 saccharides, were generated by digesting high molecular weight HA with testicular ovine hyaluronidase. Oligomers were purified in multi-hundred milligram quantities using a large-scale size exclusion column. Coupling reactions generated HA_4 – HA_8 lipid conjugates in 40-60% yields, after purification. Lipids conjugated to HA-O via the reducing end were facilely incorporated into liposome formulations. The minimum length of HA that binds CD44 is reported to be below 10 saccharides. Liposomes containing HA_4 through HA_8 ligands did not bind to CD44-overexpressing cells. Further synthesis of ligands, which reduce steric hindrance by separating the saccharide from the liposome surface, did not enhance binding. Linkers included a six or twelve carbon chain, PEG(200) and PEG(2000). Methods to synthesize longer saccharide ligands by modulating component solubility were explored. Acidified solutions of heated, aprotic solvents did not improve solubility or reaction yield. Exchanging HA to either a hydrogen or tetrabutyl ammonium salt form

did not result in more complete dissolution. Room temperature ionic liquids successfully dissolved both the saccharide and lipid components but did not improve the reaction yield. CD44 expression on cells was verified with fluorescence assisted cell sorting (FACS) with CD44 specific antibodies. Surface expressed CD44 bound fluorescent, high molecular weight HA. Alternative targeting methods, such as antibodies, or techniques to conjugate higher monodispersed lipid ligands, are still required for effective targeting of liposomes to CD44-expressing cells.

2.2 Introduction

Hyaluronan (HA) binds to the cell surface receptor CD44. HA-conjugates can target CD44-expressing cells using this highly specific ligand-receptor interaction. CD44 is overexpressed in many cancers and can internalize HA (*1-3*). When HA-conjugated drugs are endocytosed, they are more cytotoxic than non-targeted drugs (*4-8*). In circulation, HMW-HA drug conjugates are subject to clearance by the HARE receptor in the liver (*9*). Methods that use the CD44 specific targeting properties of HA and avoid liver clearance could increase targeted drug efficacy.

Liposomes use a long circulation time and the enhanced permeability and retention (EPR) effect to passively target disease regions (*10-12*). Ligands on liposomes can increase carrier-associated drug efficacy by improving the ratio between target and off target localization (*13, 14*). Utilizing both passive accumulation and active targeting, HA-modified liposomes carrying anticancer drugs avoided immediate liver clearance, localized into tumors and exhibited antitumor activity in murine tumor models (*15, 16*).

In mice bearing C26 solid foot hind pad tumors, P388/ADR ascites tumors and B16F10 or D122 metastatic lung tumors, HMW-HA-targeted liposomes, containing encapsulated doxorubicin or mitomycin C, decreased tumor growth and increased mean survival time (*15, 16*). In B16F10 lung tumor bearing mice, HA-liposomes accumulated significantly less in the liver and localized to the lungs (*15, 16*).

The polymeric structure of HA yields multiple functional side chains for chemical modification (Figure **2-1**). Both saccharides contain several hydroxyls (*17*). The acetyl group can be enzymatically removed from N-acetyl-glucosamine to yield an additional functional handle (*18*). HA modification commonly occurs at the carboxylate of glucuronic acid (*19*). The attachment between HMW-HA and the conjugate may take place at any side-chain, yielding an undefined attachment stoichiometry. For HMW-HA-conjugated liposomes, which targeted CD44 overexpressing tumors *in vivo*, HA was attached to liposome surface using the carboxylate side-chain of glucuronic acid. The attachment frequency was not reported (*20*).

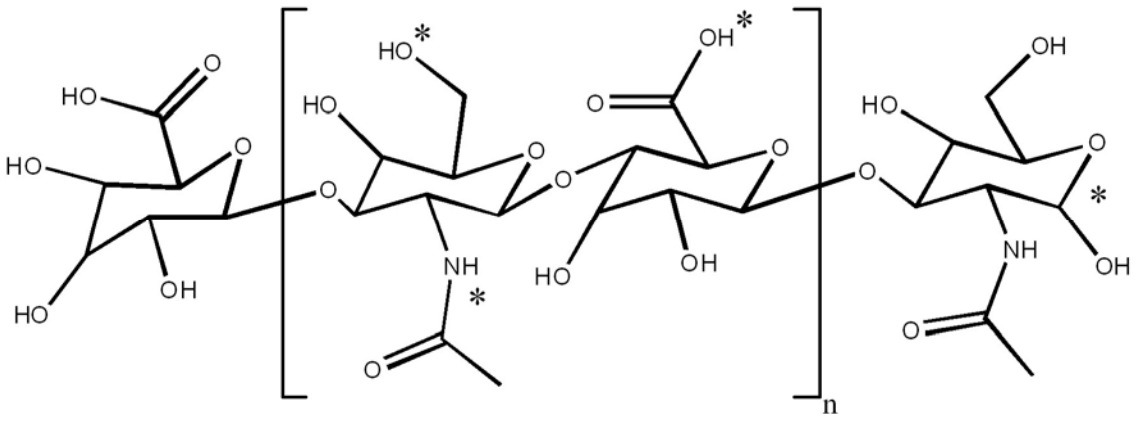


Figure 2-1. The Polymeric Repeat of Hyaluronic Acid. HA consists of a repeating disaccharide unit of β 1-3 D-glucuronic acid and β 1-4 N-acetyl-D-glucosamine. The asterisk (*) indicates possible sites of chemical conjugation.

Monodispersed ligands must be synthesized to determine which minimum HA oligosaccharide length can effectively target CD44 and avoid off-target accumulation in HA receptor-containing organs. Oligosaccharide HA can be conjugated to form a monodispersed ligand (*21*). Each oligosaccharide contains a single reducing end on the terminal glucosamine residue. The presence of this unique group allows selective modification via reductive amination. HA conjugates formed by reductive amination include lipids (*21-23*), polymers (*24*) and fluorescent tags (*25*).

Lipid conjugates of glycosaminoglycans (GAGs) were used to study cell binding and growth, or to target drug-carriers to CD44 overexpressing cell types (*21-23*). Conjugate-lipids formed with HA, heparin, heparin sulfates or chondroitin sulfates (sulfated GAGs similar to HA) of approximately 50 saccharides were used to coat cell culture dishes. These dishes were seeded with hamster kidney cells or primary fetal rat neurons to observe the binding and growth of cells in the presence of GAGs (*22, 23*). Neurite elongation was promoted by HA and unaffected by heparin (*22*). Baby hamster kidney cell adhesion was inhibited by chondroitin sulfate and unaffected by HA (*23*).

A mixture of HA-Os (4 – 12 saccharides) were conjugated to lipids and incorporated at a defined surface density into liposomes (*7, 8*). Liposome uptake was HA-CD44 specific and could be decreased by adding either free HA and anti-CD44 antibodies. (*21*). Doxorubicin-containing, HA-targeted liposomes were significantly more cytotoxic than free drug (*7, 8*).

Reductive amination will result in a population of well defined targeting ligands as long as single HA-Os can be purified from a mixture of HMW digest products. One method to generate monodispersed HA-O uses tetrasaccharide HA and enzymatically adds subsequent sugars to generate both even and odd units, up to HA_{20} (*26*). This method requires column immobilized, mutated HA synthases acting as single-action glucuronic acid transferase or N-acetylglucosamine transferase, as well as UDP-activated saccharide substrates and a monodispersed tetrasaccharide HA acceptor (*26*).

To easily produce large quantities of oligomers for HA-conjugate generation, we modified a procedure from the Day group (*27*). This protocol digests HMW-HA to an HA-O mixture. Individual oligosaccharides were purified on a Bio-Gel P-6 column followed by anion-exchange HPLC. Multimilligram quantities of the post-HPLC products could be obtained (25 mg for HA_8) (*27*).

This chapter describes a size exclusion column that can be loaded with up to 500 mg of the crude HA digest to yield homodispersed HA-Os on a hundred milligram scale.
Following HA-O production, methods were developed to synthesize HA-lipid conjugates for formulation of HA-targeted liposomes. Their interaction with CD44-overexpressing cell types was studied.

2.3 Experimental Procedures

2.3.1 Materials

All reagents and solvents were obtained from commercial suppliers and used without further purification, unless noted. Dipalmitoylphosphatidylethanolamine (DPPE), 1,2 Distearoyl-*sn*-glycero-3-phosphocholine (DSPC), 1,2 dioleoyl-*sn*-glycero-3-phosphoethanolamine-N-hexanoylamine (C_6-DOPE), 1,2 dioleoyl-*sn*-glycero-3-phosphoethanolamine-N-dodecanoylamine (C_{12}-DOPE), 1,2 distearoyl-*sn*-glycero-3-phosphoethanolamine-N-{amino(polyethylene glycol)-2000} (PEG_{2000}-DSPE) and cholesterol were obtained from Avanti Polar Lipids (Alabaster, AL). Non-sterile, EP-grade, sodium hyaluronate was purchase from Genzyme Biosurgery (Framingham, MA). Testicular ovine hyaluronidase was purchased from Calbiochem (San Diego, CA).

2.3.2 Digestion of HA

Sodium hyaluronate was dissolved in digest buffer (0.1 M sodium acetate, adjusted to pH 5.2 with glacial acetic acid) at a concentration of 1g/100 mL and stirred at room temperature for 2 days, until hydrated. Hyaluronidase (100 kilounits) was added to the dissolved HA and incubated, unstirred, for 24 h at 37 ^{o}C. The enzyme was deactivated by immersion of the flask in boiling water for 7 min. Denatured enzyme precipitated as the HA solution cooled and was removed by centrifugation at 17,000 x g (12,000 rpm) for 20 minutes at 4 ^{o}C in a Sorvall centrifuge with a SS-34 rotor (Du Pont; Newton CT). The resultant pellet was discarded and the supernatant was lyophilized to a powder (Labconco Lyph Lock 4.5; Kansas City, MO).

2.3.3 Separation of HA Oligomers by Size Exclusion Chromatography

Lyophilized HA digest (500 mg including salt) was dissolved in 1 mL of 0.05 M degassed ammonium bicarbonate buffer, filtered through a 0.45 μm filter (Millipore; Bedford, MA) and loaded via a Rheodyne 7725 manual sample injector onto a 5 cm x 100 cm column (XK 50/100 column, Amersham Biosciences; Piscataway, NJ) packed with 300 g of P-30 Biogel (medium grade resin, Biorad Laboratories; Hercules, CA). The column was equilibrated in 0.05 M ammonium bicarbonate at a flow rate of 2.3 mL/min. Blue dextran (10 mg/mL) and carboxyfluorescein (1 mg/mL) were injected to calibrate void and total volume, respectively. Fractions after the void volume (8 ml each) were collected and their absorbance measured at 210 nm. Peaks containing HA-oligomers were pooled, lyophilized and redissolved in water. Residual ammonium bicarbonate salt was removed with a hydrogen ion exchange column (Dowex 50W x 4-50 H^+, Sigma-Aldrich; St. Louis, MO). In some cases, the HA-O salt form was exchanged for tetrabutylammonium chloride using a Biorex 70 ion exchange column (Biorad Laboratories; Hercules, CA). The product was lyophilized to dryness and stored at room temperature.

2.3.4 MALDI-TOF MS Analysis of HA Oligomers and HA_n-DPPE Conjugates

All MALDI-TOF MS analyses were done on a Voyager-DE Biospectrometry Workstation (Applied Biosystems; Foster City, CA). The spectrometer was calibrated using a mixture of renin (MH^+ = 1760 Da), insulin β chain – oxidized (MH^+ = 3496.9 Da) and insulin (MH^+ = 5735.5 Da) at concentrations of 0.25, 0.09 and 0.15 μg/mL respectively, dissolved in 1:1 (v/v) H_2O and acetone saturated with a dihydroxybenzoic

acid (DHB) matrix. Samples of HA-O were dissolved in water and mixed at 1:1 (v/v) with DHB matrix in acetone, spotted on a stainless steel target and allowed to air dry. Similarly, samples of HA_n-DPPE in chloroform ($CHCl_3$) and methanol (CH_3OH) (7:3, by volume) were mixed with DHB matrix dissolved in CH_3OH (1:1, by volume). Mass spectra were recorded using both positive and negative ion modes. Peaks from a minimum of 3 column purifications were analyzed for each oligosaccharide to verify measurement consistency.

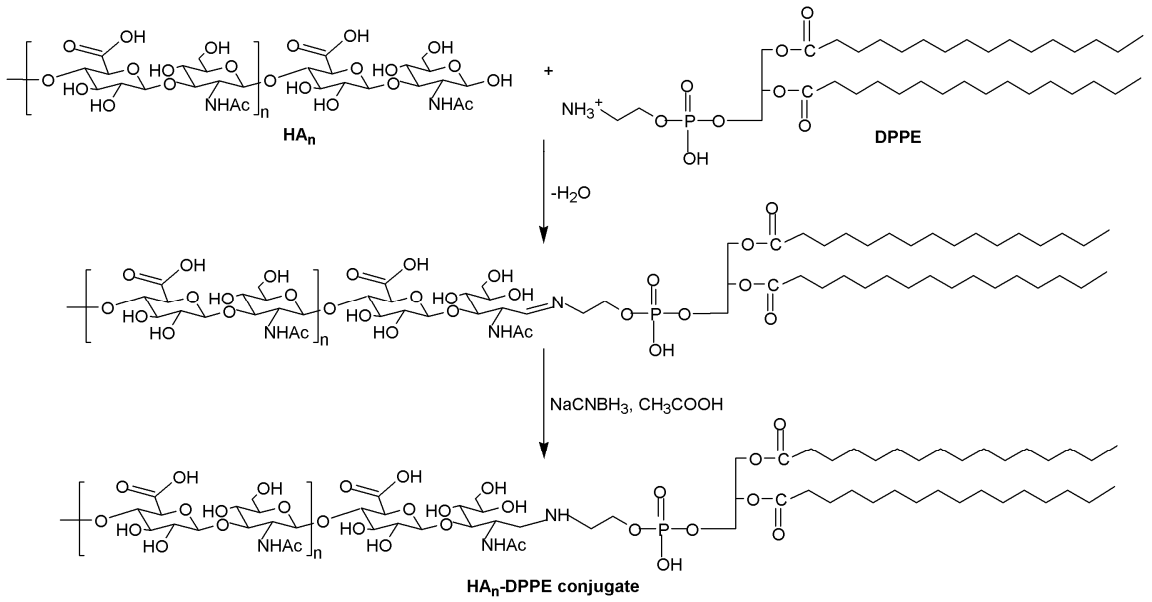
2.3.5 Coupling HA_4 to DPPE via Reductive Amination

The following method was standardized for the synthesis of the tetrasaccharide (HA_4) conjugate (Scheme **2-1**). Reaction conditions were then varied depending on HA oligomer length, as shown in Table **2-1**. HA_4 (100 mg) was suspended in DMSO (0.75 ml) and CH_3OH (2.5 mL). Two molar equivalents of DPPE (178 mg) were dissolved in 24 mL $CHCl_3/CH_3OH$ (2:1, by volume). The HA solution and the DPPE solution were combined slowly and stirred at 60 ^oC for 1.5 h. Freshly prepared reducing agent solution containing 5% w/v of tetrabutylammonium cyanoborohydride (Bu_4NCNBH_3) in $CHCl_3/CH_3OH$ (1:1, by volume) with 0.1% acetic acid was added in five 0.5 mL portions, at hourly intervals. The mixture was stirred for 24 h at 60 ^oC. For

HA_n	DMSO (mg/mL)	First Incubation (hr)	Incubation After Catalyst Addition (hr)
4	150	1.5	24
6	100	3.0	48
8	100	3.0	48
10	50	5.0	72
12	50	5.0	72

Table 2-1. Reaction Conditions for Various Length Oligomers.

HA_4 and HA_6, the solution cleared during the initial 60 ºC incubation. Reactions containing longer oligosaccharides remained turbid. Conjugation was repeated 3 times or more for each HA oligomer length to ensure reproducibility.



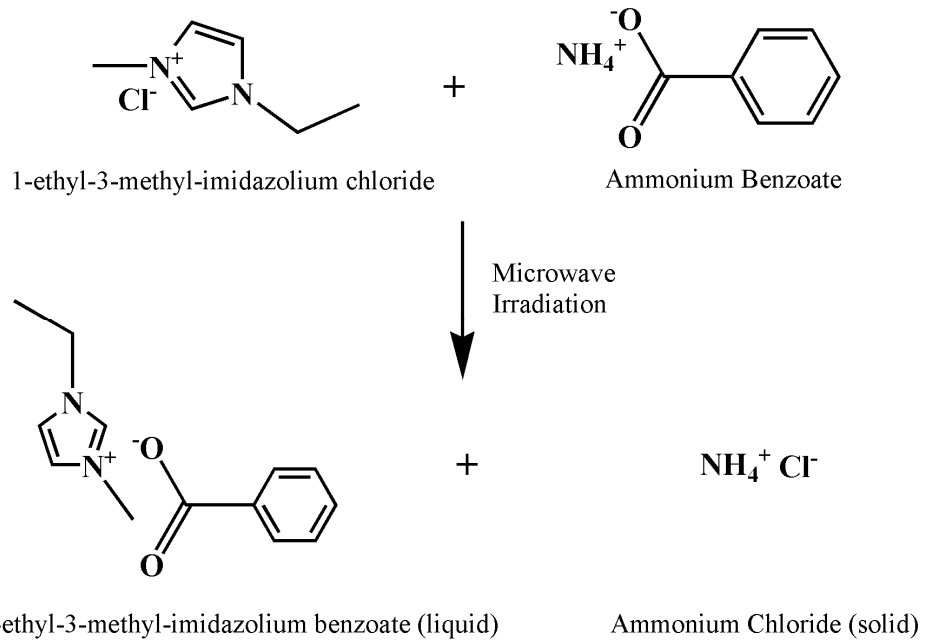
Scheme 2-1. Synthesis of HA_n-DPPE.

2.3.6 Coupling HA_n to DPPE with Alternate Solvents

Room temperature ionic liquid (RTIL) components, 1-ethyl-3-methyl-imadazolium chloride (EmImC) and ammonium benzoate (AB), were mixed in a heat-resistant, screw-top glass tube (Scheme **2-2**). The solid mixture was heated for 20 seconds in a microwave and vortexed. Heating was repeated until a liquid formed (EmImB). Upon cooling solids precipitated and the viscous liquid was decanted. An HA mixture comprised mostly of HA_{12} (6.7 µmol) and DPPE (12.7 µmol) fully dissolved in

approximately 3 mL EmImB RTIL at 70 ºC. To this 22 mg $NaCNBH_3$ or 5 mg $Sc(OTf)_3$ was added and the solution was reacted overnight. Reaction progression was evaluated with MALDI and TLC.

An HA mixture comprised principally of HA_{12} (60 µmol) was dissolved in 1 mL dry DMSO containing 12 µmol DMPE and 100 µL of acetic acid (*28*). This was heated for one hour at 60 ºC and a solution of triacetoxyborohydride ($NaBH(OAC)_3$) was added in minimal DMSO. The mixture was reacted for one week at 60 ºC and reaction progression was monitored using MALDI and TLC.



Scheme 2-2. Example Formation of a Room Temperature Ionic Liquid (RTIL).

2.3.7 Coupling HA_n with Alternative Lipids and Linkers

The standardized method for HA conjugation was used with linker lipids, containing a spacer between the amine head group and the acyl chains, substituted for DPPE (Figure **2-2**). Briefly, HA_n (0.0197 mmol) was dissolved in 150 µL DMSO and 375 µl CH_3OH. After the oligosaccharide was fully dissolved, lipid (0.038 mmol) in 3.6 mL (2:1 $CHCl_3$:CH_3OH) was added slowly and reacted at 60 ºC for 1 hour. Reducing solution was added in 0.5 mL aliquots every hour for 5 hours. The mixture reacted for 16 hours under argon. Reactions containing the ether lipid (DODPE) also included trace amounts of N,N diisopropylethylamine base. An additional 50 µl aliquot of this base was added after 1 hour incubation at 60 ºC. Reaction progress was monitored by MALDI and TLC. Products containing DOPE-C_6 or C_{12} were purified using high performance liquid chromatography and eluted at approximately 5:4:1 ($CHCl_3$:CH_3OH:H_2O).

PEG_{2000}-DSPE was reacted with HA_{12} in an aqueous based solvent system. The lipid (0.06 mmol) was dried to a film using rotary evaporation and rehydrated in 1.8 mL borate buffer (0.1 M, pH 7.3). HA_{12} (48 mg) was added to the micellar lipid suspension and the reaction mixture was heated incrementally from 35 to 75 ºC over 3 hours. Reducing solution (5 mL buffer with 58.5 mg $NaCNBH_3$ and 50 µL glacial acetic acid) was added hourly in 5-0.5 mL aliquots beginning at 3 hours.

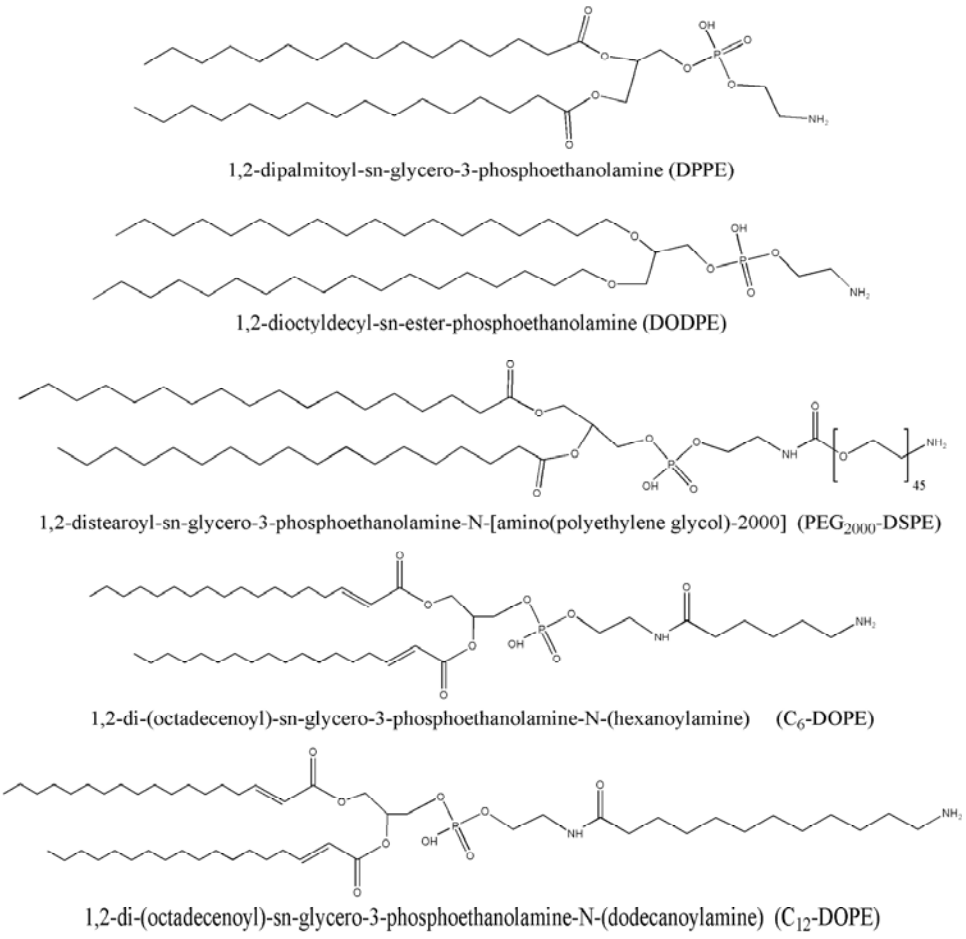


Figure 2-2. Amine-Containing Lipids Conjugated to HA via Reductive Amination.

2.3.8 HA_n-DPPE Conjugate Purification

To precipitate HA and HA-conjugated lipids, 10 volume equivalents of acetone was added. After 1 hour at 4 ºC, the mixture was centrifuged for 20 minutes at 700 x g in a Sorvall RT6000 (Du Pont; Newtown, CT). The pellet (containing unreacted HA_n, DPPE, and the HA_n-DPPE product) was resuspended in minimal $CHCl_3/CH_3OH/H_2O$ (11:9:2 by volume) and loaded onto a prepacked silica column (FLASH 12+M Cartridge Biotage; Charlottesville, VA). The column was washed with 36 mL (3 column volumes) $CHCl_3$, after which a gradient of $CHCl_3/CH_3OH/H_2O$ was run from 11:3.85:0.86 to 11:9:2 (by volume). The HA-conjugates eluted at a solvent ratio of approximately 11:6.5:1.4 ($CHCl_3/CH_3OH/H_2O$).

2.3.9 Conjugating HMW-HA to Fluorescein Amine

HMW-HA was labeled using carboxylate side-chain conjugation via the Ugi multicomponent condensation reaction (*29*). HMW-HA (74 mg) was hydrated in 8 mL of water for 3 days prior to reaction. While covered, HMW-HA was diluted with 4 mL DMSO and mixed with 0.3 mL DMSO containing 35 mg fluorescein amine and 35 µl isocyclohexane. After 5 hours, ice-cold ethanol was added and HMW-HA-fluorescein amine conjugate (HMW-HA-FA) was precipitated at -20 ºC. The precipitate was removed with tweezers, washed thoroughly in ethanol and dried under vacuum. HMW-HA-FA was synthesized in duplicate reactions to ensure reproducibility.

2.3.10 Liposome Preparation

Lipid films were prepared by drying 10 μmol of total lipid, including HA_n-DPPE, under vacuum at room temperature. Formulations contained DSPC, cholesterol, the HA-lipid conjugate (59:40:1 mole %) and 0.05 mole % of the fluorescent lipid. Liposomes were prepared by rehydrating the lipid film with 1 mL of 10 mM HEPES, 5% glucose (pH 7.4), followed by mixing by vortex mixer for 1 minute and sonication at 65 ^{o}C for 30 minutes under argon (*30*). Liposome diameter was reduced by serial extrusion through 200 and 100 nm polycarbonate membranes (Avestin; Canada). The hydrodynamic diameter of the liposomes was determined by dynamic light scattering on a Zetasizer 1000 (Malvern Instruments; UK).

2.3.11 Liposome Binding to Cells

Melanoma cells (B16F10, ATCC; Manassas, VA) were cultured in MEM Eagle's with Earle's BSS containing 10% fetal calf serum (FCS), 1% non-essential amino acids and 1% sodium pyruvate by volume. Cells ($2 * 10^5$) were placed in each well of a 6-well plate and grown overnight at 37 ^{o}C and 5% CO_2 in complete medium. The cell monolayer was rinsed once with FCS free medium. Medium containing 125 μmol/mL liposomes was then added and incubated with the cells for 3 h at 37 ^{o}C. For HA-O competition assays, crude HA hydrolysate was added at a concentration of 100 μg/mL of media for 1 hour prior to liposome addition. Liposomes were visualized based on FITC fluorescence (excitation/emission 484/510 nm, Eclipse TS100 Nikon; Japan). Cells were visualized by phase contrast using white light. Images were taken with a SPOT RT

camera (Diagnostic Instruments; Sterling Heights, MI). Binding assays were performed a minimum of 2 times for each condition studied.

For quantitative studies, liposomes contained <0.01 mole % tritiated cholesteryl hexadecyl ether. After liposome incubation, wells were washed three times and this buffer was collected and considered to contain all unbound liposomes. Cells were lysed by incubation with 0.5N sodium hydroxide for 30 minutes. Total lysate, containing cell bound liposomes, was collected. Ultima Gold (15 mL, Perkin Elmer; Boston, MA) was added and the radioactivity in each of the cell fractions was counted.

2.3.12 CD44 Analysis and Manipulation using FACS

CD44 overexpressing cells (C26 ATCC; Manassas, VA) were washed with 10 mM EDTA for 5 – 10 minutes at 37 ºC, until they detached, and were centrifuged at 800 rpm for 5 minutes. The wash was repeated twice with PBS and cells ($1 * 10^5$ per tube) were blocked with 100 µl normal goat serum at 4 ºC for 10 min. Following two PBS washes, cells were incubated with 5 µl mouse anti-CD44 (Endogen Pierce Biotechnology; Rockford, IL) in 95 µl for 20 minutes at. The cells were washed and incubated with FITC rat anti-mouse secondary antibody (Sigma) for 20-25 minutes at 4 ºC. For HA binding studies, 100 µL HMW-HA-FA binding (1 µg/mL) was added in the place of antibodies and incubated for 3 hours at 4 ºC. Competing, unlabled HMW-HA was added in equimolar concentration for 1 hour prior to sorting. Cells were washed twice with PBS. To fix, cells were incubated in 1% PFA, which was removed prior to cell sorting (FACSCalibur Invitrogen; Carlsbad, CA). Experiments were performed in duplicate.

2.4 Results

2.4.1 Digestion and Separation of HA Oligomers

High molecular weight, medical grade hyaluronan was digested with hyaluronidase over 24 hours. This incubation period digested the HMW-HA to HA_4 through HA_{12} with small amounts of larger oligosaccharides. Monodispersed saccharides were separated on a Biogel P-30 size exclusion column. This digestion and column separation combination produced well differentiated peaks with base-line separation (Figure **2-3**). Fractions from each peak contained monodispersed saccharides (Table **2-2**). These conditions separated even numbered oligosaccharides for a column loaded with up to 500 mg HA within 24 hours of running time.

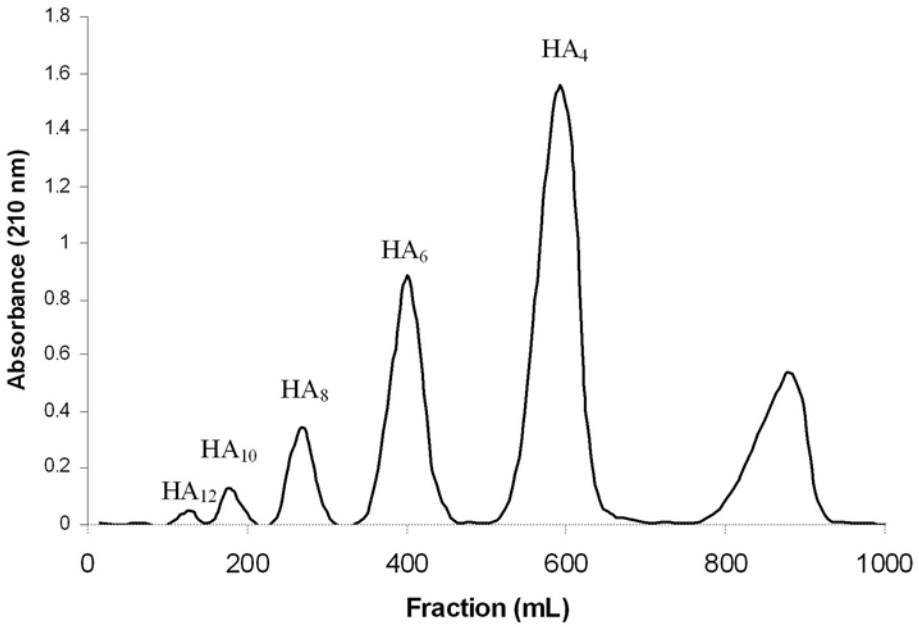


Figure 2-3. Example Size Exclusion Column Profile of HA Oligomers showing baseline separation of HA_4 through HA_{12}. Oligomer type, determined by mass via MALDI-TOF MS, is indicated above each peak. The last, unlabeled, peak is residual salt and small molecule contaminants.

HA_n	MW	Mol. Formula	Str. Formula	$[M-H]^-$	Recorded Mass
4	776.65	$C_{28}H_{44}N_2O_{23}$	$[GlcUA\text{-}GlcNAc]_2$	775.65	775.26
6	1155.34	$C_{42}H_{65}N_3O_{34}$	$[GlcUA\text{-}GlcNAc]_3$	1154.34	1154.54
8	1535.28	$C_{56}H_{86}N_4O_{45}$	$[GlcUA\text{-}GlcNAc]_4$	1534.28	1534.97
10	1914.60	$C_{70}H_{107}N_5O_{56}$	$[GlcUA\text{-}GlcNAc]_5$	1913.60	1913.06
12	2293.92	$C_{84}H_{128}N_6O_{67}$	$[GlcUA\text{-}GlcNAc]_6$	2292.92	2292.44

Table 2-2. MALDI-TOF MS Results for HA Oligosaccharides. These masses correspond to pooled fractions of HA oligosaccharide peaks from size exclusion column purification. All masses are given in daltons, molecular weight (MW) is the average molecular mass.

2.4.2 Synthesis of Lipooligosaccharides

We investigated a number of coupling conditions using different reductants, solvents and reaction times. The conditions that follow are those that produced the highest, reproducible yields (Scheme **2-1**, Table **2-1**). Oligosaccharide fragments were dissolved in a mixture of DMSO and CH_3OH before the lipid solution in $CHCl_3$ was added. The combined mixture of lipid and HA became turbid. Slow addition of the DPPE prevented complete precipitation. The ratio of solvents ($CHCl_3$, CH_3OH, and DMSO) can be adjusted to allow several oligomer lengths to couple to lipids despite their diverse solubility requirements (Table **2-1**). The reducing agent was added in small portions over a long interval of time which gave better, reproducible results as compared to a single, larger addition.

To demonstrate that we can extend our coupling protocol, we synthesized a conjugate of HA_4 and alternative lipids. The lipid 1,2-dioctadecyl-*sn*-ester-3-phosphoethanolamine (DODPE, Figure **2-2**) contains ether linkages in place of acyl linkages. Liposomes bearing HA_n-ether lipid may be less susceptible to hydrolysis related instability than lipids with acyl linkages, which are prone to hydrolysis.

Lipids in which a linker moved the oligosaccharide away from the acyl, chains were synthesized. These lipids were then incorporated into liposomes to determine if steric hindrance was influencing oligosaccharide association with CD44 on the cell surface (MALDI-TOF M{H^+} HA_8-C_6-DOPE = 2358.05, HA_8-C_{12}-DOPE = 2560.75).

2.4.3 Coupling HA_n to DPPE with Alternate Solvents

The solvent combination that resulted in successful conjugation of HA of 4 – 8 saccharides in length could not induce solubility of HA_{10} saccharides or longer. Changing the solvent conditions to contain more aprotic or more protic solvents decreased solubility of either the saccharide or lipid component. Reactant solubility appeared to correspond to reaction yield.

Room temperature ionic liquids (RTILs) are highly charged organic salts (Scheme **2-2**). Once formed, these salts are fluid at room temperature and can be used to dissolve both saccharides and lipids. We believed that once in solution, the reducing sugar would become available for Schiff's base intermediate formation with the lipid amine. Although both components were soluble, no reaction occurred. In a solution of heated DMSO, HA fully dissolved and DMPE remained precipitated. The group that reported reaction under these conditions did not specify extent and purified the HMW-conjugate using ultrafiltration (*28*). After several days at 60 ºC no quantifiable reaction was observed in our hands.

2.4.4 Purification of Lipooligosaccharides

For high throughput purification, easy separation of HA-lipid from unreacted HA and DPPE is required. Solvents like water saturated butanol and methanol could not selectively remove DMSO and the reducing agent, without lowering product yields. Acetone, however, could precipitate the crude conjugate product while dissolving all the reducing agent. This precipitate could then be resuspended in a minimal amount of 11:9:2 ($CHCl_3$:CH_3OH:H_2O) and purified by high performance FLASH silica column chromatography (Horizon, Biotage; Charlottesville, VA) producing pure HA_n-DPPE conjugates in moderately high yields.

2.4.5 Analysis of Lipooligosaccharides

Purity of each conjugate was verified by running a TLC in $CHCl_3$:CH_3OH:H_2O (11:9:2 by volume). The product stained positive with both a carbohydrate (1 mg/mL orcinol characterized by TLC and MALDI (HA_4-DPPE, Figures **2-4, 2-5** and Table **2-3**).

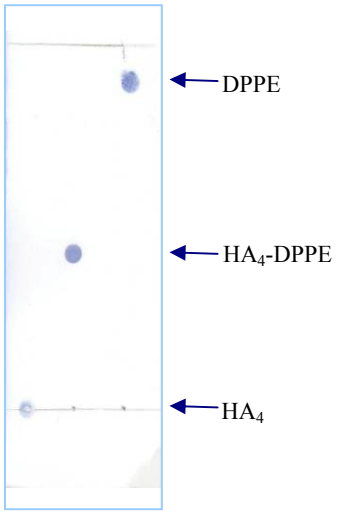


Figure 2-4. Illustrated TLC of HA_4-DPPE in chloroform:methanol:water (11:9:2 by volume). DPPE has a characteristic rf of 0.93. The HA-conjugate has an rf of 0.43. Unmodified HA does not travel from the base.

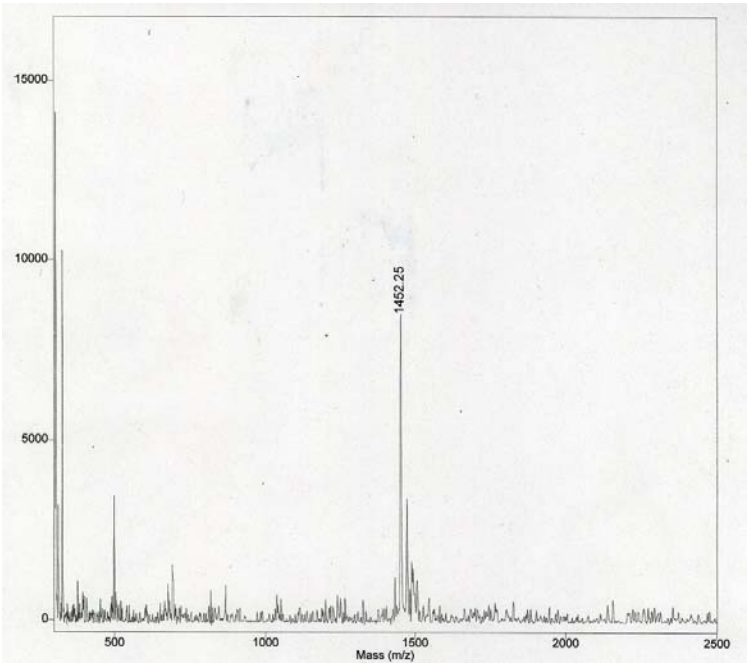


Figure 2-5. Example MALDI-TOF MS Spectrum of an HA_4-DPPE Conjugate.

HA_n-DPPE	MW	Formula	$[M-H]^-$	Recorded Mass
4	1452.61	$C_{65}H_{118}N_3O_{30}P$	1451.61	1452.25
6	1831.93	$C_{79}H_{139}N_4O_{41}P$	1830.93	1830.39
8	2211.24	$C_{93}H_{160}N_5O_{52}P$	2210.24	2210.74
10	2606.60	$C_{108}H_{185}N_6O_{63}P$	2605.60	
12	2985.92	$C_{122}H_{206}N_7O_{74}P$	2984.92	

Table 2-3. MALDI-TOF MS Results for HA_n-DPPE Conjugates. All masses are given in daltons, molecular weight (MW) is the average molecular mass.

The HA_4-DPPE was characterized by ^{1}H-NMR (Figure **2-6**) using a mixed solvent system of pyridine D_5/DCl/CD_3OD/$CDCl_3$ (1:1:2:10 by volume) (*31*). ^{1}H-NMR (400 MHz) with characteristic peaks: δ 4.76 (1H, H-1'$_\alpha$), 4.69 (2H, H-1'$_\beta$, H-1'''), 4.62 (1H, H-1''), 4.41-3.27 (sugar protons), 1.56 (4H, NH-CH_2-CH_2-), 2.25-1.29 (56H, methylene protons of DPPE), 2.01 (6H, NHCOCH_3), 0.87 (6H, terminal CH_3 of DPPE). Based on the ratio between the characteristic terminal methyl of DPPE and the methyl acetal group of N-acetyl glucosamine, the coupling is stoichiometric.

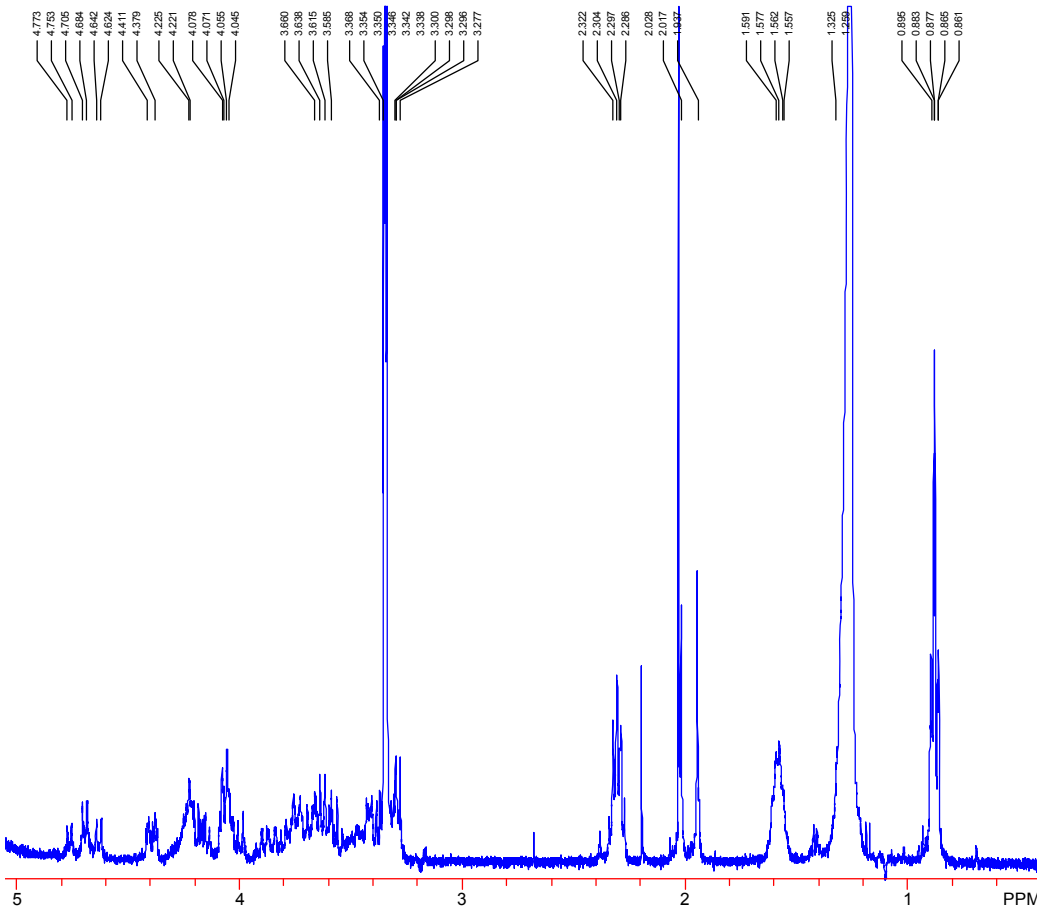


Figure 2-6. Example NMR Spectrum of an HA_4-DPPE Conjugate. Characteristic peaks at 0.96 ppm (the terminal methyl of DPPE) and 2.02 (the terminal methyl acetyl of N-acetyl glucosamine) suggest stoichiometric conjugation.

2.4.6 Binding of HA-Modified Liposomes to Cultured CD44-Expressing Cells

Initial binding assays suggested that HA_4-bearing liposomes were sufficient to mediate binding to B16F10 cells, which overexpress CD44 (Figure **2-7**). This binding was alleviated when liposome incubation was done in the presence of a heterogeneous population of short HA oligomers, suggesting that this binding is mediated by HA. Presence of CD44 on these cells was verified by FACS analysis (data not shown).

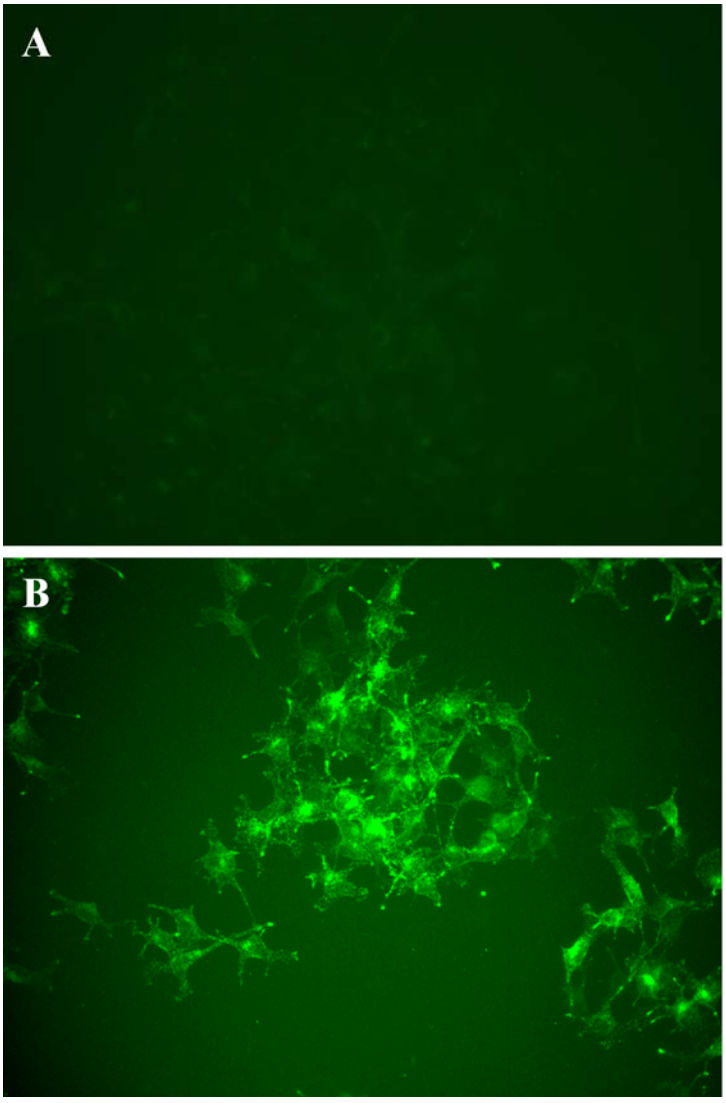


Figure 2-7. Cell Binding of HA_4-Liposomes. B16F10 cells challenged with 3% HA_4-DPPE-containing liposomes with (**A**) and without (**B**) competition from an exogenous population of heterogeneous HA oligomers.

Upon further investigation, it was shown that these liposomes also bound to control cells that did not overexpress CD44. Liposomes containing other HA conjugates were similarly unable to mediate binding between liposomes and CD44 expressing cells beyond what could be attributed to the negative charge contribution of the HA to the liposome surface (Figures **2-7**, **2-8**). This data was verified using a multi-well plate assay with liposomes containing a radioactive lipid (data not shown).

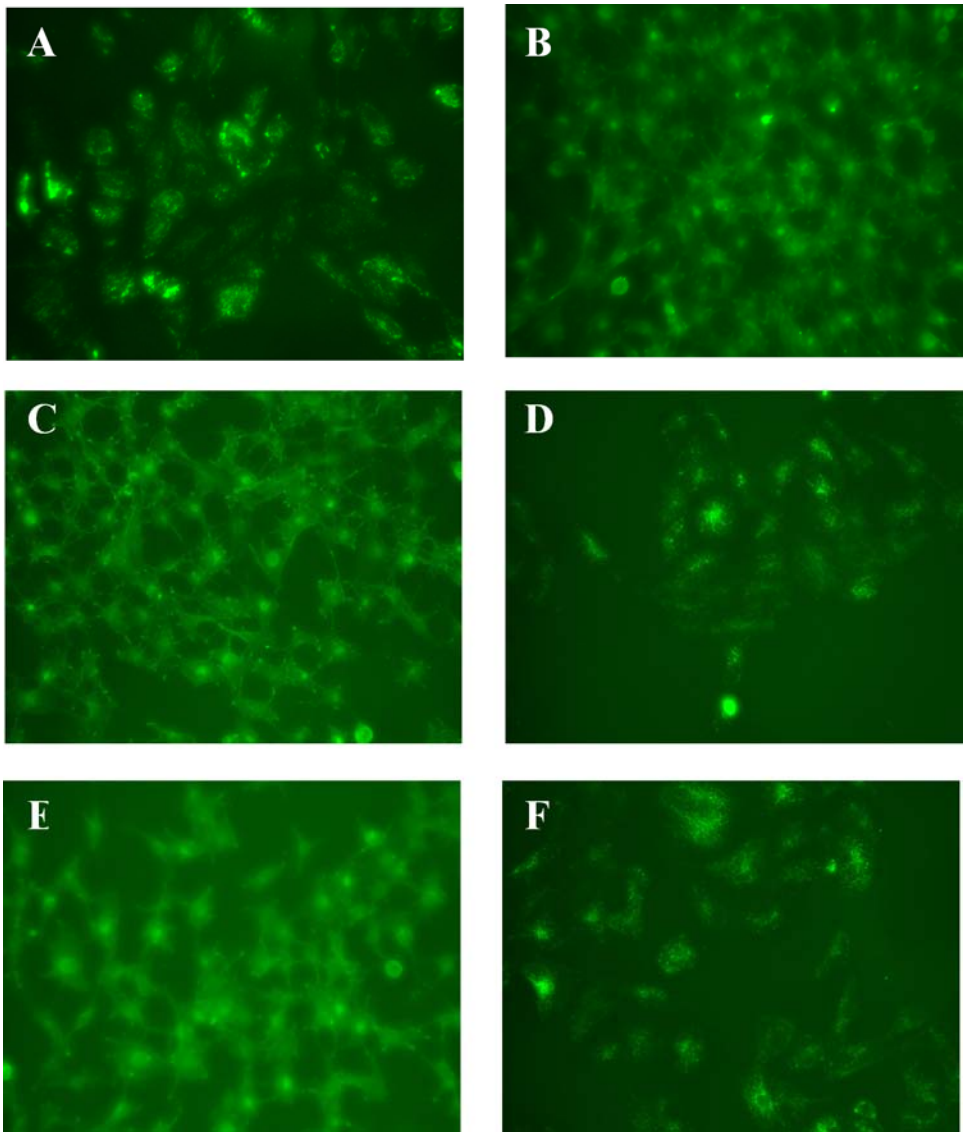


Figure 2-8. Cell Binding of HA-Linker-Liposomes containing 1% HA_8-C_6-DOPE (**A**,**B**), 1% HA_8-C_{12}-DOPE (**C**,**D**), or 5% POPG (**E**,**F**) to B16F10 (**A,C,E**) or CV1 (**B,D,F**) cells.

2.4.7 Binding of Fluorescent HMW-HA-FA to Cultured CD44-Expressing Cells

To ensure cells to bind HA, the presence of CD44 was verified by anti-CD44 antibody fluorescence FACS analysis. HMW-HA was then modified to contain a fluorescent molecule to verify that CD44 present on the cell surface was available for HA binding. Based on fluorescein amine absorbance at 490 nm, 1 in every 35-75 carboxylate side chains of D-glucuronic acid was modified. Fluorescent HMW-HA-FA bound specifically to C26 cells, which overexpress CD44. The fluorescent HMW-HA did not bind to control cells (CV1, Figure **2-9**). Competition with unlabeled HMW-HA decreased fluorescent HMW-HA binding.

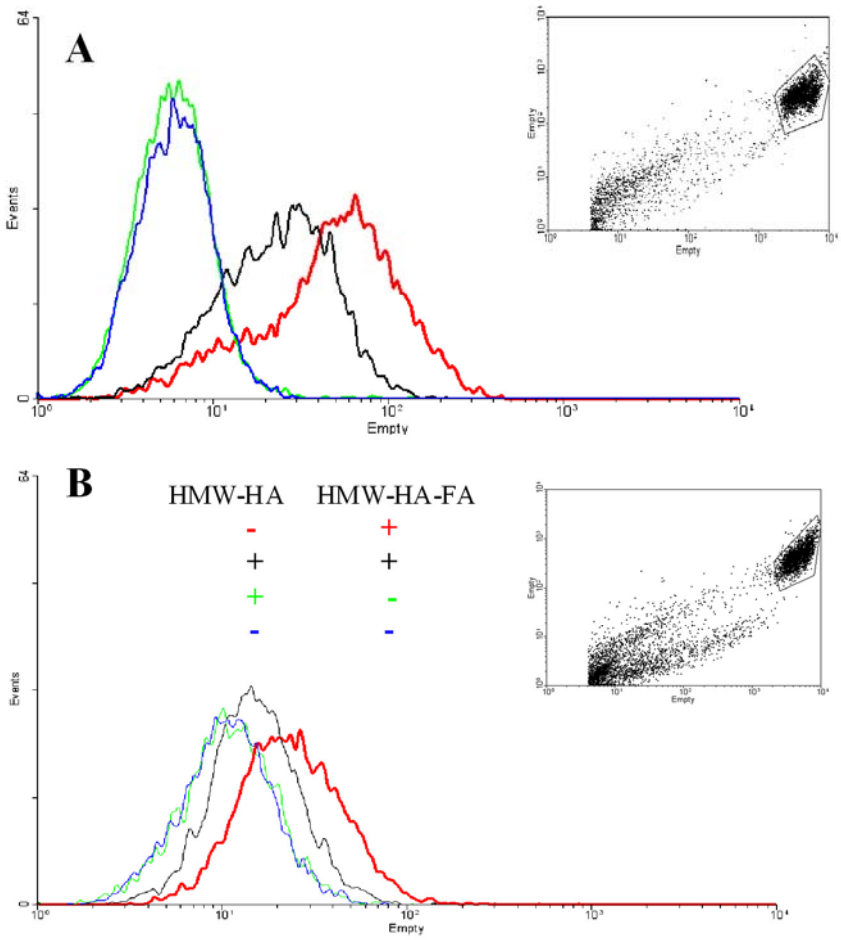


Figure 2-9. FACS Competition Assay of Unlabeled and Fluorescein Labeled HMW-HA on C26 (**A**) and CV1 (**B**) cells. Inset (**A** and **B**) indicates cell sorting and selected region of interest.

2.5 Discussion

Understanding the significance of oligomer length for receptor binding is important for furthering HA-drug targeting studies to CD44 overexpressing tumors. Other cell surface receptors, such as RHAMM and HARE, also mediate binding and internalization of circulating HA (*32*). To circumvent HA-liposome binding and clearance by these receptors, HA of the minimum saccharide number for CD44 binding should be used for targeting. Lipooligosaccharides of different and distinct lengths are needed to investigate the critical parameters for CD44 binding and internalization.

A simple method of creating short oligosaccharide fragments from HMW-HA by digestion was reported by the Day group (*27*). By directly scaling up this digestion, we were able to produce mixed HA-Os. The subsequent isolation of individual oligomers on an automated size exclusion column enabled production (multi-hundred milligram) amounts of pure HA_4, HA_6, HA_8, HA_{10} and HA_{12} (Figure **2-3**). In a single injection of 500 mg of crude HA digest, baseline purification of oligomers was completed within 24 hours, in a single-step purification, on a 100 cm long size exclusion column with manual injection and automated fraction collection.

Synthesis of an HA-lipid conjugate is a necessary prerequisite for systematic drug delivery studies where the drug is carried by HA surface modified liposomes. When constructed, it is essential that the HA-lipid conjugate retains the CD44 binding functionality of oligomer HA. Liposomes modified with high molecular weight HA have the ability to target tumors overexpressing CD44 receptors *in vivo* (*15, 16*). In these

studies HA was attached using ethyl dimethylaminopropyl carboiimide (EDC) mediated chemistry. This chemistry yields HA with multiple undefined site attachments between the liposome surface and the carboxylate side-chains.

Single point attachment of HA to lipids can provide a discrete molecule for targeting which can be fully characterized and reproduced. Reductive amination generates a well-defined molecule in which all other hydroxyl and carboxylic acid groups remain intact and available for CD44 interaction. This chemistry (*33*) has been extensively used for conjugating nano- and microgram quantities of glycosaminoglycans with various amine containing substrates. Small-scale conjugation between saccharides and lipids was done using iodine oxidation followed by extensive column purification and reaction with an amine-lipid (*23*). Synthesis schemes using reductive amination with cyanoborohydrides utilized hydrophilic amine-compounds such as poly(lysine) (*24*) and the fluorophore aminoacridone (*25*).

To obtain monodispersed HA-lipid conjugates, we developed a standardized method for their synthesis and purification that yields conjugates in moderately high, reproducible yields. The solvent system consisted of $CHCl_3$-CH_3OH with minimal DMSO to partially dissolve the HA-Os. Using the more soluble tetrabutyl ammonium salt form of the reducing cyanoborohydride, and adding it in small aliquots, improved reaction yields. With these modifications, this reaction results in a reliable and reproducible synthesis of HA_n-DPPE conjugates with moderate yields, ranging from 40 to 60% after one step column purification (Figures **2-4**, **2-5** and **2-6**). The reaction conditions are mild and can

conveniently be extended to other amine bearing lipids having variable chain lengths. However, the reaction is limited to HA_4 – HA_8; greater saccharide lengths have low yields.

Cell binding studies by our group using mixed HA-O liposomes showed promising results (*7, 8*). HA-O targeted liposomes avidly bound to and were internalized by CD44 overexpressing cell lines but not to cells that express low CD44 levels (*7, 8*). Binding of these liposomes was inhibited by HMW-HA and an anti-CD44 monoclonal antibody, demonstrating that this binding and internalization was due to CD44-HA interactions. However, the HA ligand used for liposome targeting was a heterogeneous mixture of lipid conjugated HA-Os. Further evaluating the saccharide length dependence of this targeting relationship may yield a better insight into the process by which HA on the surface of liposomes interacts with, and is internalized by, CD44.

Early crystallization experiments showed the central six saccharides of HA_8 completely occupied the CD44 binding grove and caused a conformational binding change (*34*). Although it appeared that HA_4 targeted liposomes bound to CD44 overexpressing B16F10 cells (Figure **2-7**), further binding studies suggested this interaction was not CD44 specific. Liposomes containing HA_4 to HA_8, with and without linkers, bound to both CD44 negative control cells and CD44 overexpressing cells; the HA-liposomes were not binding in a CD44 specific manner (Figure **2-8**) as the binding only occurred with high concentrations of liposomes. Most binding studies performed resulted in no visible cell binding (data not shown). To ensure that CD44 was expressed, cells were evaluated

for CD44 presence and binding ability using antibody- and HMW-HA-FA-based FACS; cells expressed CD44 and actively bound HMW-HA (Figure **2-9**).

This study clarifies the minimum binding HA saccharide length in the presence of a drug carrier but does not ascertain what minimum length is necessary. Our binding experiments suggest that the minimum oligosaccharide that binds to CD44 is slightly larger in the presence of a drug carrier than the saccharide length suggested by previous lipsome binding studies (*7, 8*) or crystallization of CD44 (*34*). Alternative synthesis methods that utilize other techniques, such as HA coupling to a resin, are being investigated as possible mechanisms to resolve HA/lipid solvent solubility.

2.6 Acknowledgements and Author Contributions

Our grateful appreciation is extended to Dr. Dipali Ruhela for mentoring in carbohydrate chemistry, original re-synthesis of HA_4-lipid conjugates, obtaining the NMR spectrum of HA_4-DPPE, participating in the intellectual and experimental investigation of lipooligosaccharide conjugation techniques and tireless creativity. This work was supported by grant NIH R01 GM061851.

2.7 Literature Cited

(1) Marhaba, R., and Zoller, M. (2004) CD44 in cancer progression: adhesion, migration and growth regulation. *J Mol Histol 35*, 211-31.

(2) Toole, B. P., Wight, T. N., and Tammi, M. I. (2002) Hyaluronan-cell interactions in cancer and vascular disease. *J Biol Chem 277*, 4593-6.

(3) Naor, D., Nedvetzki, S., Golan, I., Melnik, L., and Faitelson, Y. (2002) CD44 in cancer. *Crit Rev Clin Lab Sci 39*, 527-79.

(4) Luo, Y., and Prestwich, G. D. (1999) Synthesis and selective cytotoxicity of a hyaluronic acid-antitumor bioconjugate. *Bioconjug Chem 10*, 755-63.

(5) Luo, Y., Ziebell, M. R., and Prestwich, G. D. (2000) A hyaluronic acid-taxol antitumor bioconjugate targeted to cancer cells. *Biomacromolecules 1*, 208-18.

(6) Luo, Y., Bernshaw, N. J., Lu, Z. R., Kopecek, J., and Prestwich, G. D. (2002) Targeted delivery of doxorubicin by HPMA copolymer-hyaluronan bioconjugates. *Pharm Res 19*, 396-402.

(7) Eliaz, R. E., Nir, S., Marty, C., and Szoka, F. C., Jr. (2004) Determination and modeling of kinetics of cancer cell killing by doxorubicin and doxorubicin encapsulated in targeted liposomes. *Cancer Res 64*, 711-8.

(8) Eliaz, R. E., Nir, S., and Szoka, F. C., Jr. (2004) Interactions of hyaluronan-targeted liposomes with cultured cells: modeling of binding and endocytosis. *Methods Enzymol 387*, 16-33.

(9) Harris, E. N., Weigel, J. A., and Weigel, P. H. (2004) Endocytic function, glycosaminoglycan specificity, and antibody sensitivity of the recombinant human 190-kDa hyaluronan receptor for endocytosis (HARE). *J Biol Chem 279*, 36201-9.

(10) Maeda, H., Seymour, L. W., and Miyamoto, Y. (1992) Conjugates of anticancer agents and polymers: advantages of macromolecular therapeutics in vivo. *Bioconjug Chem 3*, 351-62.

(11) Sapra, P., Tyagi, P., and Allen, T. M. (2005) Ligand-targeted liposomes for cancer treatment. *Curr Drug Deliv 2*, 369-81.

(12) Noble, C. O., Kirpotin, D. B., Hayes, M. E., Mamot, C., Hong, K., Park, J. W., Benz, C. C., Marks, J. D., and Drummond, D. C. (2004) Development of ligand-targeted liposomes for cancer therapy. *Expert Opin Ther Targets 8*, 335-53.

(13) Sapra, P., and Allen, T. M. (2003) Ligand-targeted liposomal anticancer drugs. *Prog Lipid Res 42*, 439-62.

(14) Allen, T. M., and Cullis, P. R. (2004) Drug delivery systems: entering the mainstream. *Science 303*, 1818-22.

(15) Peer, D., and Margalit, R. (2004) Tumor-targeted hyaluronan nanoliposomes increase the antitumor activity of liposomal Doxorubicin in syngeneic and human xenograft mouse tumor models. *Neoplasia 6*, 343-53.

(16) Peer, D., and Margalit, R. (2004) Loading mitomycin C inside long circulating hyaluronan targeted nano-liposomes increases its antitumor activity in three mice tumor models. *Int J Cancer 108*, 780-9.

(17) Coradini, D., Pellizzaro, C., Miglierini, G., Daidone, M. G., and Perbellini, A. (1999) Hyaluronic acid as drug delivery for sodium butyrate: improvement of the anti-proliferative activity on a breast-cancer cell line. *Int J Cancer 81*, 411-6.

(18) Chen, F., Kakizaki, I., Yamaguchi, M., Kojima, K., Takagaki, K., and Endo, M. (2009) Novel products in hyaluronan digested by bovine testicular hyaluronidase. *Glycoconj J 26*, 559-66.

(19) Akima, K., Ito, H., Iwata, Y., Matsuo, K., Watari, N., Yanagi, M., Hagi, H., Oshima, K., Yagita, A., Atomi, Y., and Tatekawa, I. (1996) Evaluation of antitumor activities of hyaluronate binding antitumor drugs: synthesis, characterization and antitumor activity. *J Drug Target 4*, 1-8.

(20) Peer, D., and Margalit, R. (2000) Physicochemical evaluation of a stability-driven approach to drug entrapment in regular and in surface-modified liposomes. *Arch Biochem Biophys 383*, 185-90.

(21) Eliaz, R. E., and Szoka, F. C., Jr. (2001) Liposome-encapsulated doxorubicin targeted to CD44: a strategy to kill CD44-overexpressing tumor cells. *Cancer Res 61*, 2592-601.

(22) Oohira, A., Kushima, Y., Tokita, Y., Sugiura, N., Sakurai, K., Suzuki, S., and Kimata, K. (2000) Effects of lipid-derivatized glycosaminoglycans (GAGs), a novel probe for functional analyses of GAGs, on cell-to-substratum adhesion and neurite elongation in primary cultures of fetal rat hippocampal neurons. *Arch Biochem Biophys 378*, 78-83.

(23) Sugiura, N., Sakurai, K., Hori, Y., Karasawa, K., Suzuki, S., and Kimata, K. (1993) Preparation of lipid-derivatized glycosaminoglycans to probe a regulatory function of the carbohydrate moieties of proteoglycans in cell-matrix interaction. *J Biol Chem 268*, 15779-87.

(24) Asayama, S., Nogawa, M., Takei, Y., Akaike, T., and Maruyama, A. (1998) Synthesis of novel polyampholyte comb-type copolymers consisting of a poly(L-lysine) backbone and hyaluronic acid side chains for a DNA carrier. *Bioconjug Chem 9*, 476-81.

(25) Calabro, A., Benavides, M., Tammi, M., Hascall, V. C., and Midura, R. J. (2000) Microanalysis of enzyme digests of hyaluronan and chondroitin/dermatan sulfate by fluorophore-assisted carbohydrate electrophoresis (FACE). *Glycobiology 10*, 273-81.

(26) DeAngelis, P. L., Oatman, L. C., and Gay, D. F. (2003) Rapid chemoenzymatic synthesis of monodisperse hyaluronan oligosaccharides with immobilized enzyme reactors. *J Biol Chem 278*, 35199-203.

(27) Mahoney, D. J., Aplin, R. T., Calabro, A., Hascall, V. C., and Day, A. J. (2001) Novel methods for the preparation and characterization of hyaluronan oligosaccharides of defined length. *Glycobiology 11*, 1025-33.

(28) Arpicco, S., Stella, B., Fattal, E., Bolognesi, S., and Cattel, L. . (2008) Hyaluronic Acid-Modified Liposomes: Preparation and Preliminary Biological Characterization. *Annual Meeting of the Controlled Release Society.*

(29) Ugi, I. (1962) The alpha-addition of immonium ions and anions to isonitriles accompanied by secondary reactions. *Angew. Chem. International Ed. 1*, 8-21.

(30) Szoka, F., Olson, F., Heath, T., Vail, W., Mayhew, E., and Papahadjopoulos, D. (1980) Preparation of unilamellar liposomes of intermediate size (0.1-0.2 μmol) by a combination of reverse phase evaporation and extrusion through polycarbonate membranes. *Biochim Biophys Acta 601*, 559-71.

(31) Wang, Y., and Hollingsworth, R. I. (1995) A solvent system for the high-resolution proton nuclear magnetic resonance spectroscopy of membrane lipids. *Anal Biochem 225*, 242-51.

(32) Day, A. J., and Prestwich, G. D. (2002) Hyaluronan-binding proteins: tying up the giant. *J Biol Chem 277*, 4585-8.

(33) Toomre, D. K., and Varki, A. (1994) Advances in the use of biotinylated diaminopyridine (BAP) as a versatile fluorescent tag for oligosaccharides. *Glycobiology 4*, 653-63.

(34) Banerji, S., Wright, A. J., Noble, M., Mahoney, D. J., Campbell, I. D., Day, A. J., and Jackson, D. G. (2007) Structures of the Cd44-hyaluronan complex provide insight into a fundamental carbohydrate-protein interaction. *Nat Struct Mol Biol 14*, 234-9.

Chapter 3

Influence of Multivalent Nitrilotriacetic Acid Lipid-Ligand Affinity on the Circulation Half-Life in Mice of a Liposome-Attached His_6-Protein

3.1 Abstract

Metal chelation-ligand interactions, such as occur between nitrilotriacetic acid (NTA)-nickel and multihistidines, enable the non-covalent attachment of histidine-modified proteins to liposomes and other particles. We compared three lipids: a mono-NTA lipid (circa 10 uM affinity) and two tris-NTA lipid derivatives (circa 3 nM and 0.2 nM affinity) in their ability to retain two different his_6-containing proteins on NTA liposomes in the presence of fetal calf serum and after intravenous injection in mice. At nanomolar affinities the off-rate of a his_6 ligand is sufficiently long so that his_6-proteins attached to particle surfaces will remain with the particle for hours; thus, we hypothesized that the increased his_6 affinity of multivalent NTA-modified liposomes would retain his_6-proteins longer both *in vitro* and *in vivo*. For each of the three lipids, we found a robust association and complete activity retention of two his_6-modified proteins: a far red-fluorescent protein, monomeric Katushka (mKate), and a prodrug-converting enzyme, yeast cytosine deaminase (yCD). Proteins associated more tightly *in vitro* with tris-NTA liposomes than with mono-NTA liposomes in the presence of refiltered fetal calf serum. Free yCD exchanged with previously associated mKate for tris-NTA binding sites on the liposome surface. The amount of yCD on the surface was similar if the proteins were co-associated or if mKate was pre-associated. This exchange confirms that NTA associated proteins are in a dynamic state and can exchange with multihistidine proteins in the biological milieu. There was no difference in circulation time of the protein when it was

intravenously administered by itself or attached to any of the NTA-modified liposomes because *in vivo* the protein was rapidly released from the NTA liposomes. The reason for the rapid protein dissociation from the liposome *in vivo* is not clear; it could be due to displacement by endogenous histidine-containing proteins or to natural chelators that remove nickel from the NTA. Regardless of the cause, improvements in chelator or ligand design are needed before metal chelation will be capable of retaining histidine-modified proteins on NTA liposomes after *in vivo* administration.

3.2 Introduction

Nickel chelation chromatography, and similar technologies that depend upon non-covalent interactions between a nickel chelator and a multihistidine-ligand, are widely used to purify proteins and associate proteins with surfaces (*1, 2*). The affinity of first generation nitrilotriacetic acid (NTAs) is about 10 micromolar whereas affinities of newer trivalent-NTAs (tris-NTAs) are in the nanomolar range (*3-5*).

NTA mediated protein association is a useful investigative tool that is mild enough to retain protein activity and requires only a simple modification of the amino acid sequence - the addition of a string of histidines (*1, 6*). This interaction is reversible by stripping the chelated nickel from the NTA or allowing molecules to compete with the protein for NTA association (*2*). Proteins remain in a lateral surface orientation (*7-9*) and free of surface involvement (*10*). The stable, well-defined orientation allows proteins to be imaged and their structure or function investigated (*11, 12*). NTA coated surfaces improve AFM-based protein imaging and have been used to measure real-time substrate

degradation (*13*). Active, surface-immobilized proteins can also be used to exploit the activity of these proteins in microarrays and biosensors (*6, 7, 14, 15*).

Modifications to the linkage area of the NTA headgroups change the molecules affinity for his-tagged proteins. The addition of poly(ethyleneglycol) (PEG) increases protein capture efficiency (*14, 15*). Multivalent NTAs improve affinity by allowing multiple chelated nickels within the NTA cluster to interact with a single his-tag (*16-18*).

Advances in protein production by recombinant techniques have largely removed protein availability as a limitation for protein related therapies (*19*). The stability and rapid clearance of proteins *in vivo* are barriers that can reduce their therapeutic potential (*20*). These limitations can be overcome, in part, by using nanocarriers to alter protein pharmacokinetics or increase protein stability (*21-23*). Additional problems arise as chemical conjugation of proteins to carrier surfaces can damage the protein and the percent of protein attached to the carrier can be low (*24*). Multivalent NTAs have the potential to increase the efficiency, simplify the modification of nanocarriers and enable a 'toolkit' approach for *in vivo* therapeutic use. Coupling proteins to carriers using a non-covalent NTA also avoids harsh conjugation chemistries. At low nanomolar affinities, the off-rate of a his_6 ligand from an NTA-nickel is sufficiently long so that the his_6-proteins bound to particle surfaces will remain with the particle for hours. Thus, an appropriate NTA-lipid would enable the creation of NTA-modified liposomes that could be functionalized with any his_6-containing protein.

The increased affinity of a multivalent NTA for a his-tagged protein is strong enough to make the interactions stable *in vitro* (*3-5, 17, 18, 25*). Immunoliposomes generated by associating single-chain antibody fragments to liposomes with mono-NTA lipids were found to be suitable for rapid *in vitro* screening. However, incubation with human plasma proteins as a surrogate for *in vivo* studies caused the protein to dissociate from the mono-NTA (*26*).

Other groups have shown success *in vivo.* His-tagged epitopes have been associated with both mono and multivalent-NTA nanoparticles to mediate immunotherapies (*3, 25, 27*). A his-tagged peptide designed to be membrane penetrating and immunostimulatory was shown to induce splenocytic immune stimulation in BALB/c mice when associated with NTA-DOGS-liposomes (*25*). Using the same NTA-DOGS-lipid, an NTA-wax nanoparticle induced immune response against an HIV Gag protein (*27*). Potential vaccines were also formulated from plasma membrane vesicles derived from tumor cells modified to contain tris-NTA lipid (*3*). When mice were immunized by subcutaneous injection of these vesicles, containing encapsulated cytokines, they exhibited decreased tumor growth when challenged two weeks after immunization (*3*). In all three studies, the nanoparticles were injected subcutaneously and were not exposed to blood. The stability of the protein-vesicle association *in vivo* was not monitored so the duration of protein retention is not known.

In this study, we compare the behavior of liposomes modified with three different NTA-lipids of increasing affinities for his-tagged proteins: mono-NTA-DOGS, tris-NTA-LYS-

DOD, and tris-NTA-DAP-DOD (Figure **3-1**). Liposome formulations containing NTA-lipids robustly associated both yCD and mKate without decreasing protein activity but association with the NTA liposomes did not increase the protein's circulation time.

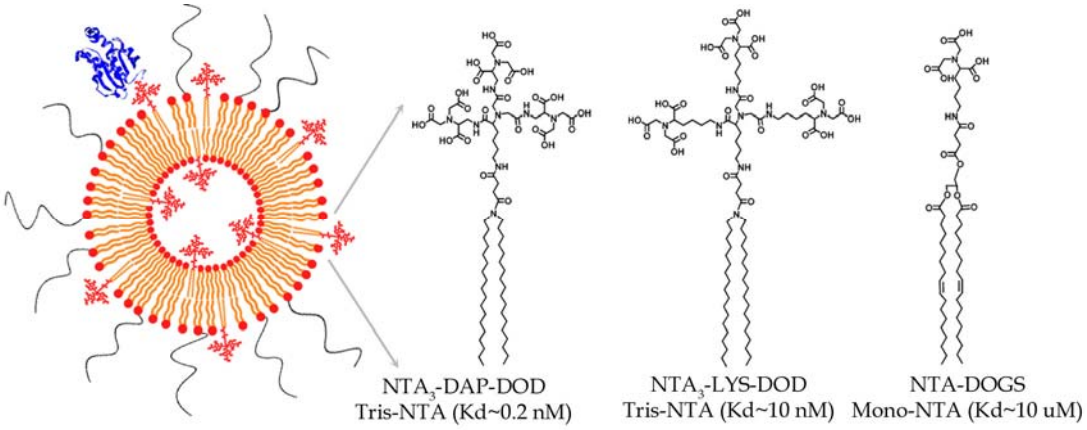


Figure 3-1. Illustration of Nitrilotriacetic Acid (NTA)-Containing PEGylated Liposomes with an Associated His-Tagged Protein. Reported equilibrium dissociation constants are given for a his_6 peptide ligand *(5, 17)*.

3.3 Experimental Procedures

3.3.1 Materials

All reagents and solvents obtained from commercial suppliers were used without further purification. Palmitoyloleoylphosphatidyl choline (POPC), palmitoyloleoylphosphatidyl glycerol (POPG), Methoxy polyethyleneglycol 2000 disteroylphosphatidyl ethanolamine (mPEG (2000)-DSPE) and cholesterol were obtained from Avanti Polar Lipids (Alabaster, AL). Ni-NTA-DOGS (1,2-dioleoyl-sn-glycero-3-{(N-(5-amino-1-carboxypentyl)iminodiacetic acid)succinyl}) was purchased from Avanti Polar Lipids preloaded with nickel. Refiltered fetal calf serum (FCS) was obtained from the UCSF Cell Culture Facility and was prepared by filter-purifying serum, not heat inactivation, thus retaining active portions of the complement cascade.

3.3.2 Synthesis of tris-NTA-LYS-DOD and tris-NTA-DAP-DOD

The tris-NTA-lipids, were synthesized via the methods described by Huang *et al* (*4, 5*). Tris-NTA-lipids contained a base of diaminopropionic acid (DAP) or lysine (LYS) for tris-NTA-DAP-DOD and tris-NTA-LYS-DOD, respectively (Figure **3-1**). Lipids were stored dry and dissolved in organic solvents immediately prior to use. To load the NTA_3 head groups with nickel, $NiCl_2$ was dissolved in minimal H_2O followed by methanol. NTA_3-lipids were incubated with nickel in the methanol-water solution (3 molar equivalents $NiCl_2$ per mol NTA_3) at 60 ºC for 15 min. The solution was allowed to cool to room temperature before adding it to the lipid formulation mixture. Preloading the nickel prior to liposome formation prevented dilution during removal of the excess nickel. Ni-NTA-DOGS was used as received from Avanti Polar Lipids.

3.3.3 Synthesis of FITC-DSPE

The fluorescent lipid was synthesized by Kareen Riviere via direct coupling of FITC to DSPE. To a solution of DSPE (50 mg) in dry chloroform (5 mL) and triethylamine (37.3 µL) was added FITC (52.1 mg, 2 equiv.) in minimal dimethyl sulfoxide (DSMO). The mixture reacted overnight at room temperature in the dark. Crude product solution was concentrated by rotary evaporation and purified on a Biotage Horizon HPFC system with pre-packed silica columns (Charlottesville, VA). The elution gradient consisted of 3 segments (solvent A:chloroform, B: methanol); 0%-20% B, 24 mL; 20%-20% B, 48 mL; 20%-30% B, 72 mL. Fractions of pure product were pooled, evaporated and dried under high vacuum overnight. Rf = 0.38 in chloroform:methanol (4:1 v/v). The product was dissolved and stored in chloroform at -40 ºC. During synthesis, handling

and use, FITC-DSPE was protected from photo-bleaching by minimizing exposure to light and heat. Structure of the product was confirmed with ^{1}H NMR and MALDI mass spectrometry.

3.3.4 Formation of Liposomes

Liposomes were prepared by the sonication and extrusion method (*28*). Briefly, lipids dissolved in organic solvents were added to depyrogenated borosilicate glass tubes. Solvent was evaporated while rotating under reduced pressure at room temperature to form a lipid film. Residual solvent was removed under high vacuum overnight. Films were then rehydrated in 1 mL HEPES buffer (20 mM HEPES, 140 mM NaCl, pH 7.4) with intermittent vortexing and sonicated under argon for 10 minutes at 23 ºC to form vesicles. Liposome diameter was reduced by serially extruding 11 times through 200 nm, 100 nm and 80 nm polycarbonate membranes with a hand-held extruder (Avestin; Ontario, Canada). Formulations contained either NTA_3-LYS-DOD, NTA_3-DAP-DOD, or NTA-DOGS (POPC/Chol/mPEG/NTA 55:40:5:n, molar ratio, where n corresponds to the mole percent NTA for each formulation). All liposomes contained 5 mol % mPEG(2000), unless noted. Control liposomes contained 1.5 mol % POPG to mimic the charge density of a 0.3% NTA_3-containing liposome formulation.

In some experiments, a tris-NTA-containing formulation without nickel was also used as a negative control. Liposome diameter and zeta potential were measured using a Zetasizer 3000 (Malvern Instruments; UK) for 3 or more liposome preparations of each formulation. The fluorescent signal from FITC-DSPE lipid, incorporated into the

formulation to allow for tracking of the liposome (at 0.05 mol % unless noted), was not significantly decreased once liposomes formed. Lipid concentration in solution was calculated from the FITC signal based on control liposomes containing the same NTA concentration. Inclusion of NTA lipids caused both a slight fluorescence decrease and a negative charge.

3.3.5 Protein Production

Genes for thermostabilized yeast cytosine deaminase (yCD; 18 kDa) (*29*) and monomeric Katushka (mKate; 27 kDa) (*30*) were constructed from gene fragments. Briefly, an optimized gene sequence for E. coli K12 (high) codon bias was designed and 27 or 32 primers (for yCD and mKate respectively) were used to construct a complete gene sequence using PCR. PCR was performed with GoTaq DNA polymerase (Promega; Madison, WI) in a GeneAmp PCR System 2400 thermal cycler (Perkin Elmer; Waltham, MA). Synthesized genes were then ligated into pET15b vector for amplification and expression.

Protein was expressed in BL21-Codon Plus (DE3)-RIPL E.coli cells (Stratagene; La Jolla, CA). E. coli were grown in LB culture medium containing 30 μg/mL kanamycin and 50 μg/mL chloramphenicol at 37 ºC until the OD600 nm reached 0.6-0.9. Protein expression was induced with 1 mM isopropyl α-D-1- thiogalactopyranoside (IPTG) with 0.5 mM zinc acetate. After overnight expression at room temperature, protein was purified from the cell supernatant by lysing the cells using freeze thaw followed by sonication. His-tagged proteins were purified from other cellular proteins on a

HisTrapFF affinity column (Amersham Biosciences; Piscataway, NJ) and eluted with 300 mM imidazole. The remaining yCD protein contaminants were removed by size exclusion chromatography on a HiPrep Sepharose S-100HR 16/60 size exclusion column (Amersham Biosciences; Piscataway, NJ). Buffers were exchanged using a PD10 desalting column (GE Healthcare; UK). OD280 nm was measured to obtain the fractions containing protein.

3.3.6 Liposome-Protein Association

His-tagged proteins were associated with liposomes at room temperature. Liposomes (2 μmol total lipid) were incubated with 270 μg mKate-his_6 or 180 μg yCD-his_6 in 0.2 mL HEPES buffer. For a 1% NTA containing formulation, this solution corresponds to a 1:1 molar ratio of surface NTA to his_6. To quantitate the extent of protein-liposome association, samples containing at least 2 μmol total lipid were passed through a pre-equilibrated 1 x 20 cm Sepharose CL-4B column under gravity flow. Fractions collected every 20 seconds (0.5 mL) were assayed for the presence of protein and liposomes. Liposomes eluted in the void volume and were measured by fluorescence (excitation/emission 490/520 nm). Protein concentration was quantified with a Bradford Protein Assay (Biorad Laboratories; Hercules, CA). This experiment was performed in triplicate for each protein/liposome formulation to ensure reproducibility.

3.3.7 Protein Activity

mKate activity was measured by fluorescence (excitation/emission 544/590 nm) in a Fluorostar 403 microplate reader (BMG Lab Technologies; Durham, NC). Enzymatic

conversion of 5-FC to 5-FU per μg of yCD was measured using previously described methods (*31*). Briefly, 1 μg yCD or yCD on liposomes was incubated in 1 mL PBS containing 5 mM 5-FC at 37 ºC. Aliquots of the reaction mixture (20 μL) were removed at 10, 20 and 30 minutes and enzymatic conversion quenched by dilution to 1 mL in 0.1 N HCl in PBS. The amount of 5-FU formed in the reaction was determined by measuring the UV absorbance at 255 and 290 nm. Concentration (mM) of 5-FU was calculated as 0.185 * (Abs 255) - 0.049 * (Abs 290) to adjust for presence of unconverted 5-FC. The activity of each sample was measured in triplicate.

Amount of enzyme activity per unit of lipid was measured after free protein was removed to ensure all active protein was associated with the surface of the liposome. Liposome concentration was estimated based on presence of a FITC-DSPE fluorophore within the membrane.

3.3.8 Protein Dissociation in Fetal Calf Serum

The dissociation of protein from liposomes was measured by challenging already associated protein with refiltered fetal calf serum (FCS). Liposomes with associated protein were mixed 1:1 in refiltered FCS and incubated at 37 ºC for a predetermined time. After incubation, samples were passed through a 1 x 20 cm Sepharose CL-4B column under gravity flow to separate free from bound protein. Liposome-containing fractions were collected and yCD concentrations were measured based on conversion activity. mKate activity was measured by fluorescence. The experiment, including liposome formulation, was performed in triplicate.

3.3.9 His-Tagged Protein Competition

Liposomes were prepared as described above and incubated to give 1:1 surface NTA to mKate ratio. After 1 hour, surface association was challenged with yCD. Proteins were allowed to equilibrate for an additional hour at room temperature and then passed over a Sepharose CL-4B column. Total protein was measured using the Bradford protein assay. Fluorescence of mKate and liposomes were monitored as described above. The competition assay was performed in triplicate for each formulation.

3.3.10 Protein Half-Life *in vivo*

Liposomes were prepared at 20 mM lipid by hydrating films in sterile PBS, as described above. Once liposome diameter was reduced to approximately 80 nm, liposomes were sterilized with 0.2 micron filters. Each protein was iodinated following the Iodogen iodination protocol (Pierce Biotechnology, Rockford IL). Briefly, an iodination tube was washed with 1 mL PBS. To the tube was added 0.1 mL 0.2M HEPES, pH 7.4 and 10 μL NaI^{125} (≈ 1 mCi). Approximately 0.5 mg protein was added to the tube and the solution was reacted at room temperature for 10 minutes. The reaction mixture was diluted with non-radioactive protein and serially purified on a pre-packed PD10 desalting column followed by a 1 x 15 cm Sephadex G-50 column. Fractions containing radioactive protein were collected and reaction efficiency calculated. The protein was then further diluted to give one million counts per dose of protein. Diluted, iodinated protein was mixed with liposomes to give one protein per surface available NTA and incubated for 1 hour at room temperature prior to injection.

All animal procedures were conducted in accordance with the policies of the UCSF Institutional Animal Care and Use Committee. Mice (Jackson Laboratories; Bar Harbor, ME) were housed in an official UCSF facility. For periods of less than 48 hours, during experimentation, mice were housed in UCSF approved laboratory conditions. BALB/c or Swiss-Webster mice (6-8 weeks old) were divided into treatment groups of 3 animals. Each group received 10 mM total lipid with 1.35 mg/mL iodinated mKate or 0.89 mg/mL iodinate yCD in 200 μL PBS via tail vein injection (one million I^{125} counts per dose; injection accounts for approximately a 15% increase in total blood volume).

Radioactivity in the blood obtained from submandibular cheek pouch bleeds at 5 minutes and 1 hour (50 μL; less than 5% total blood volume) with a final bleed at 6 hours (0.5 to 1 mL; 30 to 60% total blood volume) was quantified by gamma scintillation counting (Wallac Wizard, Perkin Elmer; Waltham, MA). Liver, lung and spleen were collected and analyzed for accumulation of radioactivity.

Non-iodinated mKate and liposomes containing 0.5% FITC-DSPE were monitored in the blood by heart puncture at 15 minutes. Serum was collected by centrifugation at 14,000 g and liposomes were separated from the bulk free protein with a Sepharose CL-4B column. mKate fluorescence was measured (excitation/emission 544/590 nm) to quantify mKate remaining with the liposomes.

3.4 Results

3.4.1 Liposome Formulation and Construction

An illustration of a liposome and the NTA lipids used in this study is shown in Figure **3-1**. The reported equilibrium dissociation constants for each lipid with a multihistidine peptide are also given (*4, 17*). Liposome diameter and stability was largely unaffected by the presence of NTA lipids (up to 3 mol %). We estimated, using the protein diameter (UCSF Chimera; San Francisco, California) and NTA-lipid surface density on the liposome (*32*), that steric hindrance between adjacent NTA binding sites should effect association around 3% NTA with a 1:1 surface NTA to protein loading ratio. The liposome diameter and charge as measured by the zeta potential were similar for all formulations (Table **3-1**).

	3 % NTA, 5% mPEG	1% NTA, 5% mPEG	1% NTA, 0% mPEG	0.3% NTA, 5% mPEG
		tris-NTA-DAP		
Diameter (nm)	88.0 ± 6.4	82.1 ± 2.5	88.3 ± 6.6	95.2 ± 15.1
ζ potential (mV)	-21.0	-18.3 ± 2.7	-18.6 ± 1.3	-19.3
		tris-NTA-LYS		
Diameter (nm)	107.9 ± 3.8	96.0 ± 11.5	96.6 ± 12.1	82.9 ± 7.6
ζ potential (mV)	-22.8	-18.6 ± 0.2	-20.1	-15.3
		NTA-DOGS		
Diameter (nm)	78.7 ± 14.7	75.4 ± 12.3	85.0 ± 7.8	71.5 ± 1.0
ζ potential (mV)	-18.9	-16.9 ± 0.6	-16.1	-12.6
		Control (1.5% POPG, 5% mPEG)		
Diameter (nm)		80.5 ± 6.5		
ζ potential (mV)		-15.6 ± 1.6		

Table 3-1. Liposome Diameter and Zeta-Potential of NTA-Containing Liposomes with 3, 1 or 0.3% NTA and 5 mol % mPEG or 1% NTA without mPEG. Control liposomes contained 1.5 mol % POPG to mimic the charge of 0.3% NTA-containing liposomes. (n=3)

3.4.2 His-Tagged Protein Association with Surface Displayed NTA on Liposomes

Liposomes containing any of the three NTA-lipids associated with protein to near the maximal expected amount. Free protein was separated from liposome bound protein to determine the extent of association. Liposomes, along with their associated protein, elute in the void volume of a Sepharose CL-4B size exclusion column, non-associated protein elutes at a larger volume. A representative example of protein separation in each fraction is shown in Figure **3-2**. Liposomes with 3, 1 or 0.3% NTA_3-DAP associated with yCD to near saturation, with no free yCD visible in later fractions. BSA did not associate with 1% NTA_3-DAP liposomes.

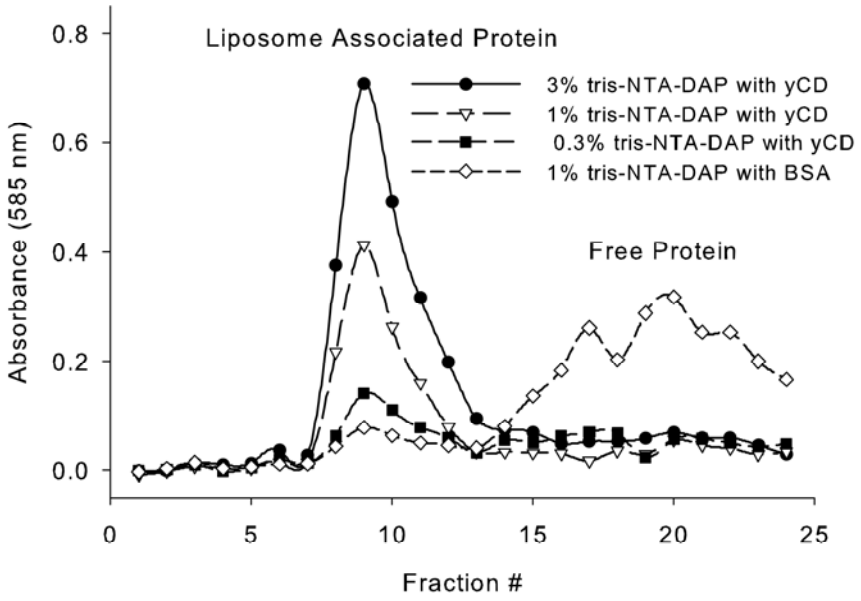


Figure 3-2. Representative Association of Proteins with the Surface of NTA-Liposomes. Liposomes bearing tris-NTA-DAP at 3% (circles), 1% (triangles) or 0.3% (squares) were associated with his-tagged yCD to saturate the available surface NTA. BSA was associated with 1% tris-NTA-DAP liposomes as a control (diamonds).

The concentration of liposomes in each fraction was calculated based on FITC-DSPE fluorescence. It was assumed that NTA lipids would distribute evenly between the inner and outer liposome surface. Hence, complete association was deemed to be a 1:1 ratio of his-tagged protein to expected surface available NTA (Table **3-2**).

Liposomes that contained NTA but not nickel did not associate with protein. BSA, which does not contain a his-tag, did not associate with NTA-nickel-containing liposomes. Control liposomes, containing both mPEG and POPG and having a similar surface charge as 0.3% NTA liposomes, associated with a minor amount of protein. The addition of EDTA, a strong chelator for nickel, to any NTA-containing liposome eliminated protein binding. Thus a chelated nickel on the liposome surface and a his-tagged protein are necessary for this technology to be effective. When those elements are present, the amount of bound protein is stoichiometric with the amount of Ni-NTA on the liposome surface. yCD is a dimer so it might be expected that greater than 100% association would occur but this was rarely seen. This indicates that both his-tags of the dimer are engaged to the NTAs on the liposome surface. The amounts of mKate associated with 3, 1 and 0.3 mol % NTA containing liposomes are given in Figure **3-3**.

mol % NTA with 5% mPEG		tris-NTA-DAP		tris-NTA-LYS		NTA-DOGS	
(NTA:protein) ratio		mg/µmol lipid	% of expected	mg/µmol lipid	% of expected	mg/µmol lipid	% of expected
3.0% (1:1)		0.28 ± 0.02	103 ± 7	0.28 ± 0.03	102 ± 12	0.27 ± 0.05	99 ± 16.8
3.0% (3:1)		0.09 ± 0.02	91 ± 16	0.10 ± 0.01	105 ± 9	0.09 ± 0.01	94 ± 7.3
1.0% (1:1)		0.10 ± 0.02	103 ± 16	0.12 ± 0.01	128 ± 11	0.10 ± 0.01	108 ± 12.2
0.3% (1:1)		0.04 ± 0.01	108 ± 15	0.04 ± 0.00	131 ± 1	0.03 ± 0.00	94 ± 12.9
0.3% (1:3)		0.03 ± 0.01	118 ± 21	0.04 ± 0.00	118 ± 3	0.06 ± 0.01	189 ± 16.4
1.0% (1:1)	No mPEG[a]	0.09 ± 0.01	104 ± 14	0.11 ± 0.01	119 ± 6	0.10 ± 0.02	104.2 ± 23.8
1.0% (1:1)	BSA[b]	0.01 ± 0.00	11 ± 3	0.01 ± 0.00	12 ± 4	0.01 ± 0.00	8.6 ± 1.0
1.0% (1:1)	No nickel[c]	0.02 ± 0.01	20 ± 6	0.02 ± 0.00	23 ± 2		
1.5 % POPG	No NTA[d]	0.01 ± 0.00	13 ± 3				

Table 3-2. Measurement of yCD Association with NTA-Containing Liposomes using the Bradford protein assay after unbound protein removal. Two variables are indicated. Percent NTA present in the liposome formulation is indicated by mol % NTA. Protein added to formed liposomes is indicated as a ratio (NTA:protein).

Control liposomes of various formulations were used to validate NTA-nickel-his-tag interactions.

[a] Liposomes formulated without a 5% mPEG coat associated similar amounts of yCD as those containing mPEG.

[b] BSA, a control protein that does not contain a his-tag, had limited association with liposomes containing NTA-nickel.

[c] Liposomes formulated with NTA, but without nickel, associated less yCD than those with nickel.

[d] Liposomes containing POPG, to mimic the charge of NTA-containing liposomes, had minimal yCD association.

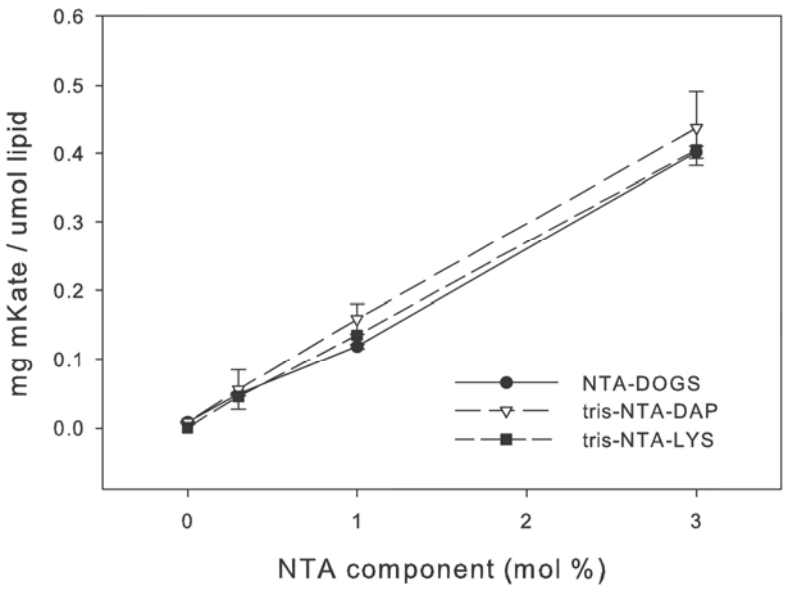


Figure 3-3. **Association of mKate with the Surface of NTA-Liposomes.** The amount of protein per µmol liposomes containing 3, 1 and 0.3 mol % NTA-DOGS (circles), tris-NTA-DAP (triangles) or tris-NTA-LYS (squares). (n=3)

3.4.3 Activity Retention of Surface Associated Proteins

Covalent attachment methods often partially or fully inactivate proteins (*24*). We measured the retention of activity of both yCD and mKate after binding to the NTA liposome. yCD converts the prodrug 5-FC to the cytotoxic drug 5-FU and the association of yCD with the surface of liposomes does not hinder 5-FC prodrug conversion. yCD retains full enzymatic activity when on the surface of a liposome (Figure **3-4A**). Some proteins exhibit increased function and experience less product inhibition (to which yCD is susceptible) when in close proximity to a lipid bilayer (*21*); a slight increase in activity is observed in the liposome bound yCD.

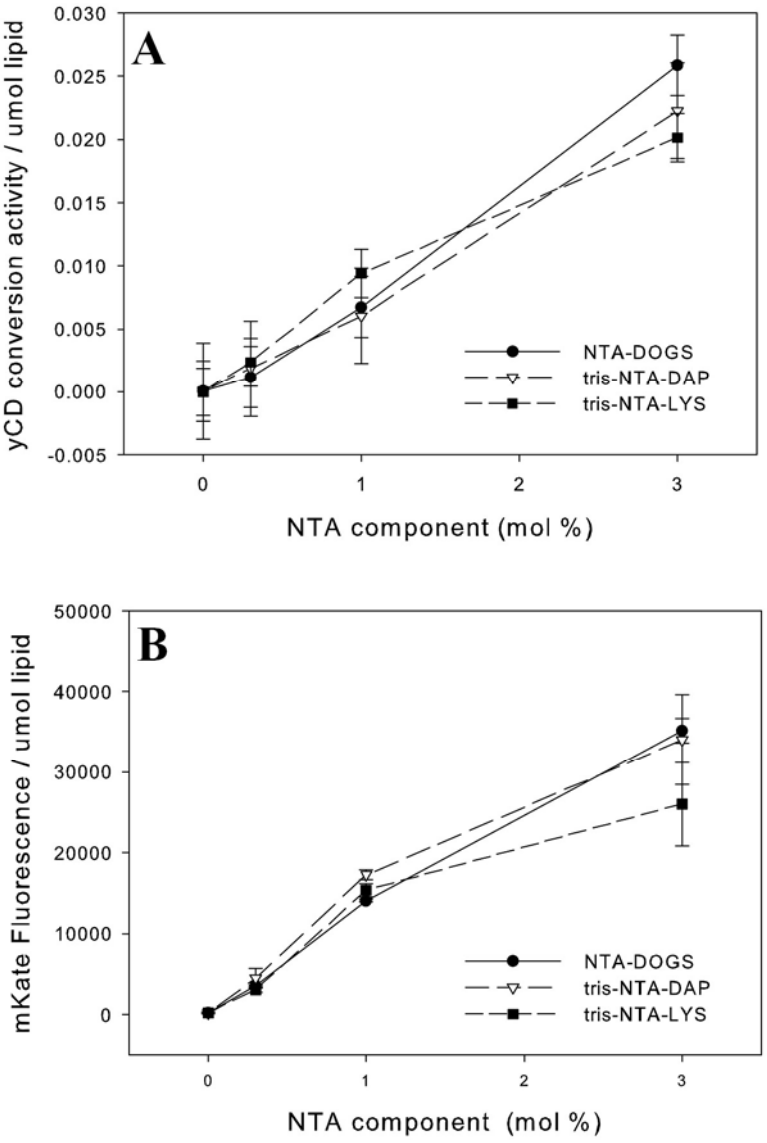


Figure 3-4. Retained Protein Activity of yCD (A) or mKate (B) on the Surface of NTA-Liposomes. The protein activity per μmol liposomes containing 3, 1 and 0.3 mol % NTA-DOGS (circles), tris-NTA-DAP (triangles) or tris-NTA-LYS (squares). (n=3)

mKate also completely occupied all of the available sites on NTA-bearing liposomes at the NTA surface densities studied (Figure **3-4B**). The activity of these liposomes was based on the fluorescence of the mKate. Unlike the observed increase in yCD activity when associated with the NTA-liposome there was no increase in fluorescence for mKate.

3.4.4 Protein Dissociation in the Presence of Refiltered FCS

Liposomes bearing NTA pre-associated with mKate or yCD were mixed at a 1:1 volume ratio with refiltered FCS. Figure **3-5** shows the retained protein on the surface of 1% NTA, 5% mPEG liposomes. The estimated amount of protein retained by the liposome is based on active protein and thermostabilized yCD has an activity half-life of over 50 hours (*29*). The decrease in fluorescent activity of mKate over 24 hours in FCS corresponds to approximately 5 – 10% of the total mKate fluorescence. This fluorescence decrease is equivalent to that seen in the loss of total fluorescence from free mKate in FCS at 37ºC over the same time period.

NTA_3-DAP has a higher affinity for histidine-tags than does NTA_3-LYS (*5*). Tris-NTAs in turn have significantly higher affinity (0.2-10 nM) than mono-NTA (10 μM) (*17*). For both yCD and mKate, retention in refiltered FCS is related but not directly proportional to the relative affinity for the NTA lipids.

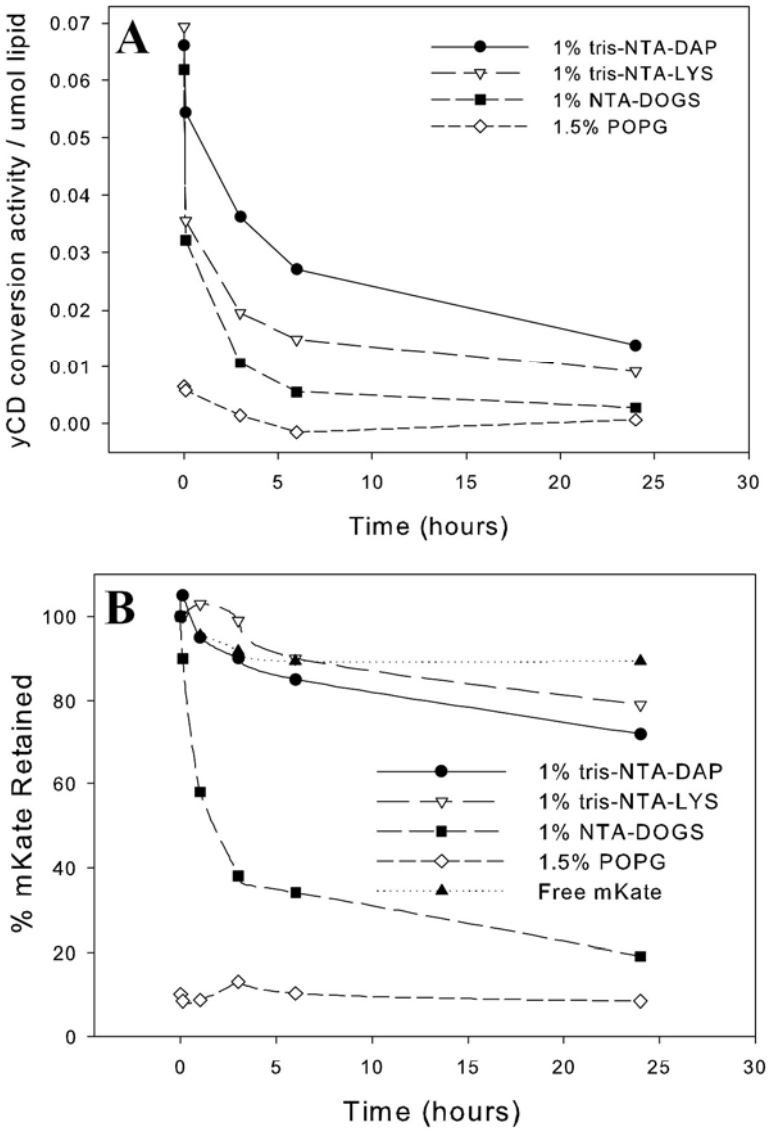


Figure 3-5. Dissociation of yCD (A) or mKate (B) from NTA-Liposomes in Refiltered FCS. Enzyme activity per unit of liposome (for yCD) or percent retained mKate fluorescence after unbound protein has been removed for each of four liposome types: 1% tris-NTA-DAP (circles), 1% tris-NTA-LYS (triangles), 1% NTA-DOGS (filled squares) and control liposomes containing 1.5% POPG (diamonds). (yCD, n=1; mKate, n=3)

3.4.5 Competition between NTA-Liposome Bound His_6-Proteins and Subsequently Added His_6-Proteins.

mKate that was stably associated with the liposome surface was challenged with added his_6-yCD. Despite the slightly higher affinity of tris-NTA-lipids for mKate (K_d=0.69 nM) than for yCD (K_d=3.02 nM) (*5*), yCD exchanged with pre-associated mKate for positions on the liposome surface (Figure **3-6**). Upon addition of a competing protein, proteins redistributed to yield the stoichiometric distribution of proteins on the surface of the liposome regardless of their reported affinity. For example, if yCD and mKate are at the same final concentration in solution, there will be an equal amount of yCD and mKate on the surface of the liposome and in solution. This arrangement will occur regardless of which protein is first incubated with the liposomes. When pre-bound mKate was challenged with BSA, which lacked a his-tag, no mKate dissociated; however, BSA non- specifically associated with the liposome so that the total amount of liposome-bound protein increased.

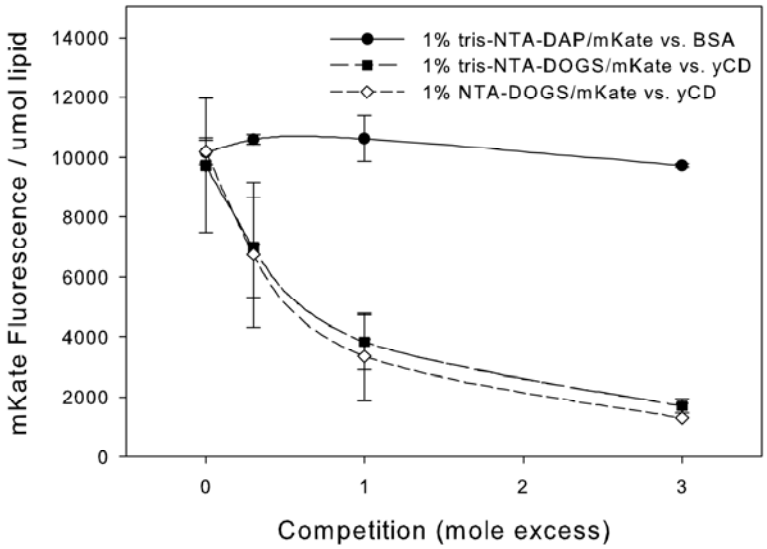


Figure 3-6. Competition of Proteins with Pre-Associated mKate. Competition of BSA for pre-associated mKate on 1% tris-NTA-DAP (circles) or yCD for pre-associated mKate on 1% tris-NTA-DAP (squares) and 1% NTA-DOGS (diamonds). (n=3)

3.4.6 Serum Half-Life of NTA-Liposome Associated Proteins Upon Intravenous Administration

The association of iodinated protein with NTA-liposomes did not increase the residence time of either protein in the blood after intravenous injection (Figure **3-7**). To ensure that iodination was not responsible for protein loss from the liposome, non-iodinated mKate was associated with fluorescent tris-DAP-NTA-liposomes and injected into mice. After 15 minutes, blood was collected and the mKate-NTA liposomes remaining in serum were separated on a Sepharose CL-4B column. A majority of the liposomes remained in circulation but only a small fraction of the injected mKate was associated with the liposome fractions from the column (Figure **3-7B**, inset). This verified that the mKate rapidly dissociated from the liposome upon contact with blood.

3.5 Discussion

We characterized the effect of increasing affinity in a series of Ni-NTA/his_6 pairs, on his_6-protein-NTA liposome association, his_6-protein activity and his_6-protein retention on NTA-liposomes under a variety of conditions. The surprising finding is that despite the retention of the his_6-protein on the NTA liposome in FCS, the NTA-liposome-attached protein rapidly dissociated from the liposome upon intravenous administration and hence was eliminated from circulation as rapidly as the injected 'free' protein. The rapid elimination occurred regardless if the liposome contained a low affinity NTA lipid or a high affinity NTA lipid and was not consistent with the measured off-rates of the same protein on a NTA Biacore chip.

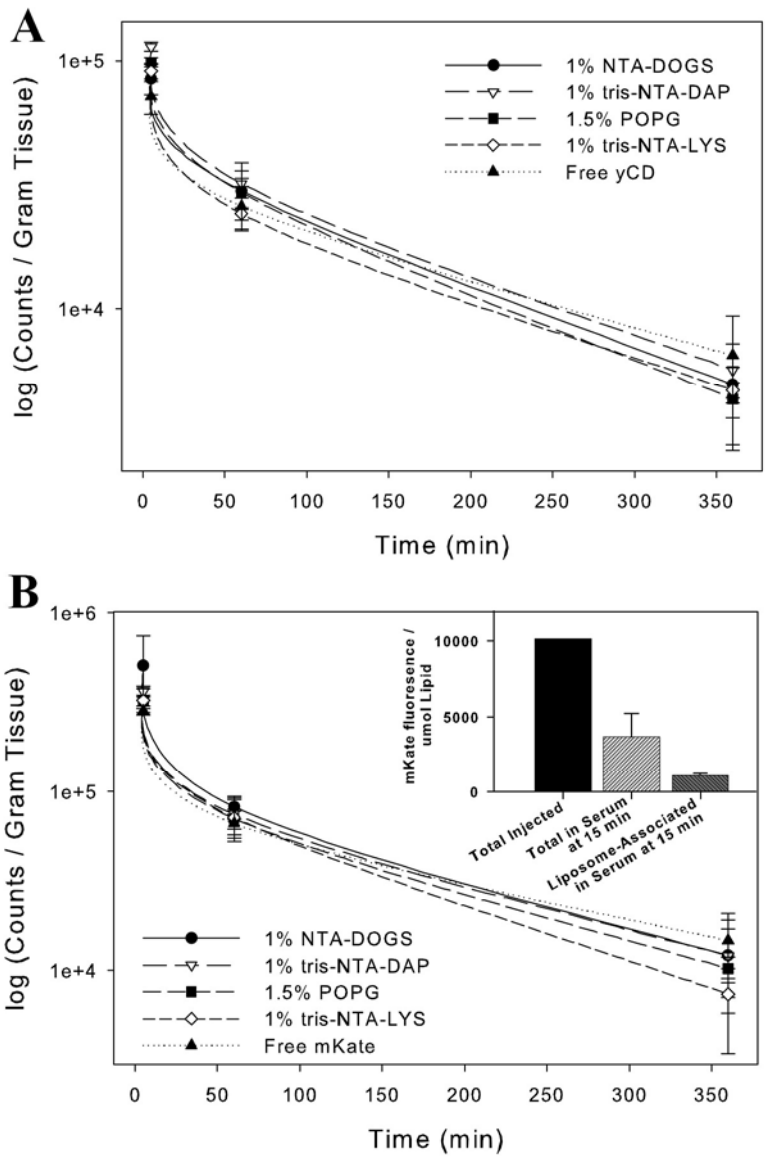


Figure 3-7. Half-Life of Iodinated yCD (A) or mKate (B) *in vivo* (filled triangles) on four liposome types: 1% tris-NTA-DAP (open triangles), 1% tris-NTA-LYS (diamonds), 1% NTA-DOGS (circles) or control liposomes containing 1.5% POPG (squares). Each animal was injected with one million I^{125} counts per dose. Non-iodinated mKate (**B**-inset) fluorescence remaining bound 15 minutes after injection on 1% tris-NTA-DAP liposomes. (n=3)

Our experiments were enabled by the synthesis of a series of tris-NTA chelators with increasing affinity for the his_6-tag (*5*). We synthesized tris-NTA-lipids with two different carbon lengths between each NTA headgroup to examine the effect of linker spacing on binding affinity. yCD and mKate retained activity when associated with the surface of NTA-containing liposomes, so the interaction holds forth the prospect of a modular system for easily constructing liposomes modified with any protein that has a his_6-tag.

Retention time for the his_6-proteins on the surface of a Biacore chip modified with the various NTA derivatives increased as NTA linker length decreased. Dissociation rates for the same NTA derivative also varied between his_6-proteins; this was ascribed to differences in the accessibility of the his-tag (*5*). Assuming that the protein is rapidly eliminated when released from the liposome, the blood residence time of a his_6-protein attached to an NTA-liposome after intravenous administration can be calculated from the dissociation rate. For the tris-NTA-LYS headgroup, with four carbons in the linker region, the half-time of release from the surface of a Biacore chip was 14 minutes with yCD (k_d=0.83 * 10^{-3}/sec). If the linker is decreased by one carbon, the half-time was 20 minutes with yCD (k_d=0.59 * 10^{-3}/sec) and 50 minutes with mKate (k_d=0.22 * 10^{-3}/sec). When the linker region was decreased by another carbon, the computed half-time with mKate increased to over 2 hours (k_d=.089 * 10^{-3}/sec) (*5*).

Proteins associated with the higher affinity NTA-liposomes were retained on the liposome much better when exposed to FCS then when on the mono-NTA modified liposomes (Figure **3-5**). The magnitude of this increased association time is related to the

affinity of each NTA-protein pair (Figure **3-5**). At 24 hours, approximately 80% of the initially bound mKate remained associated with either the tris-NTA-LYS and tris-NTA-DAP liposomes, whereas only 20% mKate remained bound to liposomes containing NTA-DOGS. yCD dissociated to a greater extent from the surface of the liposome than did mKate which is consistent with the difference in affinity (K_d=0.69 and 3.02 nM) for mKate and yCD, respectively. However, as expected for a reversible interaction, his_6-proteins could exchange with proteins in solution even from the lipid with the highest affinity, the tris-NTA-DAP. This reflects the dynamic nature of this system (Figure **3-6**).

While tris-NTA-DAP increased retention of both proteins as compared to NTA-DOGS in FCS, it did not improve protein association *in vivo* (Figure **3-7**). All of the formulations studied exhibited a similar clearance rate as free protein. PEGylated liposomes of this diameter have a circulation half-life of half a day or more (*33*). If the disassociation rate was the prime determinant of protein loss from the liposome, tris-NTA association should have afforded some improvement in circulation time for the liposome bound protein over the free protein. The dynamic nature of non-covalent association with NTA may allow any multihistidine-containing protein in the body to actively compete with the associated protein, even if the affinity of the nascent, competing protein is much lower than that of the associated protein. However if loss of protein is a simple equilibrium phenomenon, the off-rate would still control the residence time of the protein on the liposome. Therefore there must be other factors that contribute to the rapid disassociation after intravenous injection.

For instance, plasma proteins may play a crucial role in the disruption of his_6-NTA association. Some plasma proteins may interact preferentially with the surface of NTA-liposomes (*26*) and may contribute to protein dissociation or loss of nickel from the chelator (Figure **3-8**). Endogenous bio-chelators may be an additional destabilizing factor by removing bound nickel from the NTA (*34*).

Several groups have published the robust association of his-tagged proteins with NTA containing nanolipoparticles (*3, 4, 25-27, 35*). Our findings must be reconciled with a number of papers where proteins associated with liposomes or lipid particles containing mono-NTA or tris-NTA mediate a number of immune response (*3, 25, 27*). Protein-NTA particles generated a measurable immune response based on specific serum IgG levels (*27*) or an increase in splenocytes secreting cytokines (*25*). Mice immunized with tris-NTA containing plasma membrane vesicles showed decreased tumor growth (*3*). In these studies the NTA particle was injected via the subcutaneous route. After subcutaneous administration the particles are exposed to an order of magnitude lower concentration of endogenous proteins and the NTA liposome and its attached protein are eliminated more slowly than after intravenous administration. Second, the immune response is exquisitely sensitive to a protein antigen and even small quantities of protein that remained associated with the particle might have been responsible for the observed effects. Thus it is not possible to deduce the amount of protein that these various particles delivered from the observed responses.

Our results indicate that improvements in metal chelation methodologies are required if this technology is to be useful for *in vivo* applications. Our lab is exploring methods to improve the affinity of the system and reduce loss of nickel chelation. It remains to be discovered whether such improvements will be sufficient to stabilize NTA-protein-his_6 complexes *in vivo*.

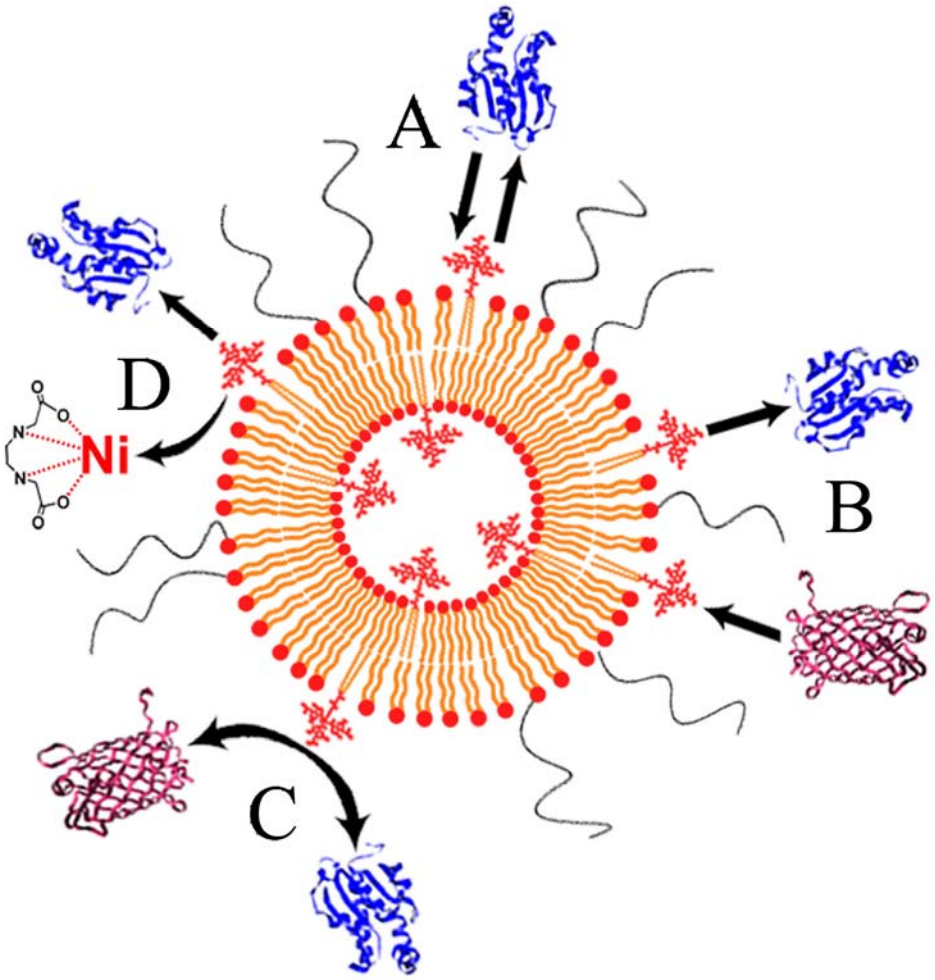


Figure 3-8. The Interaction of His-Tagged Proteins with NTA-Containing PEGylated Liposomes. Proteins bearing a his-tag associate and dissociate from the liposome surface (**A**). Upon dissociation, other proteins may associate with the newly available NTAs (**B**), proteins may directly compete for NTA binding (**C**) or nickel may be removed by endogenous chelators (**D**).

3.6 Acknowledgements and Author Contributions

We gratefully thank Katherine Jerger for her assistance with animal experiments. This work was supported by grant NIH R01 GM061851. Protein production and the salary of Dr. Cao were supported by UC discovery grant Bio 60-10618 and Halozyme, Inc.

Our appreciation is extended to Dr. Zhaohua Huang for design of the tris-NTA production scheme and synthesis of the original tris-NTA lipids and Dr. Kareen Riviere for synthesis of the FITC-DSPE. Their support and availability for discussion is acknowledged and greatly appreciated.

3.7 Literature Cited

(1) Sigal, G. B., Bamdad, C., Barberis, A., Strominger, J., and Whitesides, G. M. (1996) A self-assembled monolayer for the binding and study of histidine-tagged proteins by surface plasmon resonance. *Anal Chem 68*, 490-7.

(2) Ueda, E. K., Gout, P. W., and Morganti, L. (2003) Current and prospective applications of metal ion-protein binding. *J Chromatogr A 988*, 1-23.

(3) van Broekhoven, C. L., and Altin, J. G. (2005) The novel chelator lipid 3(nitrilotriacetic acid)-ditetradecylamine (NTA(3)-DTDA) promotes stable binding of His-tagged proteins to liposomal membranes: potent anti-tumor responses induced by simultaneously targeting antigen, cytokine and costimulatory signals to T cells. *Biochim Biophys Acta 1716*, 104-16.

(4) Huang, Z., Park, J. I., Watson, D. S., Hwang, P., and Szoka, F. C., Jr. (2006) Facile synthesis of multivalent nitrilotriacetic acid (NTA) and NTA conjugates for analytical and drug delivery applications. *Bioconjug Chem 17*, 1592-600.

(5) Huang, Z., Hwang, P., Watson, D. S., Cao, L., and Szoka, F. C. (2009) Tris-Nitrilotriacetic Acids of Subnanomolar Affinity Toward Hexahistidine Tagged Molecules. *Bioconjug Chem 20*, 1667-72.

(6) Balland, V., Hureau, C., Cusano, A. M., Liu, Y., Tron, T., and Limoges, B. (2008) Oriented immobilization of a fully active monolayer of histidine-tagged recombinant laccase on modified gold electrodes. *Chemistry 14*, 7186-92.

(7) Dietrich, C., Schmitt, L., and Tampe, R. (1995) Molecular organization of histidine-tagged biomolecules at self-assembled lipid interfaces using a novel class of chelator lipids. *Proc Natl Acad Sci U S A 92*, 9014-8.

(8) Dorn, I. T., Pawlitschko, K., Pettinger, S. C., and Tampe, R. (1998) Orientation and two-dimensional organization of proteins at chelator lipid interfaces. *Biol Chem 379*, 1151-9.

(9) Tinazli, A., Tang, J., Valiokas, R., Picuric, S., Lata, S., Piehler, J., Liedberg, B., and Tampe, R. (2005) High-affinity chelator thiols for switchable and oriented immobilization of histidine-tagged proteins: a generic platform for protein chip technologies. *Chemistry 11*, 5249-59.

(10) Schuy, S., Treutlein, B., Pietuch, A., and Janshoff, A. (2008) In situ synthesis of lipopeptides as versatile receptors for the specific binding of nanoparticles and liposomes to solid-supported membranes. *Small 4*, 970-81.

(11) Keller, T. A., Duschl, C., Kröger, D., Sévin-Landais, A.-F., Vogel, H., Cervigni, S. E., and Dumy, P. (1995) Reversible oriented immobilization of histidine-tagged proteins on gold surfaces using a chelator thioalkane. *Supramolecular Science 2*, 155-160.

(12) Barklis, E., McDermott, J., Wilkens, S., Schabtach, E., Schmid, M. F., Fuller, S., Karanjia, S., Love, Z., Jones, R., Rui, Y., Zhao, X., and Thompson, D. (1997) Structural analysis of membrane-bound retrovirus capsid proteins. *Embo J 16*, 1199-213.

(13) Dorn, I. T., Eschrich, R., Seemuller, E., Guckenberger, R., and Tampe, R. (1999) High-resolution AFM-imaging and mechanistic analysis of the 20 S proteasome. *J Mol Biol 288*, 1027-36.

(14) Zhen, G., Zurcher, S., Falconnet, D., Xu, F., Kuennemann, E., and Textor, M. (2005) NTA-Functionalized Poly(L-lysine)-g-Poly(Ethylene Glycol): A Polymeric Interface for Binding and Studying 6 His-tagged Proteins. *Conf Proc IEEE Eng Med Biol Soc 1*, 1036-1038.

(15) Kang, E., Park, J. W., McClellan, S. J., Kim, J. M., Holland, D. P., Lee, G. U., Franses, E. I., Park, K., and Thompson, D. H. (2007) Specific adsorption of histidine-tagged proteins on silica surfaces modified with Ni2+/NTA-derivatized poly(ethylene glycol). *Langmuir 23*, 6281-8.

(16) Guignet, E. G., Hovius, R., and Vogel, H. (2004) Reversible site-selective labeling of membrane proteins in live cells. *Nat Biotechnol 22*, 440-4.

(17) Lata, S., Reichel, A., Brock, R., Tampe, R., and Piehler, J. (2005) High-affinity adaptors for switchable recognition of histidine-tagged proteins. *J Am Chem Soc 127*, 10205-15.

(18) Lata, S., Gavutis, M., Tampe, R., and Piehler, J. (2006) Specific and stable fluorescence labeling of histidine-tagged proteins for dissecting multi-protein complex formation. *J Am Chem Soc 128*, 2365-72.

(19) Leader, B., Baca, Q. J., and Golan, D. E. (2008) Protein therapeutics: a summary and pharmacological classification. *Nat Rev Drug Discov 7*, 21-39.

(20) Werle, M., and Bernkop-Schnurch, A. (2006) Strategies to improve plasma half life time of peptide and protein drugs. *Amino Acids 30*, 351-67.

(21) Nagami, H., Yoshimoto, N., Umakoshi, H., Shimanouchi, T., and Kuboi, R. (2005) Liposome-assisted activity of superoxide dismutase under oxidative stress. *J Biosci Bioeng 99*, 423-8.

(22) Spira, J., Plyushch, O. P., Andreeva, T. A., and Andreev, Y. (2006) Prolonged bleeding-free period following prophylactic infusion of recombinant factor VIII reconstituted with pegylated liposomes. *Blood 108*, 3668-73.

(23) Yatuv, R., Dayan, I., Carmel-Goren, L., Robinson, M., Aviv, I., Goldenberg-Furmanov, M., and Baru, M. (2008) Enhancement of factor VIIa haemostatic efficacy by formulation with PEGylated liposomes. *Haemophilia 14*, 476-83.

(24) Colletier, J. P., Chaize, B., Winterhalter, M., and Fournier, D. (2002) Protein encapsulation in liposomes: efficiency depends on interactions between protein and phospholipid bilayer. *BMC Biotechnol 2*, 9.

(25) Chikh, G. G., Li, W. M., Schutze-Redelmeier, M. P., Meunier, J. C., and Bally, M. B. (2002) Attaching histidine-tagged peptides and proteins to lipid-based carriers through use of metal-ion-chelating lipids. *Biochim Biophys Acta 1567*, 204-12.

(26) Ruger, R., Muller, D., Fahr, A., and Kontermann, R. E. (2006) In vitro characterization of binding and stability of single-chain Fv Ni-NTA-liposomes. *J Drug Target 14*, 576-82.

(27) Patel, J. D., O'Carra, R., Jones, J., Woodward, J. G., and Mumper, R. J. (2007) Preparation and characterization of nickel nanoparticles for binding to his-tag proteins and antigens. *Pharm Res 24*, 343-52.

(28) Szoka, F., Olson, F., Heath, T., Vail, W., Mayhew, E., and Papahadjopoulos, D. (1980) Preparation of unilamellar liposomes of intermediate size (0.1-0.2 μmol) by a combination of reverse phase evaporation and extrusion through polycarbonate membranes. *Biochim Biophys Acta 601*, 559-71.

(29) Korkegian, A., Black, M. E., Baker, D., and Stoddard, B. L. (2005) Computational thermostabilization of an enzyme. *Science 308*, 857-60.

(30) Shcherbo, D., Merzlyak, E. M., Chepurnykh, T. V., Fradkov, A. F., Ermakova, G. V., Solovieva, E. A., Lukyanov, K. A., Bogdanova, E. A., Zaraisky, A. G., Lukyanov, S., and Chudakov, D. M. (2007) Bright far-red fluorescent protein for whole-body imaging. *Nat Methods 4*, 741-6.

(31) Senter, P. D., Su, P. C., Katsuragi, T., Sakai, T., Cosand, W. L., Hellstrom, I., and Hellstrom, K. E. (1991) Generation of 5-fluorouracil from 5-fluorocytosine by monoclonal antibody-cytosine deaminase conjugates. *Bioconjug Chem 2*, 447-51.

(32) Scherer, J. R. (1989) Dependence of lipid chain and head group packing of the inverted hexagonal phase on hydration. *Biophys J 55*, 965-971.

(33) Lasic, D. D., Martin, F. J., Gabizon, A., Huang, S. K., and Papahadjopoulos, D. (1991) Sterically stabilized liposomes: a hypothesis on the molecular origin of the extended circulation times. *Biochim Biophys Acta 1070*, 187-92.

(34) Bell, S. G., and Vallee, B. L. (2009) The metallothionein/thionein system: an oxidoreductive metabolic zinc link. *Chembiochem 10*, 55-62.

(35) Fischer, N. O., Blanchette, C. D., Chromy, B. A., Kuhn, E. A., Segelke, B. W., Corzett, M., Bench, G., Mason, P. W., and Hoeprich, P. D. (2009) Immobilization of his-tagged proteins on nickel-chelating nanolipoprotein particles. *Bioconjug Chem 20*, 460-5.

Chapter 4

Antibody Response in Mice to Polyhistidine-Tagged Peptide and Protein Antigens Attached to Liposomes via Lipid-Linked Nitrilotriacetic Acid

This work is coauthored by Dr. Douglas Watson.

4.1 Abstract

Particulate delivery systems enhance antibody responses to protein subunit antigens. However, covalent conjugation of protein antigens can alter the humoral immune response to their epitopes. In this report, we evaluate metal chelation via nitrilotriacetic acid (NTA) as a non-covalent method to attach proteins to liposomes. We determined the relationship between affinity of antigen-liposome interactions and the antibody response to model antigens in mice. Two model antigens, ovalbumin (OVA) and a peptide derived from the membrane proximal region of HIV-1 gp41 (N-MPR), were polyhistidinylated and attached to liposomes via monovalent NTA (mono-NTA, $K_D \sim 10$ μM), trivalent NTA (tris-NTA, $K_D \sim 1$ nM) or a covalent linkage. When BALB/c mice were immunized with N-MPR-his_6 attached to liposomes via an NTA linkage, anti-N-MPR IgG was detected in sera of 4 of 4 mice, whereas an unattached N-MPR-his_6 peptide admixed with liposomes lacking NTA failed to generate a response (0 of 4 mice). However, a tris-NTA linkage that has a greater affinity to the polyhistidine tag than mono-NTA did not increase the antibody response to either N-MPR or OVA as compared to the mono-NTA linkage. For both antigens, covalently attaching them to a lipid elicited significantly stronger antibody responses than NTA-anchored antigens (OVA: Titer $3.4 * 10^6$ vs. $1.4\text{-}1.6 * 10^6$, $p < 0.001$; N-MPR: Titer $4.4 * 10^4$ vs. $5.5\text{-}7.6 * 10^2$, $p < 0.003$). The data indicate that NTA linkages may be useful to increase antibody titers to

weak antigens (e.g. N-MPR) but may not increase titers for larger, more potent antigens (e.g. OVA) as compared to admixed formulations. Thus, additional improvements of NTA-mediated conjugation technology are necessary to achieve a universally effective, non-destructive method to increase the humoral response to antigens in particulate vaccines.

4.2 Introduction

Preventative vaccination is the most cost-effective approach to combating infectious disease. In recent years, recombinant vaccines have been developed as alternatives to traditional killed or inactivated preparations (*1*). Recombinant protein subunit vaccines are attractive because their composition can be precisely controlled and they offer superior safety profiles (*2*). Currently available vaccines against hepatitis B virus and human papillomavirus are two examples of successful protein subunit vaccines (*3, 4*). However, protein subunit preparations elicit weak antibody and T lymphocyte responses when administered without adjuvants (*5*).

Vaccine adjuvants that enhance humoral and cellular immunity to co-delivered antigens are divided into two functional categories: molecular immunopotentiators and particulate delivery systems (*6*). Molecular immunopotentiators, such as cytokines and toll-like receptor agonists, activate discrete signaling pathways to promote activation or function of immune cells. Particulates, including emulsions, gels, liposomes and microparticles, facilitate delivery to antigen presenting cells, provide prolonged antigen presentation through a "depot effect," and in some cases generate pro-inflammatory "danger" signals

(*1, 6, 7*). Achieving high potency generally requires that the subunit antigen be chemically or physically associated with the particulate (*1*). Precipitation or adsorption onto aluminum salts is the traditional approach and alum remains the only vaccine adjuvant approved for use in the United States (*8, 9*). Alternatively, proteins can be associated with lipidic or polymeric particulates via encapsulation or chemical conjugation (*10-13*). However, these strategies present significant challenges – for example, encapsulation techniques can result in protein denaturation through exposure to harsh emulsification processes or organic solvents (*14*). Covalent conjugation relies on chemical modification of the protein surface and can alter or destroy vital epitopes (*15, 16*). Adsorption to solid particles, such as poly(lactide-co-glycolide) (PLG) microparticles, represents an improvement over these methods but does not allow precise control of antigen orientation and display (*17, 18*).

Non-covalent chemical attachment methodologies have been proposed to address these issues. One promising approach to non-covalent antigen conjugation involves metal chelation, in which polyhistidine-tagged proteins are attached to nitrilotriacetic acid-containing liposomes and microparticles with micromolar affinity (*19-21*). Since NTA-Ni(II)-histidine binding is site-specific, the physical orientation of the antigen on the particulate surface can be controlled. This is of particular importance for delivery of membrane protein antigens such as HIV-1 gp41 and other viral envelope glycoproteins, where presentation of key neutralizing determinants in their native orientation within a membrane context is desired (*22*).

A recent study reported the use of lipid-anchored NTA for attachment of polyhistidine-tagged HIV-1 Gag p24 antigen to wax nanoparticles (*23*). These formulations elicited superior anti-p24 antibody and T lymphocyte responses as compared to p24 admixed with nanoparticles lacking Ni(II) or to p24 adsorbed onto alum. However, the NTA-conjugated preparation was not compared to a formulation in which the antigen was covalently attached to the nanoparticles. Additionally, concerns have been raised regarding the stability of the NTA-Ni(II)-histidine interaction in biological fluids (*24*).

Recently, we and others reported the synthesis of multivalent nitrilotriacetic acid adaptors with nanomolar affinities for polyhistidine-tagged proteins (K_D ~ 10 μM and ~1 nM for monovalent and trivalent NTA, respectively; Figure **4-1**) (*19, 25, 26*). Here, we hypothesized that the increased affinity of the antigen-particulate interaction would result in enhanced antibody responses as compared to a monovalent NTA linkage. We assessed the effect of the antigen-liposome linkage on antibody responses to two model antigens, a peptide derived from the membrane proximal region of HIV-1 gp41 (N-MPR) and a traditional strong antigen, ovalbumin (OVA). The data indicate that NTA linkages between antigens and liposomes are useful for increasing antibody titers to weak antigens (e.g. N-MPR) but further improvements are required to achieve titers achieved by covalent attachment of the antigen to a lipid anchor.

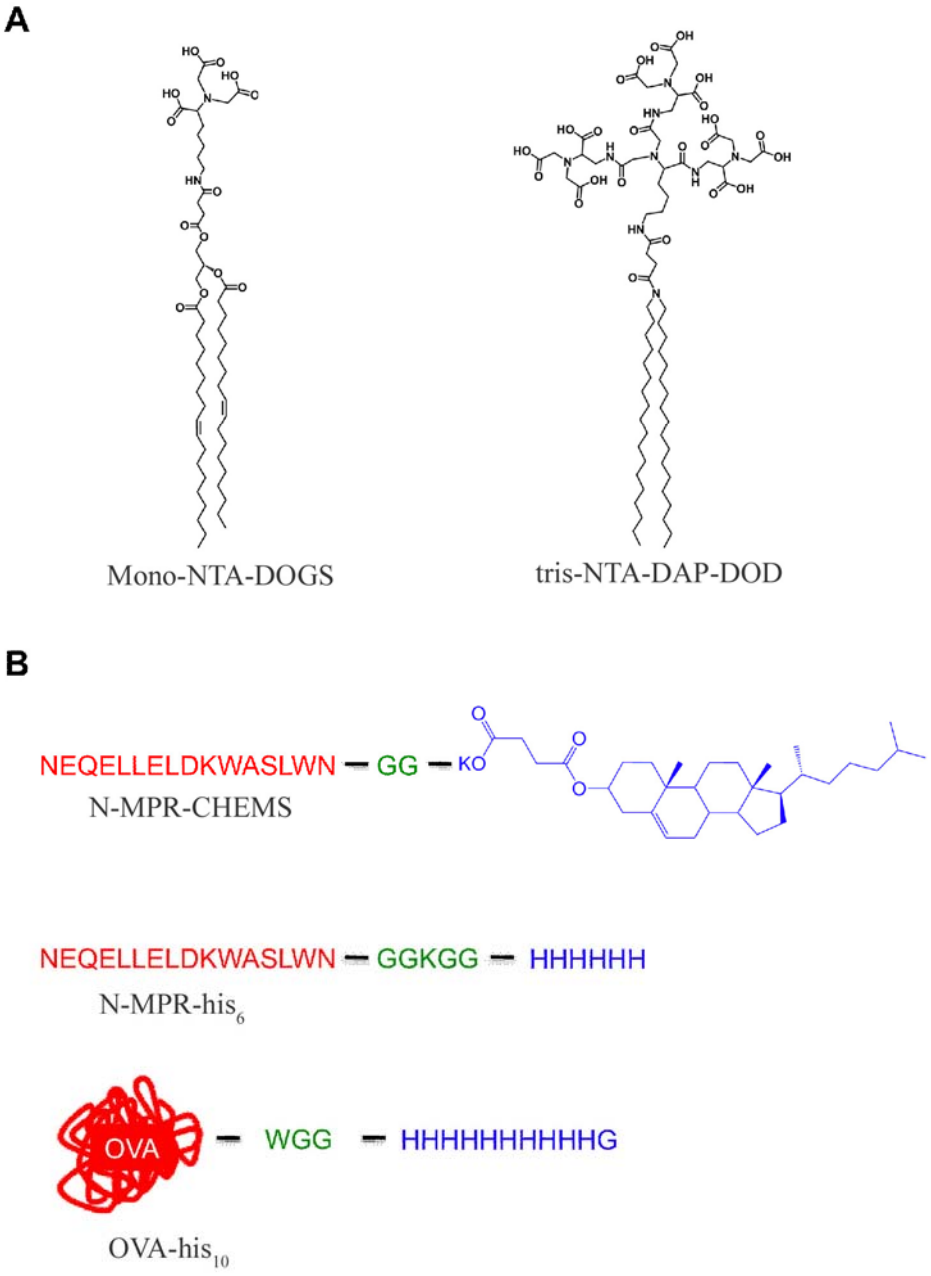


Figure 4-1. Structures of NTA-Lipids and Polyhistidine-Tagged Antigens. Mono-NTA-DOGS, tris-NTA-DAP, N-MPR-CHEMS, N-MPR-his_6, OVA-his_{10}

4.3 Experimental Procedures

4.3.1 Materials

Amino acid building blocks, resins and coupling agents were obtained from Novabiochem (Darmstadt, Germany), Anaspec (San Jose, CA) or ChemPep (Miami, FL). Cholesterol, dimyristoylphosphatidyl choline (DMPC), dimyristoylphosphatidyl glycerol (DMPG), 1,2-di- (9Z-octadecenoyl) -*sn*-glycero-3- {(N-(5-amino-1-carboxypentyl) iminodiacetic acid) succinyl} (nickel salt) (NTA-DOGS; mono-NTA) and 1,2-dioleoyl-*sn*-glycero-3-phosphoethanolamine-N-{4-(p-maleimidophenyl)butyramide} (MPB-PE) were obtained from Avanti Polar Lipids (Alabaster, AL). Cholesteryl hemisuccinate (CHEMS) and maleimidoproprionic acid (MPA) were obtained from Sigma-Aldrich. Anhydrous solvents of 99.8% or greater purity were obtained from Acros Organics (Geel, Belgium). Monophosphoryl lipid A derived from Escherichia coli (MPL; #L6638), aluminum hydroxide gel (Alum; #A8222) and ovalbumin (Grade V; #A5503) were obtained from Sigma-Aldrich. Endotoxin-free buffers were obtained from the UCSF Cell Culture Facility. Unless otherwise specified, all other reagents were obtained from Sigma-Aldrich.

4.3.2 Synthesis of Peptides and Lipids

Peptides were synthesized on Rink Amide MBHA or NovaPEG resin in an automated solid phase synthesizer (ABI 433A; Applied Biosystems, Foster City, CA) with standard fluorenylmethyloxycarbonyl/ o-benzotriazole -N,N,N',N' -tetramethyl- uronium-hexafluoro-phosphate/ n-hydroxybenzotriazole (FMOC/HBTU/HOBT) protocols. Peptides containing N-MPR were synthesized on NovaPEG resin with an orthogonally

protected lysine (Fmoc-Lys(1-(4,4-Dimethyl-2,6-dioxo-cyclohexylidene)-3-methyl-butyl)-OH; Fmoc-Lys(ivDde)-OH) incorporated at the C terminus for on-resin conjugation of lipid, polyhistidine or biotin. For N-MPR peptides, the N terminus was Boc-protected; for other peptides N terminal Fmoc protection was utilized. Removal of the orthogonal ivDde group was accomplished by 3 x 15 minute treatments of the peptidyl resin with 2% hydrazine hydrate in dimethylformamide (DMF; 10 mL per g resin). The resin was washed in DMF (3 x 10 mL) and dichloromethane (DCM; 3 x 10 mL) and dried under vacuum.

Attachment of CHEMS to N-MPR was accomplished via amidation of a carboxylated lipid and a deprotected lysyl ε amine at the C terminus as described (*27*). Essentially, CHEMS (270 μmol) was activated with 270 μmol each of HBTU, HOBT and diisopropylethylamine (DIEA) in anhydrous DMF/DCM (DCM as needed for lipid solubilization) for 30 minutes at room temperature followed by addition of 67.5 μmol resin and continued reaction under argon for 24 hours at room temperature. Following the reaction, the resin was washed with DMF (4 x 10 mL) and DCM (4 x 10 mL) to remove unreacted lipids and dried under vacuum. N-MPR-CHEMS were cleaved from the resin by treatment with trifluoroacetic acid containing 2.5% water, 2.5% ethanedithiol and 1% triisopropylsilane for 4 hours under argon. Cleaved peptides were precipitated into cold ethyl ether. The precipitate was pelleted by centrifugation at 3000 rpm (RT6000, Sorvall, Waltham, MA) and washed once with cold ethyl ether. The ether was poured off and the pellet was re-dissolved in methanol (MeOH), transferred to a round bottom flask, dried by rotary evaporation under reduced pressure and further dried under

high vacuum. The lipopeptide was further separated from unconjugated peptide by reverse phase high pressure liquid chromatography (RP-HPLC; DX 500, Dionex, Sunnyvale, CA) on a semi-preparative C4 column (214TP510; Grace Vydac, Deerfield, IL) until unconjugated peptide was no longer detectable by MALDI-MS. Lipopeptide fractions were identified by MALDI-MS in 2,5-dihydroxybenzoic acid matrix, pooled and lyophilized. Stock lipopeptide solutions were prepared in MEOH and stored under argon at -20 ^{o}C.

Biotinylated N-MPR was prepared for use in ELISA by an analogous method. Biotin was attached to the deprotected C terminal amine by activation of 500 μmol D-biotin with 500 μmol HBTU/HOBT/DIEA in 1.65 mL anhydrous 1:1 DMF/dimethylsulfoxide (DMSO) for 30 minutes followed by addition of resin and continued reaction under argon for 24 hours at room temperature. Following the reaction, the resin was washed with 1:1 DMF/DMSO (3 x 10 mL), DMF (3 x 10 mL) and DCM (3 x 10 mL) and dried under vacuum. Biotinylated peptides were cleaved and purified as described above. Biotin content was quantified by 4′-hydroxyazobenzene-2-carboxylic acid dye exclusion (Sigma #H2153) according to the manufacturer's instructions.

Synthesis of N-MPR-his$_6$ was accomplished by appending the C terminus of N-MPR with a hexahistidine tag. The orthogonally protected lysyl ε amine was deprotected and appended by automated solid phase synthesis with Fmoc protection as described above. The peptide was cleaved and purified as described, and a stock solution was prepared in sterile water and stored at -20 ^{o}C.

Maleimide functionalized decahistidine (his_{10}-maleimide) was prepared by on-resin modification of the deprotected peptidyl N terminus with maleimidoproprionic acid (MPA). MPA (290 μmol) was activated with 290 μmol HBTU, 290 μmol HOBT and 580 μmol DIEA in 3 mL anhydrous DMF for 30 minutes at room temperature under argon. Peptidyl resin (74 μmol) was added and shaken at room temperature under argon for 2.5 hours. The resin was washed with DMF (4x) and DCM (4x) and dried under high vacuum overnight. The modified peptide was cleaved and purified as described above, except the cleavage cocktail did not contain ethanedithiol. Molecular weights of all peptides were confirmed by MALDI-MS in dihydroxybenzoic acid matrix. Peptide concentration of stock solutions was confirmed by A280 of tryptophan residues with extinction coefficient calculated by the method of Pace (*28*). Nomenclature, sequences and molecular weights of peptides used in this study are summarized in Table **4-1**.

Dioctadecyl-tri(nitrilotriacetic acid) (tris-NTA-DOD; tris-NTA) was synthesized and characterized as described in detail elsewhere (*26*). Prior to liposome formation, tris-NTA-DOD was loaded with Ni(II) by incubation with a 2.85:1 molar excess of $NiCl_2$ at 60 °C for 15 minutes and cooled to room temperature.

Name	Peptide Sequence	MW (exp)	MW (obs)
N-MPR-CHEMS	NEQELLELDKWASLWNGGK-CHEMS	2698.3	2718.2 (Na^+)
N-MPR-his_6	NEQELLELDKWASLWNGGKGGHHHHHH	3166.5	3163.0
N-MPR-biotin	NEQELLELDKWASLWNGGK-biotin	2455.6	2455.0
his_{10}-maleimide	WGGHHHHHHHHHHG	1896.9	1901.0

Table 4-1. Sequences and Molecular Weights of Peptide Antigens.

4.3.3 Preparation of Polyhistidinylated Ovalbumin

Endotoxin contamination of ovalbumin was reduced by centrifugal filtration of a 10 mg/mL solution in PBS through 100 kDa membrane (Amicon Ultra; Millipore, Billerica, MA) twice to remove aggregates followed by passage down a polymyxin B endotoxin removal column (Detoxi-Gel; Pierce, Rockford, IL). Protein prepared in this manner contained less than 0.15 EU/mg endotoxin as determined by an endpoint chromogenic LAL assay (QCL-100; Lonza, Allendale, NJ). Prior to polyhistidinylation, ovalbumin (73 nmol) was thiolated by treatment with 0.6 mM 2-iminothiolane (1.6 μmol) in sodium phosphate buffer (0.1 M $NaPO_4$, 50 mM NaCl, pH 7.53) for 1.5 hours at room temperature. Thiolated ovalbumin (OVA-SH) was separated from excess 2-iminothiolane by passage down a desalting column (PD-10; GE Healthcare, Piscataway, NJ). Concentration of purified OVA-SH was determined by the Bradford method (Bio-rad, Hercules, CA) and preparations were stored at 4 ^{o}C until use.

Polyhistidinylation of OVA-SH (100 nmol) was accomplished by reaction with three-fold molar excess of his_{10}-maleimide (300 nmol) in sodium phosphate buffer overnight at room temperature. To purify polyhistidinylated OVA (OVA-his_{10}) from unreacted OVA-SH, imidazole was added to a final concentration of 20 mM and the protein was loaded onto a 1 mL Ni(II)-NTA column (HisTrapFF; GE Healthcare). The column was washed with 10 mL sodium phosphate buffer containing 20 mM imidazole and OVA-his_{10} was eluted in sodium phosphate buffer containing 500 mM imidazole. To remove imidazole and excess his_{10}-maleimide, the solution was dialyzed at a sample to dialysate volume ratio of 1:150 overnight in sterile PBS with 3 buffer changes (Slide-A-Lyzer,

10,000 MWCO; Pierce, Rockford, IL). Protein stability and extent of modification were monitored by sodium dodecylsulfate polyacrylamide gel electrophoresis. Protein concentration was determined by the Bradford method and preparations were stored at 4 ^{o}C until use. Synthesis was performed in triplicate to verify reproducibility.

4.3.4 Preparation of Fluorescent Proteins

A far-red fluorescent protein (mKate) was used as a surrogate protein for characterization of polyhistidine-tagged protein binding to NTA liposomes (*29*). mKate was expressed and purified as described (Chapter 3). Briefly, the gene was codon-optimized for E. coli K12 and synthesized by overlap PCR (*30*) with GoTaq DNA polymerase (Promega, Madison, WI). Synthesized genes were ligated into pET15b for amplification and expression. Protein was expressed in BL21 Codon Plus (DE3)-RIPL E. coli (Stratagene, La Jolla, CA). E. coli were grown in LB culture medium containing 30 μg/mL kanamycin and 50 μg/mL chloramphenicol at 37 ºC until the OD600 nm reached 0.6-0.8, at which time expression was induced with 0.5 mM isopropyl α-D-1-thiogalactopyranoside (IPTG) with 0.5 mM zinc acetate. After overnight expression at room temperature, protein was purified from the cell supernatant by lysing the cells using freeze thaw followed by sonication. Polyhistidine-tagged mKate was affinity purified from cellular proteins (HisTrapFF; Amersham Biosciences, Piscataway, NJ) and eluted with 500 mM imidazole. Protein-containing eluent fractions were identified by OD280 and buffer exchanged into PBS using a PD10 desalting column (GE LifeSciences, Piscataway, NJ). Protein concentration was determined by the Bradford method and preparations were stored at 4 ^{o}C until use.

4.3.5 Liposome Preparation

Peptide and protein antigens were formulated in liposomes comprised of 15:2:3:0.3 DMPC:DMPG:Cholesterol:MPL (*31*). NTA-containing and maleimide-containing liposomes comprised of DMPC:DMPG:Cholesterol:MPL and either tris-NTA-DOD, NTA-DOGS, or MPB-PE were formed at a molar ratio of 15:2:3:0.3:0.3. Prior to use, glassware was rinsed with MeOH and $CHCl_3$ and dried for at least 90 minutes at 150 ^oC to destroy pyrogens. Lipid solutions were combined in borosilicate glass tubes and dried to a thin film by rotary evaporation under reduced pressure. For liposomes containing N-MPR-CHEMS, lipopeptide in MeOH was added to the lipid solution prior to drying. Films were further dried under high vacuum overnight. Lipids were hydrated in endotoxin-free PBS (UCSF Cell Culture Facility, San Francisco, CA) by intermittent vortexing and liposomes were prepared by bath sonication for 10 minutes at room temperature under argon. Liposomes prepared in this manner contained endotoxin levels less than 0.15 EU/mL when disrupted with 1.5% (v/v) $C_{12}E_{10}$ detergent (*32*) and assayed for endotoxin activity by an endpoint chromogenic LAL assay (QCL-1000, Lonza, Walkersville, MD).

N-MPR-his_6 and OVA-his_{10} were associated with NTA-containing liposomes for 1 hour at room temperature immediately prior to injection. Covalent attachment of OVA to liposomes was accomplished by addition of OVA-SH to liposomes containing MPB-PE immediately after liposome formation and continued reaction overnight at 4 ^oC. The final formulations contained 0.1 mg/mL OVA derivative or 0.5 mg/mL N-MPR derivative and 0.5 mg/mL monophosphoryl lipid A in 20 mM carrier lipid. Vesicle size was

characterized by dynamic light scattering (Zetasizer 3000; Malvern Instruments, UK). Liposomes were stored at 4 ^{o}C under argon until use. As a control, OVA-his$_{10}$ was adsorbed onto alum according to the manufacturer's instructions.

4.3.6 Liposome-Antigen Association *in vitro*

Association of OVA-his$_{10}$ with NTA-containing liposomes was characterized by size exclusion chromatography. Immediately after animal injections, residual liposome preparations were passed down a 1 x 20 cm Sepharose CL-4B column under gravity flow. Liposomes eluted in the void volume and were assayed for the presence of OVA by the Bradford method. Controls included liposomes containing covalently bound OVA, liposomes lacking NTA and liposomes lacking protein. Association was measured after every liposome preparation for animal injections.

The disassociation of polyhistidine-tagged protein from liposomes in the presence of serum was monitored using a surrogate 27 kDa fluorescent protein, mKate. Dissociation from liposomes was measured by challenging pre-associated protein with refiltered fetal calf serum (FCS; UCSF Cell Culture Facility). Liposomes comprised of 60:40 POPC:Cholesterol and 1 mol % NTA lipid (where indicated) were prepared as described above. Protein was added to liposomes at a 1:2 molar ratio of protein to NTA lipid and incubated for 1 hour at room temperature. Liposomal protein was mixed with FCS at a 1:1 volume ratio and incubated at 37 ºC for the indicated time. After incubation, liposomes containing 2 μmol total lipid per sample were passed down a 1 x 20 cm Sepharose 4B-CL column under gravity flow to separate free protein from liposome-

associated protein. Liposomes eluted in the void volume and were assayed for the presence of mKate by fluorescence (excitation/emission 544/590; Fluostar 403, BMG LabTechnologies GmbH, Durham, NC). Free protein without liposomes was also monitored for fluorescence degradation over time and fluorescence intensity was unchanged after 24 hours (data not shown). Disassociation was monitored for triplicate liposome preparations.

4.3.7 Animal Immunizations

All animal procedures were conducted by Douglas Watson and Katherine Jerger in accordance with the policies and approval of the UCSF Institutional Animal Care and Use Committee. 10 week-old female BALB/c mice (Jackson Laboratories, Bar Harbor, ME) were housed in a UCSF specific pathogen-free barrier facility. Animals received subcutaneous immunizations in alternating hind hocks on Days 0 and 14 as described (*33*). Each injection contained 5 μg OVA derivative or 25 μg N-MPR derivative, 25 μg MPL and 1 μmol lipid vehicle in 50 μL sterile phosphate-buffered saline. OVA/alum injections contained 5 μg OVA adsorbed onto 325 μg alum (6.5 mg/mL) per the manufacturer's instructions. On Day 28 blood was collected from the submandibular vein (approximately 250 μL; 15% total blood volume) for characterization of antibody responses. Cells and clotted material were removed by centrifugation at 14,000 rpm for 15 minutes (5415C; Eppendorf, Westbury, NY) and sera were stored at -80 ^{o}C until use.

4.3.8 ELISA

ELISAs were developed by Douglas Watson to quantify binding of immune sera to N-MPR or OVA. Peptide ELISAs were conducted using N-MPR biotinylated as described above and captured on 96 well streptavidin-coated plates (#15120; Pierce, Rockford, IL). Assays were performed according to the manufacturer's instructions with the following modifications. Biotinylated peptide was added to wells in PBS containing 0.1% Tween-20 (PBS-T) and incubated for 2 hours at 37 ^{o}C. Following a wash step, sera were serially diluted in PBS containing 0.1% casein (#C7078 Sigma-Aldrich) (PBS-C), added to wells and incubated for 30 minutes at 37 ^{o}C. After reconstitution, horseradish peroxidase-conjugated IgG secondary antibody (Jackson Immunoresearch; West Grove, PA) was diluted 1:1 in glycerol for long-term storage at -20 ^{o}C and further diluted 1:1000 in PBS-C immediately prior to use. Following a wash step, secondary antibody was added to wells and incubated for 30 minutes at 37 ^{o}C. Following a final wash step, a tetramethylbenzidine substrate solution (#T0440; Sigma-Aldrich) was added to wells and incubated for 30 minutes at room temperature. The reaction was stopped with 0.5M H_2SO_4 and the yellow product was monitored at 450 nm (Optimax, Molecular Devices, Sunnyvale, CA). All incubations were done in 100 µL volumes and wells were washed 6 times with PBS-T between each step. Titer was defined as the reciprocal dilution of immune sera yielding an optical density twice that of 1:200 pre-immune sera after subtraction of background wells lacking serum. All samples were assayed in duplicate.

OVA ELISAs were performed as follows: ovalbumin was diluted from a 5 mg/mL PBS stock solution to 0.1 mg/mL in carbonate-bicarbonate coating buffer (15 mM Na_2CO_3,

35 mM $NaHCO_3$, pH 9.6). OVA (10 μg in 100 μL) per well was added to flat-bottomed high capacity immunoassay plates (Costar). Plates were sealed with parafilm and incubated at 4 ^oC overnight. Plates were blocked with 0.5% casein for 2 hours. After a wash step, immune sera were serially diluted in PBS-C and incubated in wells for 30 minutes. Wells were washed and peroxidase-conjugated anti-mouse IgG was diluted 1:1000 in PBS-C and added to wells for 30 minutes. Following a wash step, plates were then developed and read as indicated above. All incubations were done in 100 μL volumes at 37 ^oC and wells were washed 6 times with PBS-T between each step. Titer was defined as described above and all samples were assayed in duplicate.

4.3.9 Statistical Analysis

Statistical significance was assessed by analysis of variance and two-tailed Student's t test. Differences were considered significant if they exhibited p values < 0.05 in the Student's t test. Data analyses were performed using Microsoft Excel and SigmaPlot.

4.4 Results

4.4.1 Preparation of Antigens and Liposomes

Nitrilotriacetic acid-mediated attachment has garnered interest as a means for tethering polyhistidine-tagged peptide and protein antigens to particulate vaccine carriers (*19, 20, 23*). The goal of this investigation was to determine the role of NTA-Ni(II)-histidine-antigen affinity on antibody responses to two antigens in mice. Liposomes were an appropriate delivery system for this study because they deliver associated antigens efficiently to antigen presenting cells (*34*), stimulate potent immune responses when

adjuvanted with monophosphoryl lipid a (MPL) (*10*) and lipid-anchored NTA molecules can be readily incorporated into the formulation (*20, 26*).

The N terminal peptide of the membrane proximal region of HIV-1 gp41 (N-MPR) was selected because this sequence is a key target for development of vaccines that elicit neutralizing antibodies (*35*). Since the N-MPR peptide is smaller than OVA and contains fewer antigenic determinants, we believed it would provide insight into the use of NTA linkages for delivery of less potent antigens. Moreover, broadly neutralizing antibodies that target the MPR exhibit lipid binding activity and it has been postulated that elicitation of similar antibodies will require presentation of MPR immunogens in a lipid bilayer environment (*36*). Thus, a site-specific NTA-mediated tether could also allow control over directional orientation and presentation of the structure in its native orientation.

A hexahistidine-tagged N-MPR peptide was synthesized in which the polyhistidine tag was attached at the C terminus via an orthogonal protecting group (Figure **4-1**). This was done for two reasons: first, it oriented the peptide in a manner that mimics the native sequence, wherein the C terminus of the sequence is tethered to the membrane and the N terminus extends outward (*22*). Second, attachment via the ε lysyl amine permitted the structure to most closely resemble that of a previously synthesized lipid-anchored control peptide found to elicit high anti-peptide titers when administered in liposomal formulations to BALB/c mice (*27*). Vesicle sizes of N-MPR-containing formulations were not recorded because liposomes precipitated following addition of N-MPR antigens

and thus the structures presented to the immune system were likely not vesicles of defined diameter. Interestingly, in a previous study in which the N-MPR-CHEMS-containing formulations were extruded through polycarbonate membranes following sonication, rapid aggregation was not observed (*27*).

Ovalbumin was selected because it is widely used as a model antigen for assessment of humoral and cellular responses (*37, 38*). The protein was modified with decahistidine in a two step reaction in which free amines were first modified by 2-iminothiolane to generate free thiol groups (*39*). These groups were then reacted with a maleimide-functionalized decahistidine peptide to generate the final conjugate. The conjugate was assured to be free of unmodified OVA because it was purified using a NTA-Ni(II) affinity column. SDS-PAGE analysis revealed a slight increase in molecular weight upon polyhistidinylation, corresponding to 1-2 decahistidine peptides per protein molecule. It is unclear why the proteins ran in the 37-40 kDa molecular weight range, which was less than the expected molecular weight of 45 kDa (Figure **4-2**). Liposomes prepared with OVA-his_{10} exhibited vesicle diameters consistently in the 130-200 nm range regardless of introduction of NTA- or maleimide-functionalized lipids into the formulation (Table **4-2**). Moreover, vesicle sizes were qualitatively consistent over time and no visible aggregation was observed following the addition of protein.

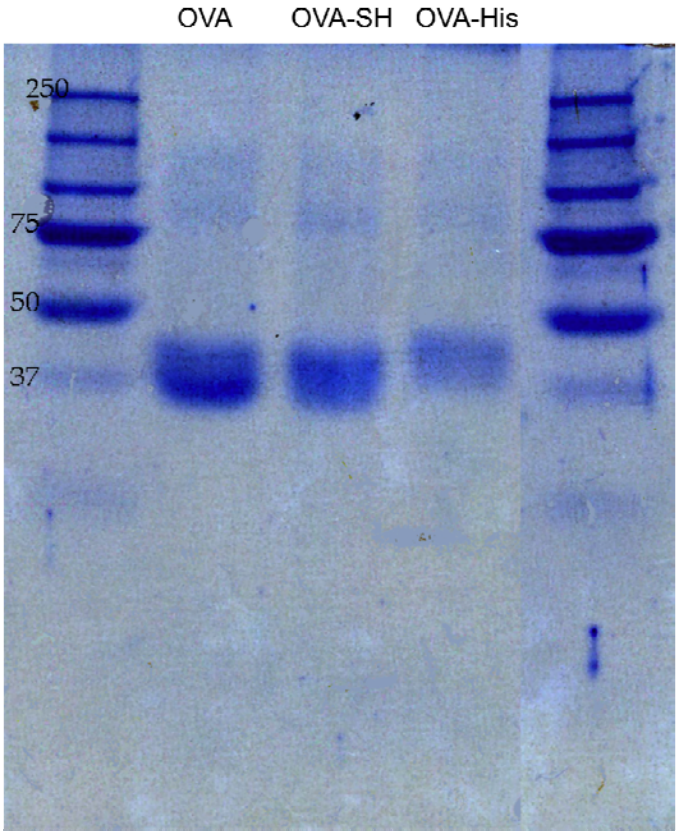


Figure 4-2. SDS-PAGE of Polyhistidinylated Ovalbumin. OVA-his_{10} ran slightly larger than OVA-SH or unmodified OVA, corresponding to the addition of 1-2 decahistidine tags to the total molecular weight.

Formulation	Vesicle Diameter (nm)	Standard Deviation (nm)
OVA-his_{10} mixed-lipo	131.5	1.3
OVA-SH covalent-lipo	157.4	3.1
OVA-his_{10} + mono-NTA-lipo	135.5	0.7
OVA-his_{10} + tris-NTA-lipo	168.2	14.8
OVA-his_{10} + tris-NTA-lipo (no MPL)	194.3	1.6

Table 4-2. Vesicle Sizes of Ovalbumin-Containing Liposome Preparations.

4.4.2 Liposome-Antigen Association

Interest in multivalent NTA adaptors arose in part due to concerns that the micromolar affinity of monovalent NTA-Ni(II)-histidine may be too unstable for in vivo applications (*24, 26*). To address this question, we determined the effect of serum on the stability of binding between liposomes containing mono-NTA-DOGS (K_D ~ 10 μM) or tris-NTA-DOD (K_D ~ 1 nM) and a surrogate hexahistidine-tagged fluorescent protein, mKate. In this experiment, protein was added to pre-formed NTA liposomes and allowed to associate for 1 hour prior to addition of fetal calf serum. At the indicated time, liposome-associated protein was separated from free protein by size exclusion chromatography. Under the conditions studied, both mono-NTA and tris-NTA liposomes initially bound 100% of the protein added (Figure **4-3**).

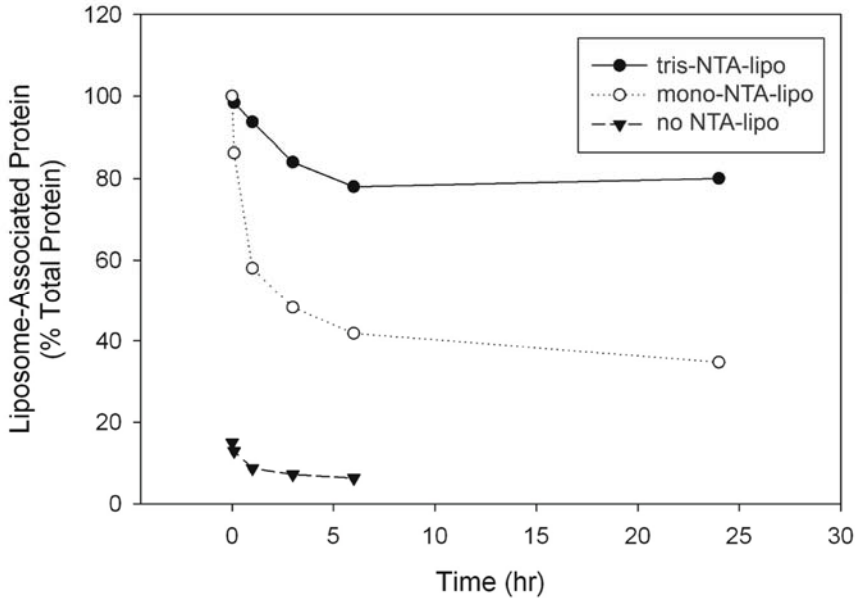


Figure 4-3. Effect of Serum on Association of a Fluorescent Hexahistidine-Tagged Protein with Liposomes Containing NTA-Lipids. The disassociation of polyhistidine-tagged protein from liposomes in the presence of serum was monitored using a surrogate fluorescent protein, mKate, by challenging liposome-associated mKate with refiltered fetal calf serum and incubating at 37 ºC for the indicated time. After incubation, free and liposome-associated mKate were separated by size exclusion. Liposomes containing tris-NTA retained nearly double the protein of mono-NTA-liposomes by 4 hours. Results are representative of two independent experiments.

However, over time protein dissociated from mono-NTA liposomes more quickly, with less than 50% of the protein remaining associated after 4 hour, whereas at the same time point approximately 80% remained associated with tris-NTA liposomes.

The association of polyhistidinylated OVA to NTA liposomes or control liposomes in PBS was determined by size exclusion chromatography with detection by the Bradford method. In formulations containing tris-NTA-DOD, the protein was entirely retained in the liposome fraction (Figure **4-4**). Mono-NTA- and maleimide-functionalized liposomes exhibited an intermediate level of protein retention, whereas control liposomes ('OVA-his_{10}') did not exhibit any protein binding above the background signal of empty liposomes. When the background contribution was subtracted and peak areas were integrated, tris-NTA-liposomes bound 77.7-83.0% of the added OVA, whereas mono-NTA- and maleimide-functionalized liposomes bound 34.4-38.6% of the protein (Table **4-3**). These results underscore the differences in protein binding between mono-NTA- and tris-NTA-containing formulations, while also revealing a considerable amount of unconjugated protein in the maleimide-functionalized liposomes. This could be caused by saturation of available thiols on the protein or steric restraints at the liposome surface.

4.4.3 Humoral Immune Responses in Mice

Antibody responses to liposome-associated OVA and N-MPR were assessed in BALB/c mice. Liposomes containing N-MPR-his_6 attached via either a mono-NTA or a tris-NTA linkage elicited anti-peptide IgG in sera of 4 of 4 mice in each group. However, N-MPR-his_6 admixed with control liposomes lacking NTA failed to elicit a detectable anti-N-

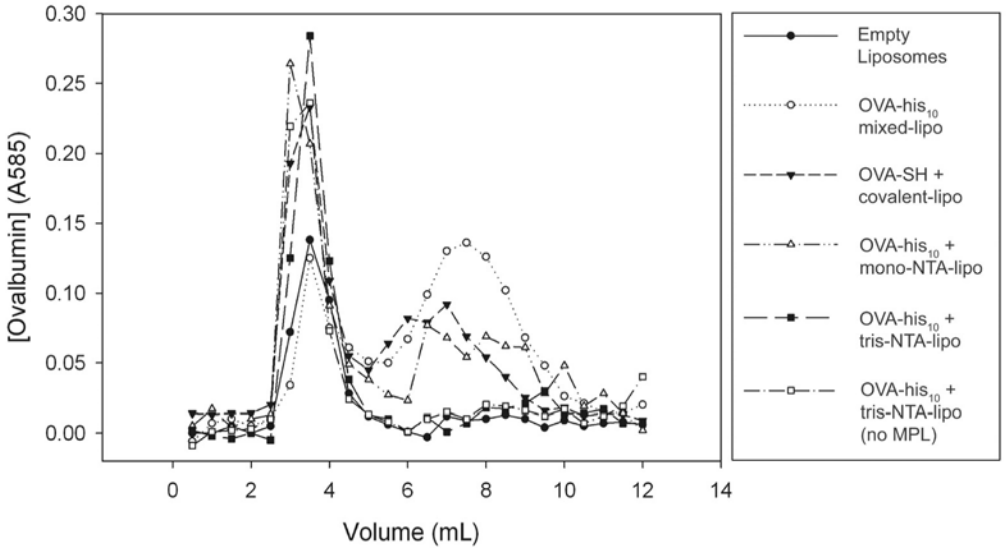


Figure 4-4. Association of Ovalbumin with Liposomes Containing NTA-Lipids. Association of OVA-his_{10} with NTA-containing liposomes was characterized by size exclusion. Liposomes containing tris-NTA were found to completely retain OVA-his_{10} under the conditions studied, whereas mono-NTA liposomes and maleimide liposomes exhibited intermediate retention. Control liposomes lacking NTA did not exhibit protein-liposome binding greater than background. Results are representative of two independent liposome preparations.

Formulation	Liposome-Associated Protein (% of total)
OVA-his_{10} mixed-lipo	0.0
OVA-SH covalent-lipo	34.4
OVA-his_{10} + mono-NTA-lipo	38.6
OVA-his_{10} + tris-NTA-lipo	77.7
OVA-his_{10} + tris-NTA-lipo (no MPL)	83.0

Table 4-3. Association of Ovalbumin with Liposomes Containing NTA-Lipids. The association of polyhistidinylated OVA to NTA liposomes or control liposomes in PBS was determined by a size exclusion chromatography method with detection by the Bradford assay. Integrated peak areas were calculated following subtraction of the background contribution of liposomes lacking protein. Percent association was calculated as associated/(associated + free) x 100. Results are representative of two independent preparations.

MPR antibody response. This is consistent with a previous study by our group in which liposomal N-MPR peptide required a lipid anchor to generate a substantial antibody response in BALB/c mice (*27*). No significant difference was observed when comparing antibody responses elicited by mono-NTA and tris-NTA linkages ($p = 0.67$). Importantly, covalent attachment of N-MPR to liposomes via a cholesteryl hemisuccinate anchor was superior to NTA-mediated conjugation for elicitation of antibody responses to N-MPR (GMT $4.4 * 10^4$ vs. $5.5\text{-}7.6 * 10^2$; $p = 0.002$ vs. mono-NTA, $p = 0.002$ vs. tris-NTA; Figure **4-5**).

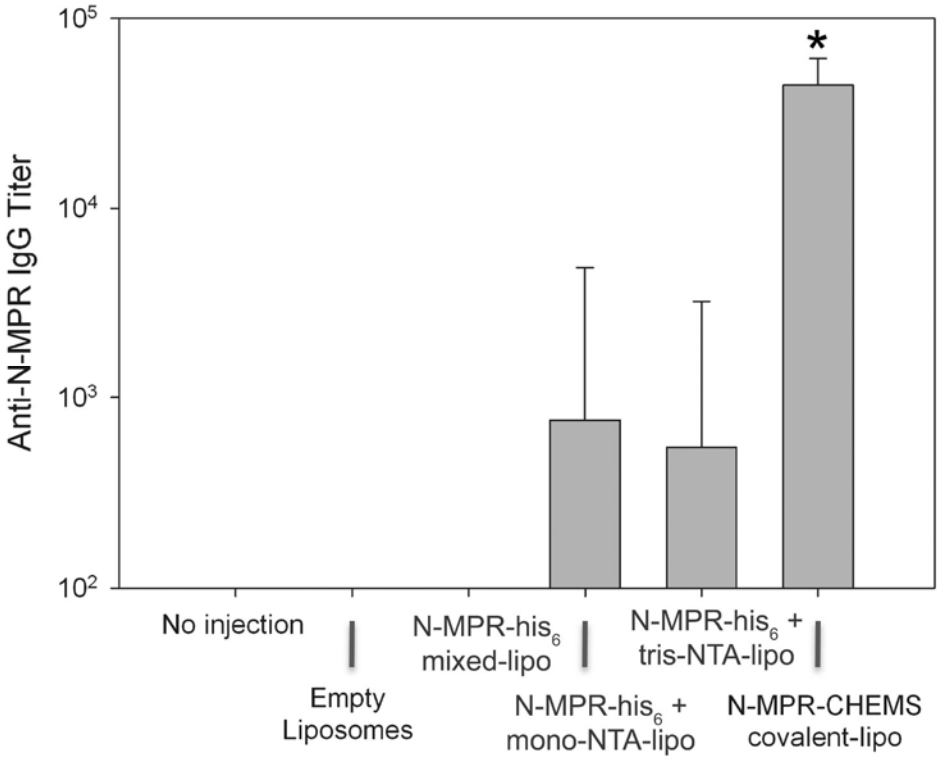


Figure 4-5. Effect of N-MPR-Liposome Linkage on Anti-N-MPR IgG Response in Mice. Covalent attachment of N-MPR to liposomes via a cholesteryl hemisuccinate anchor was superior to NTA-mediated conjugation for elicitation of antibody responses to N-MPR ($p = 0.002$ vs. mono-NTA, $p = 0.002$ vs. tris-NTA). However, polyhistidinylated N-MPR admixed with control liposomes failed to elicit a detectable anti-N-MPR antibody response. No significant difference was observed when comparing antibody responses elicited by mono-NTA and tris-NTA linkages ($p = 0.67$).

When OVA-his_{10} was the immunizing antigen, mono-NTA-DOGS-mediated attachment elicited significantly greater antibody responses than adsorption on aluminum hydroxide gel (GMT 1.6 * 10^6 vs. 4.4 * 10^5, p = 0.0002; Figure **4-6**), as reported by Patel and coworkers in the case of p24 attached to wax nanoparticles (*23*). Omission of MPL from the tris-NTA formulation resulted in an order of magnitude decrease in anti-OVA titers (GMT 1.6 * 10^5, p = 0.003). As seen in the case of N-MPR-his_6, attachment via tris-NTA did not confer any advantage over the mono-NTA linkage (p = 0.53). Moreover, both mono-NTA and tris-NTA formulations were inferior to covalently conjugated OVA (GMT 1.4-1.6 * 10^6 vs. 3.4 * 10^6, p < 0.001). Surprisingly, control liposomes in which the protein was unattached also elicited significantly greater anti-OVA titers than NTA liposomes (GMT 2.6 * 10^6; p = 0.006 vs mono-NTA, p = 0.01 vs tris-NTA). Statistical comparisons between groups, as determined by two-tailed Student's t test, are summarized in Table **4-4**.

In summary, NTA-mediated attachment was more effective than simply admixing antigen with liposomes lacking NTA for elicitation of serum IgG to N-MPR-his_6 but not to OVA-his_{10}. NTA-mediated attachment was also more effective than adsorption on alum for elicitation of serum anti-OVA IgG responses. However, the tris-NTA anchor did not provide any enhancement as compared to the mono-NTA anchor for induction of antibody to either OVA or N-MPR. Lastly, covalent conjugation elicited greater serum antibody titers to both OVA and N-MPR as compared to NTA attachment.

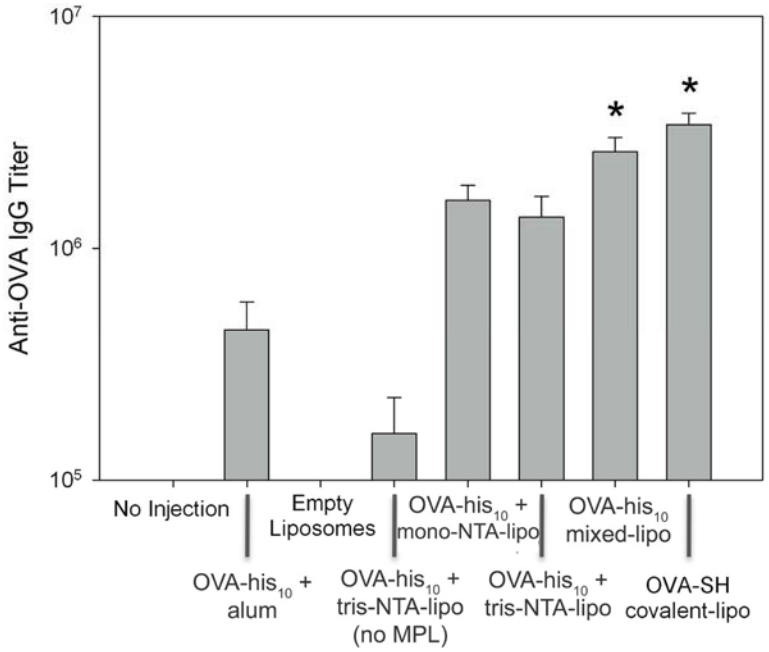


Figure 4-6. Effect of Ovalbumin-Liposome Linkage on Anti-Ovalbumin IgG Response in Mice. Antibody responses to liposome-associated OVA were assessed in BALB/c mice. DOGS-NTA-mediated attachment elicited significantly greater antibody responses than adsorption on aluminum hydroxide gel ($p = 0.0002$). However, both mono-NTA and tris-NTA formulations were inferior to covalently conjugated OVA (* = $p < 0.001$). Control liposomes in which the protein was unattached also elicited significantly greater anti-OVA titers than NTA liposomes ($p = 0.006$ vs Mono-NTA, $p = 0.01$ vs Tris-NTA). No responses were observed in control groups ('No Injection' and 'Empty Liposomes'). Statistical comparisons between groups, as determined by two-tailed Student's t test, are summarized in Table **4-3**.

	OVA-SH covalent-lipo	OVA-his$_{10}$ + mono-NTA-lipo	OVA-his$_{10}$ + tris-NTA-lipo	OVA-his$_{10}$ + tris-NTA-lipo (no MPL)	OVA-his$_{10}$ + alum
OVA-his$_{10}$ mixed-lipo	3.08E-02	5.61E-03	1.02E-02	1.98E-05	5.36E-05
OVA-SH covalent-lipo		2.87E-04	8.53E-04	4.11E-06	9.26E-06
OVA-his$_{10}$ + mono-NTA-lipo			5.28E-01	3.26E-05	2.09E-04
OVA-his$_{10}$ + tris-NTA-lipo				2.57E-03	1.02E-02
OVA-his$_{10}$ + tris-NTA-lipo (no MPL)					9.33E-03

Table 4-4. Statistical Significance of Differences in Anti-Ovalbumin IgG Titer amongst groups of mice immunized with ovalbumin-containing liposome formulations. Analyses were performed using two-tailed Student's t test assuming equal variances and differences were considered significant if p values were less than 0.05. All comparisons were significant except that of mono-NTA-lipo vs. tris-NTA-lipo (indicated in red).

4.5 Discussion

Particulate delivery systems are required to elicit robust immune responses to subunit protein antigens, and more potent alternatives are needed to replace traditional aluminum salts (*1, 5, 7*). Liposomes, polymeric particles, emulsions and other microscale and nanoscale carriers have been developed to deliver payloads efficiently to antigen presenting cells (*2, 6, 13*). Methodologies for association of antigen with these systems, including entrapment, adsorption or chemical conjugation, can damage proteins and present epitopes in an uncontrolled orientation (*14-16*). Metal chelation via NTA-Ni(II)-histidine has been suggested as a site-specific, non-destructive approach to particulate delivery of polyhistidine-tagged antigens (*20, 23*). However, concerns have arisen that the micromolar affinity of monovalent NTA for hexahistidine may be too weak for in vivo applications (*24-26*).

This study sought to characterize the importance of NTA-Ni(II)-histidine affinity in promoting antibody responses to polyhistidine-tagged antigens formulated with particulate carriers. We hypothesized that the increased affinity of trivalent NTA for polyhistidine (K_D ~ 1 nM) would translate to increased liposome association and enhanced antibody titers as compared to a monovalent NTA linkage (K_D ~ 10 μM). Antibody responses to liposomal preparations of two model proteins wherein the antigen was attached via a trivalent NTA lipid anchor, a commercially available monovalent NTA anchor or a covalent linkage were assessed in BALB/c mice.

The key findings of the study are three-fold. First, attachment of N-MPR-his_6 but not OVA-his_{10} to liposomes via an NTA lipid elicited stronger antibody responses in mice as compared to a formulation in which the antigen was simply admixed with control liposomes lacking NTA (Figures **4-5** and **4-6**). This difference may arise from the greater antigenic diversity of OVA, a large protein with many B and T cell epitopes, as compared to N-MPR, a peptide that contains only a few epitopes. In a prior study, Chikh and coworkers attached a decahistidine-tagged polypeptide containing a cytotoxic T lymphocyte epitope to mono-NTA liposomes (*20*). Although they observed increased peptide-specific splenocyte interferon gamma secretion as compared to a formulation lacking NTA following immunization of mice, the difference was not statistically significant. Additionally, the polypeptide was observed to associate somewhat with liposomes in the absence of NTA, presumably due to its hydrophobic nature. Thus, further studies will be needed to determine how the size, charge and hydrophobicity of a particular antigen affect the utility of NTA-liposome delivery for promoting antibody responses to that antigen.

The second key finding of the study was that antigen attachment via multivalent NTA linkages with greater affinity did not result in enhanced antibody responses as compared to monovalent NTA linkages despite association of a greater fraction of the antigen with tris-NTA liposomes (Figures **4-5** and **4-6**). This result is surprising since liposomal antigen persists at the injection site for days following subcutaneous administration (*40*), and differences in antigen binding to monovalent NTA and tris-NTA liposomes would manifest over this time scale. Although tris-NTA liposomes bound more than twice the

protein of mono-NTA liposomes in vitro (Figure **4-4**), no enhancement of antibody responses was observed. The extent of binding may be substantially altered in vivo, but similar differences in binding of OVA-his_{10} to mono-NTA and tris-NTA were also observed in the presence of serum (Figure **4-3**). One possible explanation for this is that the nickel may be removed from the NTA by biological chelators such as thiocompounds or zinc binding proteins such as metallothionein that are present in vivo (*41*). This would result in dissociation of the histidine-tagged antigen from the liposome. However, the weaker antigen (N-MPR) required association with the carrier, via either NTA or a covalent linkage, to elicit a response, suggesting an in vivo role for the NTA linkage in this case (Figure **4-5**).

A third important observation was that NTA linkages were inferior to covalent conjugation for elicitation of antibody responses to liposomal formulations of OVA and N-MPR (Figures **4-5** and **4-6**). In the case of OVA, antibody titers did not correspond with extent of protein-liposome binding, as essentially double the amount of OVA associated with the tris-NTA formulation as compared to the covalently attached formulation in vitro (Figure **4-4** and Table **4-3**). Thus, extent of antigen-particulate association is not a clear correlate of antibody induction in this system. This effect may be antigen-specific, since N-MPR required liposome attachment, via either an NTA linkage or covalent conjugation, to elicit an antibody response in BALB/c mice. One possible explanation for the greater serum antibody titers induced by covalent antigen attachment is that lipid conjugation confers a benefit in antigen processing downstream of particulate association and internalization (*42, 43*). Indeed, we recently observed that the

structure of the lipid anchor dramatically affected the serum IgG response to liposome N-MPR lipopeptides despite complete retention of all antigens in the liposome formulation (*27*).

Surprisingly, control liposomes in which the protein was completely unassociated elicited significantly greater anti-OVA responses than liposomes containing NTA-anchored OVA (Figure **4-4** and Table **4-3**). These findings conflict with the work of Patel and coworkers showing that NTA-Ni(II) wax nanoparticles elicited greater responses to polyhistidine-tagged p24 antigen than control nanoparticles lacking Ni(II) (*23*). This discrepancy may arise from in vivo differences in antigen retention in solid wax particles as compared to the fluid lipid formulation used in these studies. Alternatively, the disparity may be attributed to the greater immunostimulatory capacity of the MPL-adjuvanted liposomes as compared to the nanoparticles studied by Patel and coworkers (*44*). Indeed, unassociated OVA admixed with MPL-adjuvanted liposomes also elicited significantly greater antibody responses than OVA alone in PBS (GMT $3.1 * 10^4$, $p = 0.0001$), indicating a key role of the liposomes in activating the response, perhaps through toll-like receptor 4 engagement or other inflammatory pathways. Additionally, thiolation of OVA could have altered the response in the current experiment; however, thiolated bovine serum albumin was not found to elicit antibody responses when admixed with control liposomes in A/J mice in a similar experiment (*45*). Moreover, analogous modifications of other proteins generally reduce, rather than increase, immune responses (*46*).

In summary, these studies highlight the advantages and limitations of nitrilotriacetic acid lipid technology for particulate delivery of subunit vaccine antigens. Association with an MPL-adjuvanted liposomal carrier was required to elicit antibody responses to a weak antigen (N-MPR) but not a potent antigen (OVA). However, there were no differences in antibody titers when the antigens were attached via the monovalent or the trivalent NTA linkages. Additionally, covalent attachment to the carrier was superior to NTA-mediated attachment for elicitation of antibody responses. Thus, further improvements of the NTA-mediated conjugation strategy are required before it will be a universally effective method to attach antigens to particulate vaccine carriers and elicit high titer antibody responses.

4.6 Acknowledgements and Author Contributions

We gratefully thank Katherine Jerger for her assistance with animal experiments. This work was supported by grant NIH R01 GM061851 and by a grant from the National Institutes of Health, University of California, San Francisco - Gladstone Institute of Virology & Immunology Center for AIDS Research, P30-AI027763. Our appreciation is extended to Dr. Limin Cao for design and original production of his-tagged proteins, Dr. Zhaohua Huang for design of the tris-NTA production scheme and synthesis of the original tris-NTA lipids and to Dr. Douglas Watson for synthesis of peptides and lipopeptides, liposome formulation, performance of ELISA assays, data analysis and the bulk of manuscript writing.

4.7 Literature Cited

(1) Aguilar, J. C., and Rodriguez, E. G. (2007) Vaccine adjuvants revisited. *Vaccine 25*, 3752-62.

(2) Perrie, Y., Mohammed, A. R., Kirby, D. J., McNeil, S. E., and Bramwell, V. W. (2008) Vaccine adjuvant systems: enhancing the efficacy of sub-unit protein antigens. *Int J Pharm 364*, 272-80.

(3) Koff, R. (2002) Immunogenicity of hepatitis B vaccines: implications of immune memory. *Vaccine 2002*, 3695-3701.

(4) Lowy, D. R., and Schiller, J. T. (2006) Prophylactic human papillomavirus vaccines. *J Clin Invest 116*, 1167-73.

(5) Gupta, R. K., and Siber, G. R. (1995) Adjuvants for human vaccines--current status, problems and future prospects. *Vaccine 13*, 1263-76.

(6) O'Hagan, D. T., and Valiante, N. M. (2003) Recent advances in the discovery and delivery of vaccine adjuvants. *Nat Rev Drug Discov 2*, 727-35.

(7) Liang, M. T., Davies, N. M., Blanchfield, J. T., and Toth, I. (2006) Particulate systems as adjuvants and carriers for peptide and protein antigens. *Curr Drug Deliv 3*, 379-88.

(8) Glenny, A., Pope, C., Waddington, H., and Wallace, V. (1926) The antigenic value of toxoid precipitated by potassium-alum. *Journal of Pathology and Bacteriology 29*, 38-45.

(9) Fox, E. N., Waldman, R. H., Wittner, M. K., Mauceri, A. A., and Dorfman, A. (1973) Protective study with a group A streptococcal M protein vaccine. Infectivity challenge of human volunteers. *J Clin Invest 52*, 1885-92.

(10) Alving, C. R., Koulchin, V., Glenn, G. M., and Rao, M. (1995) Liposomes as carriers of peptide antigens: induction of antibodies and cytotoxic T lymphocytes to conjugated and unconjugated peptides. *Immunol Rev 145*, 5-31.

(11) Brunel, F., Darbouret, A., and Ronco, J. (1999) Cationic lipid DC-Chol induces an improved and balanced immunity able to overcome the unresponsiveness to the hepatitis B vaccine. *Vaccine 17*, 2192-203.

(12) Singh, M., Li, X. M., McGee, J. P., Zamb, T., Koff, W., Wang, C. Y., and O'Hagan, D. T. (1997) Controlled release microparticles as a single dose hepatitis B vaccine: evaluation of immunogenicity in mice. *Vaccine 15*, 475-81.

(13) Lian, T., Bui, T., and Ho, R. J. (1999) Formulation of HIV-envelope protein with lipid vesicles expressing ganglioside GM1 associated to cholera toxin B enhances mucosal immune responses. *Vaccine 18*, 604-11.

(14) Singh, M., Chesko, J., Kazzaz, J., Ugozzoli, M., Kan, E., Srivastava, I., and O'Hagan, D. T. (2004) Adsorption of a novel recombinant glycoprotein from HIV (Env gp120dV2 SF162) to anionic PLG microparticles retains the structural integrity of the protein, whereas encapsulation in PLG microparticles does not. *Pharm Res 21*, 2148-52.

(15) Weissig, V., Lasch, J., Klibanov, A. L., and Torchilin, V. P. (1986) A new hydrophobic anchor for the attachment of proteins to liposomal membranes. *FEBS Lett 202*, 86-90.

(16) Cooper, H. M., Jemmerson, R., Hunt, D. F., Griffin, P. R., Yates, J. R., 3rd, Shabanowitz, J., Zhu, N. Z., and Paterson, Y. (1987) Site-directed chemical modification of horse cytochrome c results in changes in antigenicity due to local and long-range conformational perturbations. *J Biol Chem 262*, 11591-7.

(17) Friede, M., and Aguado, M. T. (2005) Need for new vaccine formulations and potential of particulate antigen and DNA delivery systems. *Adv Drug Deliv Rev 57*, 325-31.

(18) Kazzaz, J., Neidleman, J., Singh, M., Ott, G., and O'Hagan, D. T. (2000) Novel anionic microparticles are a potent adjuvant for the induction of cytotoxic T lymphocytes against recombinant p55 gag from HIV-1. *J Control Release 67*, 347-56.

(19) van Broekhoven, C. L., and Altin, J. G. (2005) The novel chelator lipid 3(nitrilotriacetic acid)-ditetradecylamine (NTA(3)-DTDA) promotes stable binding of His-tagged proteins to liposomal membranes: potent anti-tumor responses induced by simultaneously targeting antigen, cytokine and costimulatory signals to T cells. *Biochim Biophys Acta 1716*, 104-16.

(20) Chikh, G. G., Li, W. M., Schutze-Redelmeier, M. P., Meunier, J. C., and Bally, M. B. (2002) Attaching histidine-tagged peptides and proteins to lipid-based carriers through use of metal-ion-chelating lipids. *Biochim Biophys Acta 1567*, 204-12.

(21) Dietrich, C., Schmitt, L., and Tampe, R. (1995) Molecular organization of histidine-tagged biomolecules at self-assembled lipid interfaces using a novel class of chelator lipids. *Proc Natl Acad Sci U S A 92*, 9014-8.

(22) Montero, M., van Houten, N. E., Wang, X., and Scott, J. K. (2008) The membrane-proximal external region of the human immunodeficiency virus type 1 envelope: dominant site of antibody neutralization and target for vaccine design. *Microbiol Mol Biol Rev 72*, 54-84, table of contents.

(23) Patel, J. D., O'Carra, R., Jones, J., Woodward, J. G., and Mumper, R. J. (2007) Preparation and characterization of nickel nanoparticles for binding to his-tag proteins and antigens. *Pharm Res 24*, 343-52.

(24) Van Broekhoven, C. L., and Altin, J. G. (2001) A novel system for convenient detection of low-affinity receptor-ligand interactions: chelator-lipid liposomes engrafted with recombinant CD4 bind to cells expressing MHC class II. *Immunol Cell Biol 79*, 274-84.

(25) Lata, S., Reichel, A., Brock, R., Tampe, R., and Piehler, J. (2005) High-affinity adaptors for switchable recognition of histidine-tagged proteins. *J Am Chem Soc 127*, 10205-15.

(26) Huang, Z., Park, J. I., Watson, D. S., Hwang, P., and Szoka, F. C., Jr. (2006) Facile synthesis of multivalent nitrilotriacetic acid (NTA) and NTA conjugates for analytical and drug delivery applications. *Bioconjug Chem 17*, 1592-600.

(27) Watson, D. S., and Szoka, F. C., Jr. (2009) Role of lipid structure in the humoral immune response in mice to covalent lipid-peptides from the membrane proximal region of HIV-1 gp41. *Vaccine 27*, 4672-83.

(28) Pace, C. N., Vajdos, F., Fee, L., Grimsley, G., and Gray, T. (1995) How to measure and predict the molar absorption coefficient of a protein. *Protein Sci 4*, 2411-23.

(29) Shcherbo, D., Merzlyak, E. M., Chepurnykh, T. V., Fradkov, A. F., Ermakova, G. V., Solovieva, E. A., Lukyanov, K. A., Bogdanova, E. A., Zaraisky, A. G., Lukyanov, S., and Chudakov, D. M. (2007) Bright far-red fluorescent protein for whole-body imaging. *Nat Methods 4*, 741-6.

(30) Rouillard, J. M., Lee, W., Truan, G., Gao, X., Zhou, X., and Gulari, E. (2004) Gene2Oligo: oligonucleotide design for in vitro gene synthesis. *Nucleic Acids Res 32*, W176-80.

(31) Ernst, W. A., Kim, H. J., Tumpey, T. M., Jansen, A. D., Tai, W., Cramer, D. V., Adler-Moore, J. P., and Fujii, G. (2006) Protection against H1, H5, H6 and H9 influenza A infection with liposomal matrix 2 epitope vaccines. *Vaccine 24*, 5158-68.

(32) Harmon, P., Cabral-Lilly, D., Reed, R. A., Maurio, F. P., Franklin, J. C., and Janoff, A. (1997) The release and detection of endotoxin from liposomes. *Anal Biochem 250*, 139-46.

(33) Kamala, T. (2007) Hock immunization: a humane alternative to mouse footpad injections. *J Immunol Methods 328*, 204-14.

(34) Dal Monte, P., and Szoka, F. C., Jr. (1989) Effect of liposome encapsulation on antigen presentation in vitro. Comparison of presentation by peritoneal macrophages and B cell tumors. *J Immunol 142*, 1437-43.

(35) Karlsson Hedestam, G. B., Fouchier, R. A., Phogat, S., Burton, D. R., Sodroski, J., and Wyatt, R. T. (2008) The challenges of eliciting neutralizing antibodies to HIV-1 and to influenza virus. *Nat Rev Microbiol 6*, 143-55.

(36) Alam, S. M., McAdams, M., Boren, D., Rak, M., Scearce, R. M., Gao, F., Camacho, Z. T., Gewirth, D., Kelsoe, G., Chen, P., and Haynes, B. F. (2007) The role of antibody polyspecificity and lipid reactivity in binding of broadly neutralizing anti-HIV-1 envelope human monoclonal antibodies 2F5 and 4E10 to glycoprotein 41 membrane proximal envelope epitopes. *J Immunol 178*, 4424-35.

(37) Zhou, F., and Huang, L. (1993) Monophosphoryl lipid A enhances specific CTL induction by a soluble protein antigen entrapped in liposomes. *Vaccine 11*, 1139-44.

(38) Boyle, J. S., Brady, J. L., and Lew, A. M. (1998) Enhanced responses to a DNA vaccine encoding a fusion antigen that is directed to sites of immune induction. *Nature 392*, 408-11.

(39) Dal Monte, P. R., and Szoka, F. C., Jr. (1989) Antigen presentation by B cells and macrophages of cytochrome c and its antigenic fragment when conjugated to the surface of liposomes. *Vaccine 7*, 401-8.

(40) Oussoren, C., and Storm, G. (2001) Liposomes to target the lymphatics by subcutaneous administration. *Adv Drug Deliv Rev 50*, 143-56.

(41) Bell, S. G., and Vallee, B. L. (2009) The metallothionein/thionein system: an oxidoreductive metabolic zinc link. *Chembiochem 10*, 55-62.

(42) Rees, A. D., Faith, A., Roman, E., Ivanyi, J., Wiesmuller, K. H., and Moreno, C. (1993) The effect of lipoylation on CD4 T-cell recognition of the 19,000 MW Mycobacterium tuberculosis antigen. *Immunology 80*, 407-14.

(43) Van Rhijn, I., Young, D. C., De Jong, A., Vazquez, J., Cheng, T. Y., Talekar, R., Barral, D. C., Leon, L., Brenner, M. B., Katz, J. T., Riese, R., Ruprecht, R. M., O'Connor, P. B., Costello, C. E., Porcelli, S. A., Briken, V., and Moody, D. B. (2009) CD1c bypasses lysosomes to present a lipopeptide antigen with 12 amino acids. *J Exp Med 206*, 1409-22.

(44) Alving, C. R., and Rao, M. (2008) Lipid A and liposomes containing lipid A as antigens and adjuvants. *Vaccine 26*, 3036-45.

(45) Shek, P. N., and Heath, T. D. (1983) Immune response mediated by liposome-associated protein antigens. III. Immunogenicity of bovine serum albumin covalently coupled to vesicle surface. *Immunology 50*, 101-6.

(46) Doyle, H. A., and Mamula, M. J. (2001) Post-translational protein modifications in antigen recognition and autoimmunity. *Trends Immunol 22*, 443-9.

Chapter 5

Evaluating the Potential for Hyaluronidase-Liposome Targeting to Tumors and Intratumoral Translocation

5.1 Abstract

Injection of hyaluronidase can decrease tumor growth and increase survival time in animals with models of solid tumors. Hyaluronidase alters the permeability of the tumor to macromolecular drug carriers, including liposomes, and can improve their anti-cancer efficacy. In this study, we evaluate the potential use for hyaluronidase to target liposomes or improve their motility within tumors. Ovine hyaluronidase was modified with iminothiolane to introduce sulfhydryl groups into the enzyme. The sulfhydryl-modified enzyme was further modified by attachment of a maleimide-his_{10} or by attaching the enzyme to maleimide-lipids embedded in the liposome. Hyaluronidase was present on the liposome surface via non-covalent association with NTA-lipids in the bilayer, covalent attachment directly to the liposome surface and covalent attachment to the liposome via a PEG(2000) spacer. His_{10}-modified enzyme or liposome-attached enzyme retained full activity. Hyaluronidase-liposomes diffused into an HA-gel at the same rate as liposomes admixed with free, unmodified hyaluronidase. Hyaluronidase-liposomes conjugated via a PEG(2000) spacer bound to the surface of HA-producing cancer cells in culture. Hyaluronidase-liposomes, at 350 to 700 U per dose, were eliminated more rapidly than unmodified liposomes but less rapidly than the free enzyme.

5.2 Introduction

Hyaluronan (HA) surrounds tissue and contributes to its support and hydration (*1*). This high molecular weight polysaccharide is present at high concentrations in many healthy tissues, including the skin (*2*). HA is rapidly cleared from circulation by receptors present on the liver (*3, 4*). In some cancers, HA synthesis and degradation are altered, resulting in increased HA content within the tumor extracellular matrix (*1, 5*).

Hyaluronidase degrades HA to short saccharide chains by catalyzing hydrolysis at the β1-4 glycosidic linkage (*6*). Degrading the HA-rich matrix surrounding tumors can effect survival and cancer progression (*7*). Exogenous bovine testicular hyaluronidase (300 U per dose) injected intravenously into mice with human breast carcinoma xenograft tumors decreased tumor size (*7*). After hyaluronidase treatment, tumor size decreased to approximately half of the initial tumor size while untreated tumors continued to grow. Pretreatment of carcinoma cells prior to subcutaneous injection into the mammary fat pad also decreased tumor formation (*7*).

Hyaluronidase treatment may also increase the accumulation and penetration of anti-cancer macromolecules by altering the permeability of the tumor extracellular matrix (*8-10*). Bovine testicular hyaluronidase injected intratumorally decreased the fluid pressure in solid tumors (*8, 9*). Injected intravenously, bovine testicular hyaluronidase (1500 U per dose) increased the permeation of macromolecular carriers (*11*). Hyaluronidase injection (1600 U per dose) into osteosarcoma tumors in the periosteum of mice decreased pressure within the tumor. Pressure was measured using an intratumoral wick-

in-needle technique (*8*). Mice received repeated intratumoral injections of bovine testicular hyaluronidase (1600 U of hyaluronidase at 3 day intervals). Approximately 30 minutes after each injection of hyaluronidase, mice were given an intravenous injection of antibodies. Mice not receiving hyaluronidase and those receiving fewer hyaluronidase doses had less antibody uptake within the tumor. Hyaluronidase pre-treatment did not increase uptake in other tissues (*9*).

Pretreatment of solid, subcutaneous osteosarcoma tumors with intratumoral bovine testicular hyaluronidase (1500 U per dose) decreased intratumoral interstitial fluid pressure, by 40%, one hour after injection (*12*). Intravenously injected liposomes containing doxorubicin accumulated at 4-fold higher concentrations than liposomes injected without prior hyaluronidase treatment. Liposomes were visualized by the presence of doxorubicin fluorescence. Liposomes penetrated farther into the hyaluronidase treated tumor than untreated tumor, showing 5-fold higher concentrations near the tumor center (*12*).

Co-injection of recombinant human hyaluronidase increased the spread of macromolecules (*10*). Free recombinant human hyaluronidase (0.5-5 U per dose) co-injected with a trypan blue dye into the skin of mice significantly increased dye spreading within the interstitial matrix (*10*). Intratumoral co-injection of recombinant human hyaluronidase (10 U per dose) with an adenoviral vector containing a green fluorescent protein (EGFP) expression cassette increased the area in which fluorescent protein was expressed by 50% compared to controls without hyaluronidase (*10*). Similarly, the

spread of 2 * 10^6 MW fluorescent-dextran and 200 nm fluorescent-latex beads increased (4 fold and 50%, respectively) when co-injected with recombinant hyaluronidase (25 U per dose) in the skin of mice (*10*).

Thus, the hyaluronidase-liposome complex may increase therapeutic delivery in three ways. First, increased circulation half-life of the hyaluronidase could increase protein accumulation into the tumor. Increased protein accumulation could result in immediate anti-cancer effects from hyaluronidase disruption of cell-HA interactions. Second, hyaluronidase may influence the intratumoral behavior of the conjugated-liposome. This influence may be due to matrix degradation immediately surrounding the carrier and may improve intratumoral permeation. Finally, hyaluronidase may target the conjugated liposomes to tumor because the HA-rich extracellular matrix is exposed to circulation macromolecules.

In this chapter, we measured the activity and binding properties of liposomal-hyaluronidase formed via non-covalent and covalent attachment (Figure **5-1**). Hyaluronidase was modified with maleimide-his_{10} to provide a non-covalent association partner for tris-NTA-DAP-DOD lipids present in the liposomes. For direct liposome attachment, hyaluronidase was conjugated using maleimide-DSPE or maleimide-PEG(2000)-DSPE incorporated into the liposomal bilayer. I also assessed the impact of covalent modification and liposome-attachment on hyaluronidase activity. Finally, the diffusion of hyaluronidase-liposomes in a HA-gel, binding to HA-producing cells and *in vivo* behavior of hyaluronidase-liposomes was evaluated.

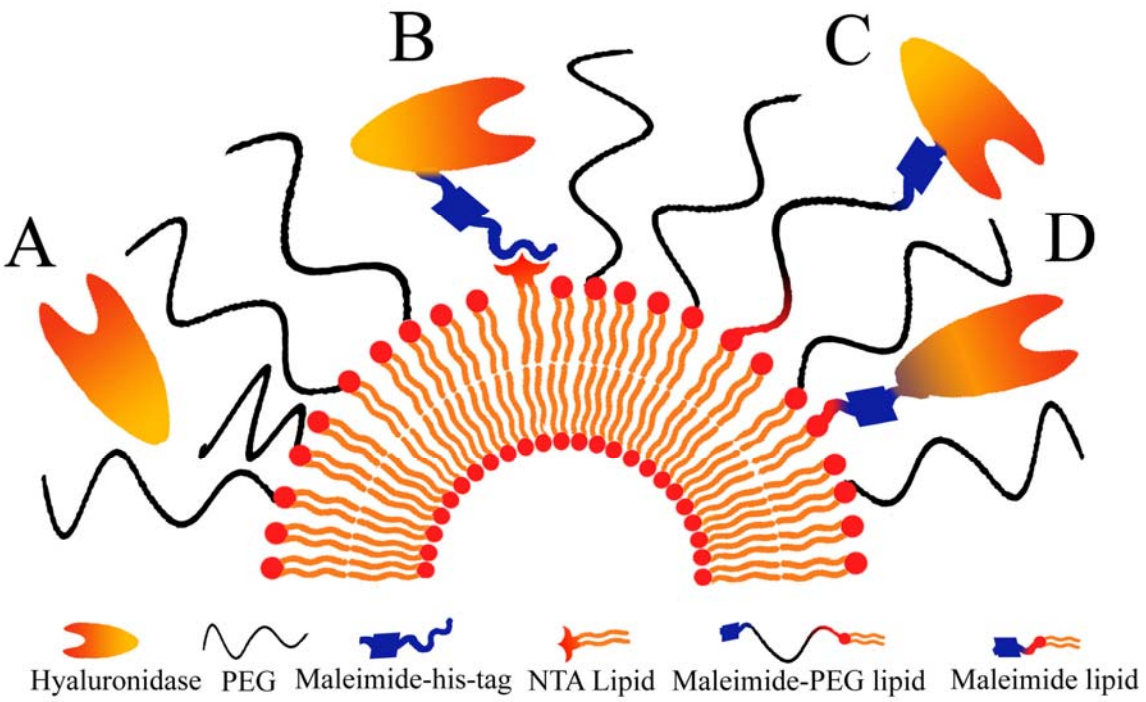


Figure 5-1. Hyaluronidase-Liposomes. Hyaluronidase interacts with liposomes via non-specific adsorption (**A**), non-covalent his_{10}-tag/tris-NTA interactions (**B**), covalent attachment to the terminus of PEG lipids (**C**) or covalent attachment to the liposome surface (**D**).

5.3 Experimental Procedures

5.3.1 Materials

All reagents and solvents obtained from commercial suppliers were used without further purification. Hyaluronidase, Ovine Testicular, was obtained from Calbiochem (8130 U/mg, EMD Biosciences; La Jolla, CA). FITC-DSPE was synthesized as reported in **Chapter 3**.

5.3.2 Modification of Hyaluronidase for Covalent Attachment

Hyaluronidase was modified to contain additional sulfhydryls for covalent attachment to maleimide. Briefly, approximately 12.3 mg hyaluronidase (55 kDa) was dissolved to

0.6 mM in 0.4 mL reaction buffer (0.1 M $NaPO_4$, 50 mM NaCl pH 7.5) containing 4.2 mM Traut's reagent (2-iminothiolane). This solution was reacted for 1.5 hours at room temperature. The mixture was placed on a PD-10 desalting column (pre-packed G-25 M, GE Healthcare; Buckinghamshire, UK) to remove unreacted Traut's reagent and 0.5 mL fractions were collected. The protein concentration of each fraction was determined with the Bradford protein assay (absorbance 585 nm, Bio-rad; Hercules, CA).

Modified hyaluronidase was conjugated to either a polyhistidine tag or directly to the surface of liposomes. A polyhistidine-tag was added by dissolving the peptide (his_{10}-maleimide) in reaction buffer. Peptide was mixed at 3-fold molar excess to sulfhydryl-containing hyaluronidase and reacted overnight at room temperature. The hyaluronidase-his_{10} was purified from unmodified hyaluronidase on a HisTrapFF column (1 mL, GE Healthcare; Uppsala, Sweden). The protein was injected into the column and washed with 10 mL reaction buffer with 20 mM imidazole. His-tagged protein was eluted with 500 mM imidazole. Unreacted his-tag was removed by dialysis into sterile PBS in a 10,000 MWCO dialysis cassette (Slide-A-Lyzer, Thermo Scientific; Rockford, IL).

5.3.3 Formation of Liposomes

Liposomes were prepared by the sonication and extrusion method (*13*). Briefly, lipids dissolved in organic solvents were added to depyrogenated borosilicate glass tubes. Formulations for non-covalent association contained tris-NTA-DAP-DOD (POPC/Chol/mPEG/NTA 55:40:5:1, molar ratio). NTA lipids were pre-incubated with nickel as described in **Chapters 3** and **4**. Liposomes for covalent attachment contained

either maleimide-DSPE or maleimide-PEG(2000)-DSPE (POPC/Chol/mPEG/maleimide 55:40:5:3, molar ratio). All liposomes contained a total of 5 mol % mPEG(2000), unless noted. Solvent was evaporated while rotating under reduced pressure at room temperature to form a lipid film. Residual solvent was removed under high vacuum overnight. Films were then rehydrated in 1 mL HEPES buffer (20 mM HEPES, 140 mM NaCl, pH 7.4) with intermittent vortexing and sonicated under argon for 10 minutes at 23 ºC to form vesicles. Liposome diameter was reduced by serially extruding 11 times through 200 nm, 100 nm and 80 nm polycarbonate membranes with a hand-held extruder (Avestin; Ontario, Canada).

5.3.4 Association of Hyaluronidase-His_{10} with NTA-Containing Liposomes

For non-covalent liposome/protein association, hyaluronidase-his_{10} was added directly to NTA containing liposomes at 1:1 hyaluronidase per surface available NTA. It was assumed that NTA distributed evenly between the inner and outer liposome membrane surfaces. For a 20 mM solution of 1% tris-NTA-DAP-containing liposomes, 200 µL liposomes were mixed with 200 µL hyaluronidase-his_{10} (5 mg/mL in reaction buffer). Hyaluronidase-his_{10}/NTA-liposomes were allowed to associate for 1 hour at room temperature and stored at 4 ºC.

For co-association of proteins on the NTA-liposome, used in HA-gel diffusion studies, hyaluronidase-his_{10} and mKate-his_6 were mixed 3:1 (molar ratio) and incubated with NTA-liposomes overnight at 4 ºC. The final ratio of NTA to total protein was 1:1;

hyaluronidase-his_{10} should occupy 75% of the NTA and mKate-his_6 should occupy the remaining 25% of the NTA sites.

5.3.5 Covalent Attachment of Modified Hyaluronidase to Liposomes

For direct covalent attachment, sulfhydryl-containing hyaluronidase was added to freshly formed, maleimide-containing liposomes at 1:10 molar ratio of hyaluronidase to maleimide. For a 20 mM solution of 3% maleimide-liposomes, 200 μL liposomes were mixed with 200 μL hyaluronidase (1.6 mg/mL in reaction buffer). The reaction proceeded for 4 hours at room temperature. Excess free cysteine (10 μL of a 20 mg/mL solution of L-cysteine in PBS) was added to block unreacted maleimide and the mixture was incubated overnight at 4 ºC.

For animal experiments, liposomes were prepared at 60 mM lipid by hydrating films in sterile PBS, as described above. Liposome formulations (POPC:Chol:mPEG:maleimide 55:40:5:3) included a tritiated cholesteryl hexadecyl ether lipid to give 1 million DPM per dose. After liposomes were extruded serially through 100 and 80 nm polycarbonate membranes they were sterilized by passing through 0.22 micron filters (13mm PVDF syringe filter, Fisher Scientific; Santa Clara, CA). Hyaluronidase (250 μL of a 7.2 mg/mL solution in reaction buffer) was mixed with liposomes (500 μL) and reacted for 4 hours at room temperature. Free cysteine (20 μL of a 20 mg/mL solution of L-cysteine in PBS) was added and the mixture was reacted overnight at 4 ºC. Free protein was removed on a Sepharose CL-4B size exclusion column (8 x 1.5 cm bed pre-equilibrated in PBS). Liposome concentration was estimated based on the presence of

tritiated cholesteryl hexadecyl ether (Beckman LS600TA scintillation counter; Beckman Coulter, Fullerton CA). Protein concentration was determined by Bradford protein assay. Control liposomes were either admixed to give the same hyaluronidase concentration as maleimide-PEG liposomes or injected without protein.

5.3.6 Quantitation of Liposome-Protein Association or Attachment

Free hyaluronidase was removed from liposomes on a Sepharose CL-4B size exclusion column (8 x 1.5 cm bed) pre-equilibrated with PBS. Hyaluronidase covalently attached or non-covalently associated with liposomes, eluted in the void volume; unbound hyaluronidase eluted at larger column volumes. Fractions (0.5 mL) were collected and assayed for protein concentration using Bradford protein assay. Liposome concentration in each fraction was calculated from FITC-DSPE incorporated into the liposomes (0.1 mol %). A standard fluorescence curved, based on control liposomes of the same formulation, was used to calibrate liposome concentration (excitation/emission 485/520 nm, Fluorstar 403, BMG Labtechnologies; Durham, NC). This experiment was performed two or more times for each liposome formulation.

5.3.7 Hyaluronidase Activity Assay

Hyaluronidase activity was determined by measuring newly released, reducing end N-acetylglucosamine (*14*). Briefly, 125 µL HA stock (1.5 mg/mL HMW-HA in 0.1 M NaCl) was placed in 1.5 mL Eppendorf tubes with 5 µL enzyme in phosphate buffer (0.2 M NaH_2PO_4, 0.1 M NaCl pH 6). Sulfhydryl-containing hyaluronidase, hyaluronidase-his_{10} or hyaluronidase-liposomes were estimated to have 8130 U/mg

hyaluronidase (based on the Hyaluronidase, Ovine Testes Package Insert) for the purpose of initial dilution. Experimental samples were diluted to an expected 10 U (1.23 μg) per 5 μL in phosphate buffer. A standard curve consisting of 25 to 1 U fresh, unreacted hyaluronidase per 5 μL was run with each assay. Hyaluronidase was allowed to degrade the HA stock for 30 minutes, 1 hour and 2 hours at 37 ºC and heated at 100 ºC for 5 minutes. After cooling, tetraborate buffer was added to each tube (25 μL, 0.5 M $K_2B_4O_7$, pH 10.5) and the mixture was heated to 100 ºC for 3 minutes. DMAB (750 μL p-dimethylaminobenzaldehyde, 1 g/100 mL 87.5% glacial acetic acid 12.5% 10N HCl) was added, vortexed thoroughly to mix and incubated at 37 ºC for 20 minutes. Enzyme precipitate was removed by centrifugation at 8,000 x g for 10 minutes. Red chromogen (3-acetamido-5-(1,2-dihydroxyethyl)furane) absorbance was measured at 585 nm. For each time point, the standard curve was plotted for calibration of U hyaluronidase per chromogen absorbance. The activity of hyaluronidase in the sample was estimated from the curve and the average of the triplicate (one sample for each time point) was recorded.

5.3.8 Liposome Diffusion Through a Hyaluronan Gel

Columns of hyaluronan gel were prepared by heating a 20 mg/mL solution of HMW-HA to 60 ºC and loading the gel into a 9-inch, glass pasteur pipette (Fisher Scientific; US division) by applying a vacuum to the top of the pipette. After the pipette was filled, the bottom of the pipette was sealed with parafilm. The top of the gel was marked on the pipette. After cooling at 4 ºC overnight, the gel was warmed to 37 ºC. Hyaluronidase or hyaluronidase-liposomes (50 μL) were added to the surface of the hyaluronan gel and the top was sealed with parafilm to prevent evaporation.

Liposome movement through the gel was quantified using liposomes containing the fluorescent lipid, FITC-DSPE, or NTA-liposomes associated with a fluorescent protein, mKate-his_6. HA-gel columns were preheated to 37 ºC and liposomes with associated proteins were gently added onto the surface of HA-gel. Liposome movement was observed at various times after liposome addition on a Kodak 4000m Image Station (Eastman Kodak Company; Rochester, NY) for FITC fluorescence (excitation/emission 465 / 535 nm) and mKate fluorescence (excitation/emission 535 / 600 nm). Images were taken using the Kodak Molecular Imaging Software. The distance moved by the liposomes, not including initial starting height of the loaded liposomes, was recorded.

5.3.9 Hyaluronidase-Liposome Interactions with HA-Expressing Cells

C26 murine colon carcinoma cells were plated to be subconfluent or confluent the next day ($0.5 * 10^4$ or $5 * 10^4$ cells per well in a 12 well plate, respectively) and incubated at 37 ºC with 5% CO_2, overnight. The wells were washed with PBS and 500, 100 or 20 U/mL hyaluronidase or hyaluronidase-liposomes were added in 1 mL media (RPMI 1640 with 10% heat inactivated FCS). Liposomes without hyaluronidase were prepared as a control. After 3 hours at 37 ºC the cells were washed twice with PBS (1 mL) and remained in PBS for imaging. Cell morphology was monitored using phase-contrast white light. Liposome binding was visualized by FITC fluorescence (484/510 nm, Eclipse TS100 Nikon; Japan). Images were taken with a SPOT RT camera using SPOT Imaging Software (Diagnostic Instruments; Sterling Heights, MI). This experiment was performed in duplicate to ensure reproducibility.

5.3.10 Hyaluronidase-Liposome Half-Life and Biodistribution in Tumored Mice

All animal procedures were conducted in accordance with the policies of the UCSF Institutional Animal Care and Use Committee. Mice (Jackson Laboratories; Bar Harbor, ME) were housed in an official UCSF facility. During experimentation, mice were housed in UCSF approved laboratory conditions for periods not exceeding 48 hours.

BALB/c mice were subcutaneously injected with $3 * 10^5$ C26 cells in 50 μL PBS into their right flank. When tumors reached approximately 100 mm^3, mice were divided into treatment groups of 8 animals. These tumors grew more slowly than is typically seen with C26 flank tumors in BALB/c mice and were treated on day 18. Each group received 15 mM total lipid with 1 million DPM tritium in 200 μL via tail vein injection. Doses which contained liposomes admixed with hyaluronidase or liposomes with hyaluronidase conjugated via maleimide-PEG(2000) had 0.41 mg/mL hyaluronidase (3300 U/mL). Liposomes containing hyaluronidase conjugated via maleimide directly on the liposome surface had 0.21 mg/mL hyaluronidase (1700 U/mL). Control liposomes contained no hyaluronidase.

Blood (approximately 50 μL; less than 5% total blood volume) was obtained from submandibular cheek pouch bleeds at 5 minutes and 1 hour, 3 hours and 6 hours with a final bleed (0.5 to 1 mL; 30 to 60% total blood volume) and sacrifice at 24 or 48 hours. Treatment groups were split in half (4 animals) for blood draws, with each set receiving 2 blood draws before sacrifice. Tritium content in blood and tissue was measured after dissolution of the blood or tissue in Solvable (PerkinElmer; Waltham MA). Blood was

place in weighed scintillation vials and dissolved in 1 mL Solvable for 2 hours at 60 ºC. The solution was neutralized by adding 0.1 mL EDTA in water (0.1 M, pH 4.5) and decolorized by adding 0.3 mL H_2O_2 (30%) at room temperature and reacted for 15 minutes prior to reheating to 60 ºC for 30 minutes. After cooling to room temperature, 15 mL Ultima Gold (PerkinElmer; Waltham, MA) was added and the capped scintillation vial was inverted repeatedly to uniformly mix the contents. Radioactivity was quantitated in a Beckman scintillation counter (LS600TA; Beckman Coulter, Fullerton CA).

Lung, liver, spleen, kidney, muscle and tumor were collected and analyzed for accumulated radioactivity. Approximately 100 mg tissue was weighed in a glass scintillation vial. To this was added 1 mL Solvable and the tissues were dissolved overnight at 60 ºC. To estimate the total radioactivity recovered per organ, organ weight in the treated animals was based upon the average organ weight of three untreated animals. Total blood volume was estimated as 7% of the average weight of three untreated animals.

5.4 Results

5.4.1 Non-Covalent Association of Hyaluronidase with NTA- Liposomes

Sulfhydryl groups were added to the hyaluronidase using iminothiolane; sulfhydryl-containing hyaluronidase retained full activity (8374 ± 690 U/mg, 103% ± 8.5) as compared to unmodified hyaluronidase. The sulfhydryl-modified hyaluronidase

maintained stable activity levels over 24 hours at 37 ºC in refiltered fetal calf serum (Figure **5-2A**).

A his_{10}-maleimide peptide was covalently attached to the hyaluronidase via the sulfhydryl groups to engineer the non-covalent association of the hyaluronidase with NTA-containing liposomes. Hyaluronidase-his_{10} was not degraded by the modification process and appeared to have a slightly increased molecular weight in an SDS-PAGE gel, corresponding to an addition of 1-2 his_{10}-tags per protein (Figure **5-2B**). This gel displays multiple hyaluronidase bands per lane, corresponding to 75 and 35 kDa, which is commonly seen when hyaluronidase SDS-PAGE gels are run with reducing conditions corresponding to endoproteolytically cleaved, disulphide-linked fragments (*15-17*). Multiple bands are present in both the commercially obtained, unmodified- (far left lane) and his_{10}-modified hyaluronidase (middle lane).

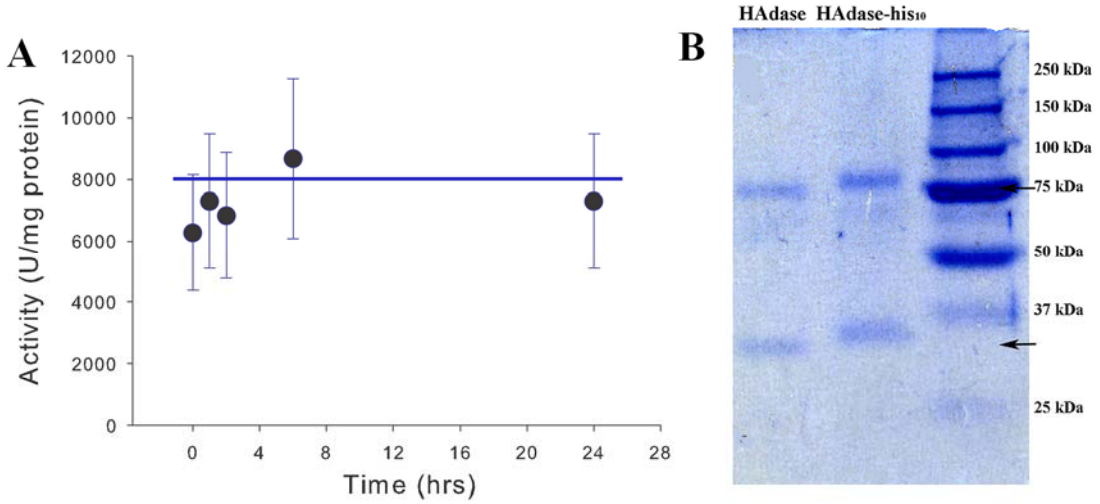


Figure 5-2. Effect of Covalent Modification on Hyaluronidase. Enzyme activity of hyaluronidase, modified to contain sulfhydryls, after incubation at 37 ºC in the presence of refiltered fetal calf serum. The solid line indicates expected activity for unmodified protein (**A**). SDS-PAGE gel of unmodified and hyaluronidase-his_{10}. Two hyaluronidase (HAdase) bands, indicated by arrows at 75 and 35 kDa, are present in each lane due to reduction conditions (average MW 55 kDa *(15-17)*) (**B**).

Hyaluronidase-his_{10} incubated with liposomes containing 1% tris-NTA-DAP fully associated with the liposome. No unassociated hyaluronidase was separated from the liposome associated on a size exclusion column (Table **5-1**). Each hyaluronidase contains at least one accessible his-tag for NTA association as hyaluronidase without his_{10}, or with inaccessible his-tags, were removed during purification of the his_{10}-modified hyaluronidase.

5.4.2 Covalent Attachment of Hyaluronidase to Liposomes

Hyaluronidase was first modified to contain additional sulfhydryls. Modified hyaluronidase was then conjugated directly to the liposome using a maleimide-DSPE or maleimide-PEG(2000)-DSPE. The maleimide-PEG(2000) is spaced above the mPEG(2000) coating while maleimide-DSPE remains shielded (Figure **5-1**). Control liposomes, containing 5 mol % mPEG(2000)-DSPE non-specifically adsorbed approximately 14% of the total hyaluronidase. Attachment efficiency of the covalent modification was 23% if the maleimide was on the liposome surface, below the mPEG, and 35% if the maleimide was present above the mPEG(2000)-DSPE (Table **5-1**). Hyaluronidase-liposome diameter and charge are similar to control liposomes with admixed hyaluronidase (Table **5-2**).

	Admixed	3% Maleimide	3% Maleimide-PEG	1% tris-NTA-DAP
% Associated	14.0 ± 1.4	22.7 ± 9.1	34.7 ± 6.5	100
Activity (U/mg)	8658 ± 3277	8211 ± 1610	8374 ± 1600	7114 ± 862
% Activity	106.5 ± 40.3	101.0 ± 19.8	103.0± 19.7	87.5 ± 10.6

Table 5-1. Hyaluronidase Association with Liposomes and Retained Enzymatic Activity. Amount of hyaluronidase associated with liposomes was determined by comparing liposome-conjugated protein versus total protein in fractions from a Sepharose CL-4B size exclusion column. Liposome-containing fractions were then pooled and assayed for retained hyaluronidase activity. Formulations consisted of POPC:Chol(55:40) with a total of 5% mPEG(2000)-DSPE and either 3% maleimide-DSPE, 3 mol % maleimide-DSPE or 1 mol % tris-NTA-DAP for non-covalent association. (n=2-6)

5.4.3 Enzymatic Activity of Hyaluronidase-Liposomes

During each assay, activity of the liposome-bound hyaluronidase was calibrated using a standard activity curve of unmodified hyaluronidase. All unbound hyaluronidase was removed from the liposome prior to the enzymatic assay. Hyaluronidase-liposomes degraded HMW-HA at the same rate as unmodified hyaluronidase, regardless of the association or conjugation method used (Table **5-1**). This data suggests that hyaluronidase activity was unaffected by presence near the surface of a liposome. Maleimide directly on the surface of the liposome, below the mPEG(2000), had a similar activity per μg protein as unmodified and hyaluronidase conjugated to liposomes via a PEG(2000) spacer.

	Control	3% Maleimide	3% Maleimide-PEG	1% tris-NTA-DAP
Diameter (nm)	79.7 ± 1.9	92.5 ± 4.0	101.9 ± 25.2	101.9 ± 15.7
ζ potential (mV)	-7.7 ± 4.0	-9.3 ± 5.7	-9.5 ± 7.6	-19.0

Table 5-2. Diameter and Zeta-Potential of Hyaluronidase-Liposomes. Formulations consisted of POPC:Chol(55:40) with a total of 5% mPEG(2000)-DSPE and either 3% maleimide-DSPE, 3 mol % maleimide-DSPE or 1 mol % tris-NTA-DAP for non-covalent association. Liposomes were extruded, incubated with hyaluronidase and purified on a Sepharose CL-4B size exclusion column. Fractions containing liposomes were pooled and measured for size and zeta-potential. (n=2-6)

5.4.4 Hyaluronidase Diffusion Through a Hyaluronan Gel

We hypothesized that active, liposome-bound hyaluronidase could mediate diffusion through a HA-rich environment by degrading the HA immediately surrounding the liposome. Hyaluronidase increased diffusion of the liposomes through a HA-gel (Figure **5-3**). The gel was unstirred during the experiment so movement can be attributed to the effects of degradation of HMW-HA. For hyaluronidase-liposomes with comparable activity (1000 U/mL) movement through the HA-gel proceeded at approximately 4 mm/day regardless of conjugation-method used (Figure **5-3C,D**).

Liposomes with tris-NTA-DAP contained both hyaluronidase-his_{10} and the fluorescent protein mKate-his_6. Visualization of the liposomes with mKate-his_6 showed movement of non-covalently associated hyaluronidase-his_{10} liposomes was similar to movement of control liposomes that are admixed with hyaluronidase-his_{10} and mKate-his_6 (Figure **5-3A**). The rate of movement was linear over the 24 hour incubation period (Figure **5-3C**).

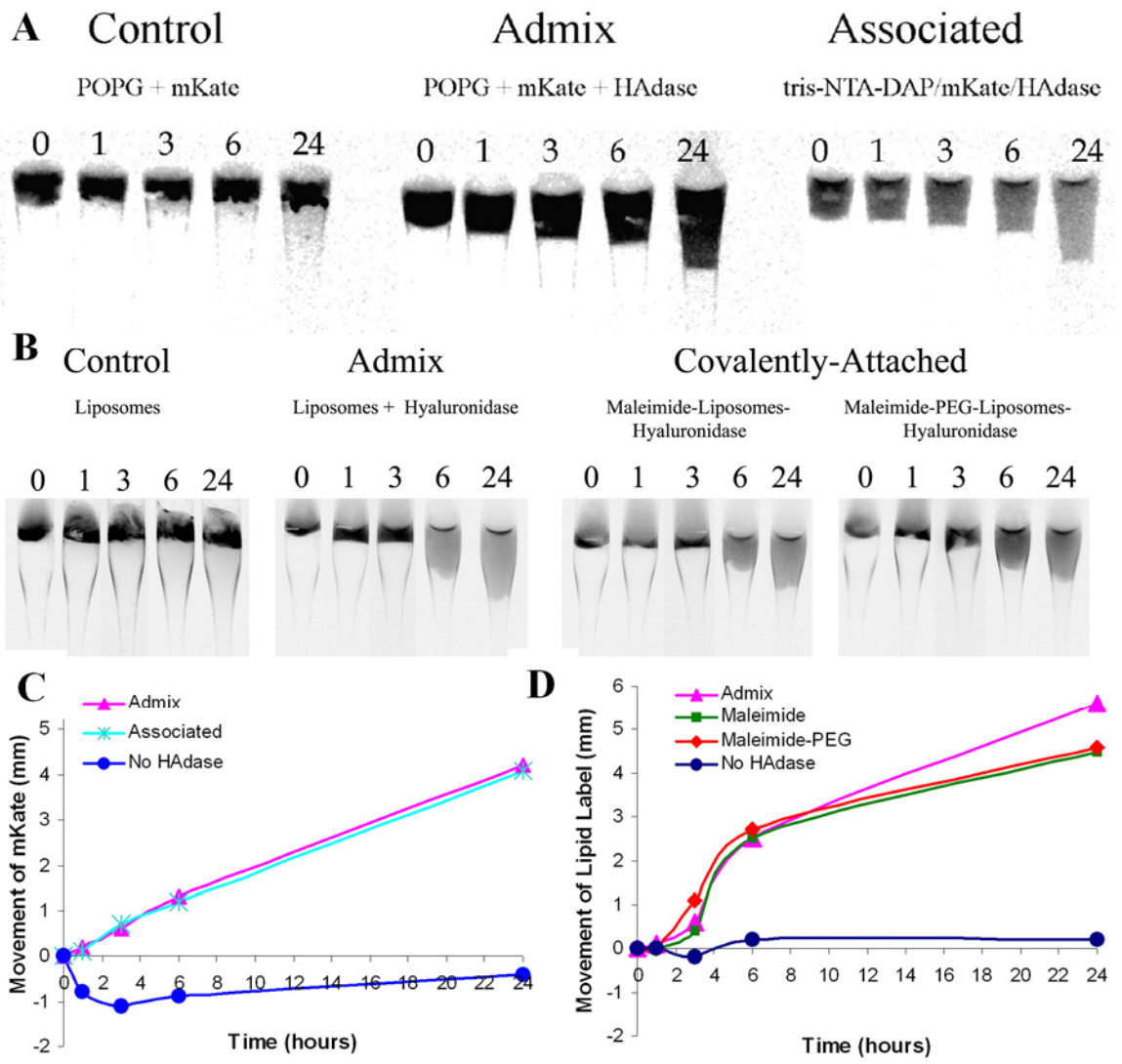


Figure 5-3. Hyaluronidase-Assisted Liposome Diffusion through an Hyaluronan-Gel (20 mg/mL) at 37 ºC over 24 hours. Hyaluronidase (HAdase) was either non-covalently associated via his_{10}/tris-NTA interactions (**A**) or covalently attached to maleimide-lipids within the liposome (**B**). Diffusion of non-covalent liposomes was visualized using a secondary his_6-containing protein (mKate, excitation/emission 535/600 nm) (**A**). Covalently modified liposomes were visualized with FITC-DSPE lipid within the liposome (excitation/emission 465/535 nm) (**B**). Each sample contained 50 µL10 mM liposome and 1000 U/mL hyaluronidase. Movement of the hyaluronidase-liposomes was calculated by their change in position (in mm) over time for hyaluronidase non-covalently associated (-*-) (**C**) or covalently attached via either maleimide-DSPE (-■-) or maleimide-PEG(2000)-DSPE (-♦-) (**D**) bound hyaluronidase. Control liposomes were either injected without protein (-●-) or admixed with hyaluronidase (-▲-).

Covalent hyaluronidase-liposomes moved through the HA-gel at a rate similar to control liposomes admixed with unmodified hyaluronidase (Figure **5-3B**). Hyaluronidase accessed the HA-gel regardless of whether it was conjugated below or above the mPEG(2000). The average movement of covalently modified hyaluronidase-liposomes was also approximately 4 mm per day; however, the movement was non-linear. The control liposomes exhibited the same movement pattern (Figure **5-3D**) suggesting the rate of movement was influenced by inconsistent environmental factors, such as slight mixing. In HA-gel columns, hyaluronidase-liposomes formed from either covalently attached or non-covalently associated hyaluronidase moved at the same rate as control liposomes admixed with hyaluronidase.

5.4.5 Hyaluronidase-Liposome Binding to HA-Expressing Cells

We hypothesized that hyaluronidase on the surface of liposomes could mediate cell-binding through the interaction with the HA-rich extracellular matrix. Murine C26 colon carcinoma cells express HMW-HA while in cell culture. Cells were plated one day prior to liposome exposure to attain low confluency (Figure **5-4B**) and high confluency (Figure **5-4D**) to compare the effects of cell density on liposome binding. Hyaluronidase-conjugated liposomes bound to HA-producing cells in culture (Figure **5-4B**) at both cell densities. Liposomes admixed with hyaluronidase did not bind (Figure **5-4E**). Only liposomes at the highest concentration (500 U hyaluronidase / mL) were able to bind. Hyaluronidase-liposomes at lower concentrations (100 U and 20 U hyaluronidase/mL) did not visibly bind more than control liposomes. Hyaluronidase, either free or liposome-conjugated, did not affect the morphology of cells over 3 hours at 37 ºC.

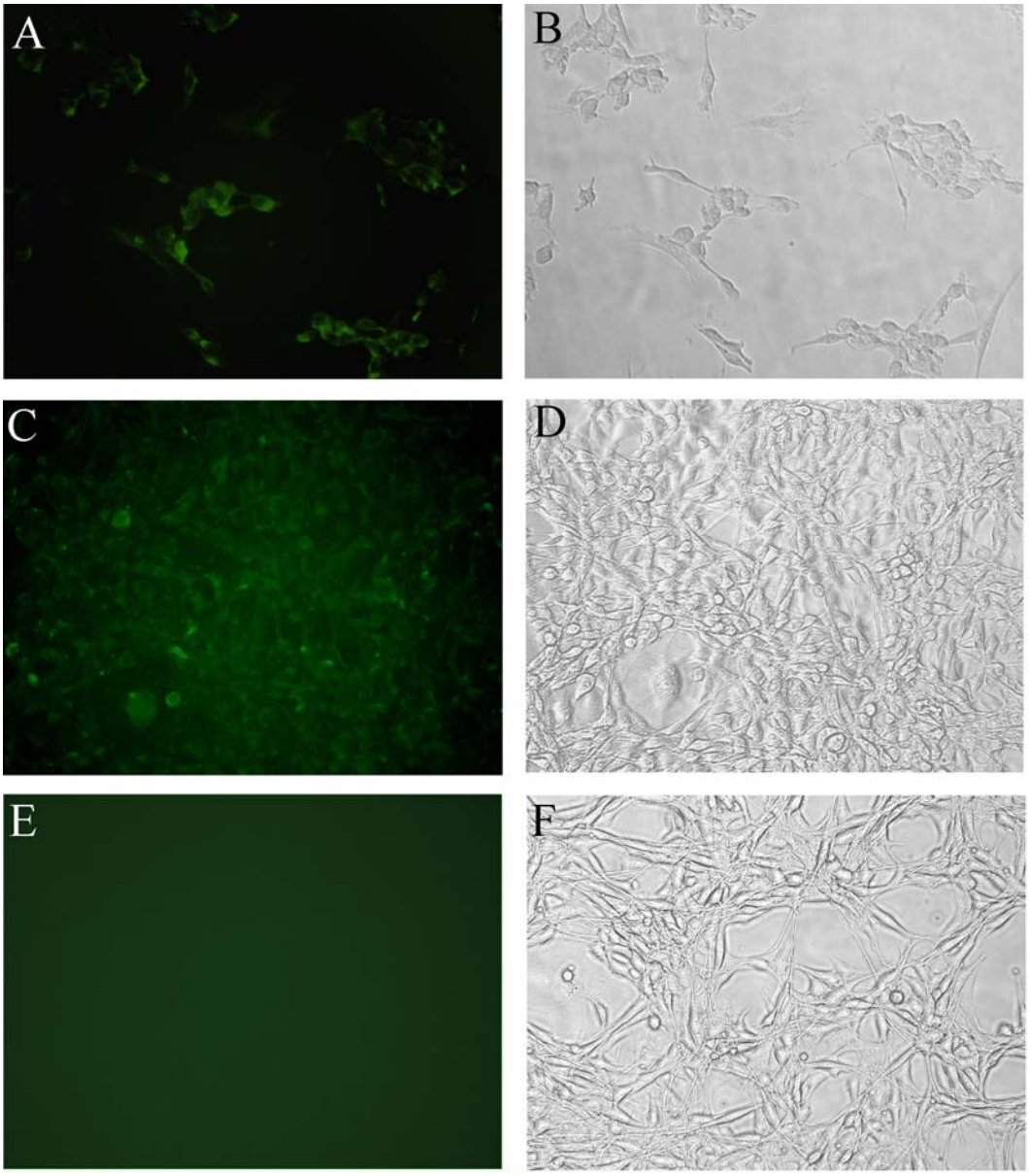


Figure 5-4. Cell Binding of Hyaluronidase-Liposomes containing 3% maleimide-PEG(2000)-DSPE lipid (**A-D**) to C26 colon carcinoma cells. Free hyaluronidase was removed prior to liposome/cell binding. Cells were plated at low (**A,B**) and high (**C-F**) confluence. Control liposomes were admixed with free hyaluronidase (**E,F**). Liposomes were visualized with FITC-DSPE fluorescence (emission/excitation 460-500/510-560 nm).

5.4.6 Hyaluronidase-Liposome Half-Life and Biodistribution in Tumored Mice

We hypothesized that hyaluronidase could also mediate liposome binding to the tumor extracellular matrix when injected intravenously. As previous studies have shown that proteins are not retained by NTA-liposome in circulation, only liposomes with covalently attached hyaluronidase were included in the *in vivo* study. Liposomes with hyaluronidase covalently attached to the surface, either directly or via a PEG(2000) spacer, resulted in liposomes that circulated with an α half-life of approximately 45 minutes (Figure **5-5**, Table **5-3**). The half-life of control and admixed liposomes, 10.4 and 10.2 hours respectively, was estimated based on single rate elimination kinetics (Table **5-3**). For liposomes conjugated to hyaluronidase, a β half-life of approximately 8.3 hours was determined using biphasic elimination.

Quantitation of radioactivity in lung, spleen, liver, kidney, muscle and tumor indicated that liposomes with covalently modified hyaluronidase accumulated in the liver and spleen more rapidly than control or admixed liposomes (Figure **5-6**, Table **5-4**). Muscle, a control organ, showed limited uptake of all liposome formulations. At 24 hours hyaluronidase conjugated to liposomes via maleimide-PEG(2000) accumulated to approximately 2-fold higher concentrations in liver than the control liposomes. Hyaluronidase-liposomes showed decreased tumor accumulation; 3 to 4-fold fewer radioactive counts were present in the tumors at both 24 and 48 hours compared to control liposomes.

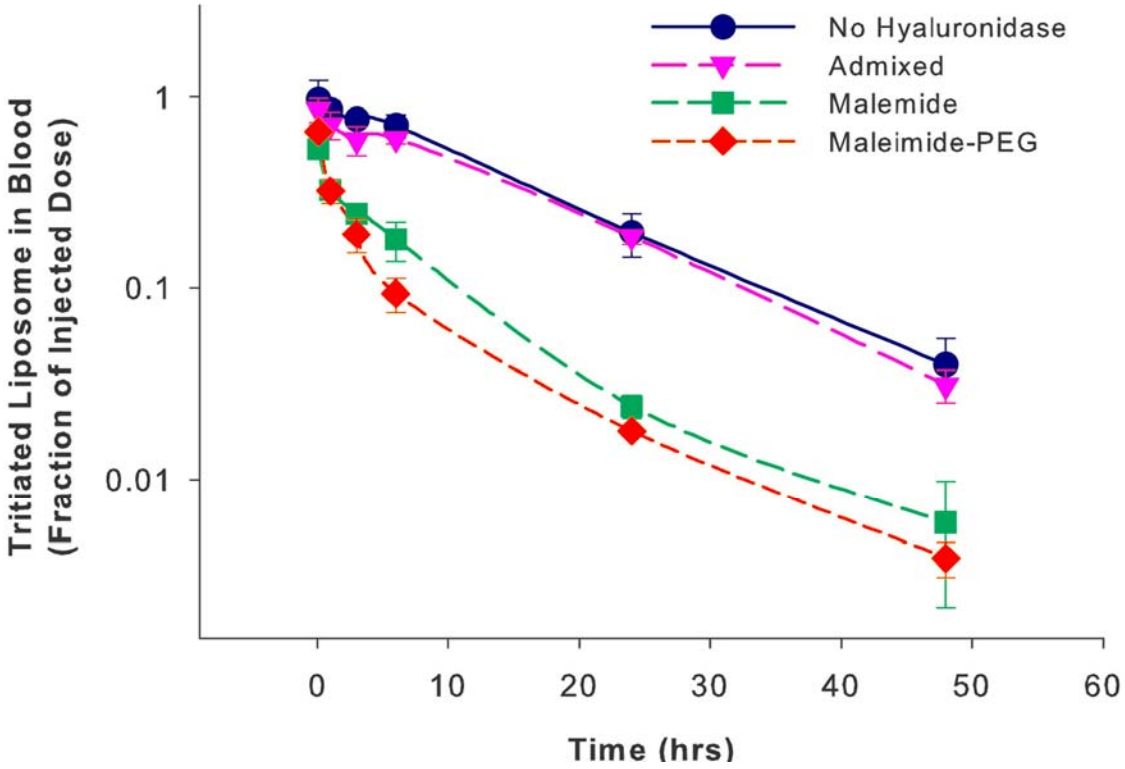


Figure 5-5. ***In vivo*** **Fraction of Injected Liposome Dose in Blood as a Function of Time** of hyaluronidase-liposomes in BALB/c mice bearing C26 subcutaneous flank tumors. Liposomes contained tritiated cholesteryl hexadecyl ether for radioactive measurements. Formulations included a total of 5% mPEG(2000)-DSPE and either 3% maleimide-DSPE (-■-) or maleimide-PEG(2000)-DSPE (-♦-) conjugated hyaluronidase. Unbound protein was removed prior to injection. Control liposomes were either injected without protein (-●-) or admixed with hyaluronidase (-▼-). Each dose consisted of 15 mM lipid and 1700-3500 U hyaluronidase per 200 µL PBS. (n=4)

	Half-life (hrs)	R^2
No Hyaluronidase	10.4	.9984
Admixed	10.2	.9915

	α Half-life (hrs)	R^2	β Half-life (hrs)	R^2
Maleimide	0.79	.8110	8.3	.9744
Maleimide-PEG	0.82	.9246	8.4	.9737

Table 5-3. Half-Life of Hyaluronidase-Liposomes within the circulation of BALB/c tumor-bearing mice was estimated based on linear data fitting of transformed data. Control liposomes without hyaluronidase and liposomes admixed with hyaluronidase were fit as a single-phase exponential decay. Maleimide and maleimide-PEG(2000) liposomes were assumed to exhibit a biphasic exponential decay. R^2 indicates strength of log-linear fit of the exponential curves.

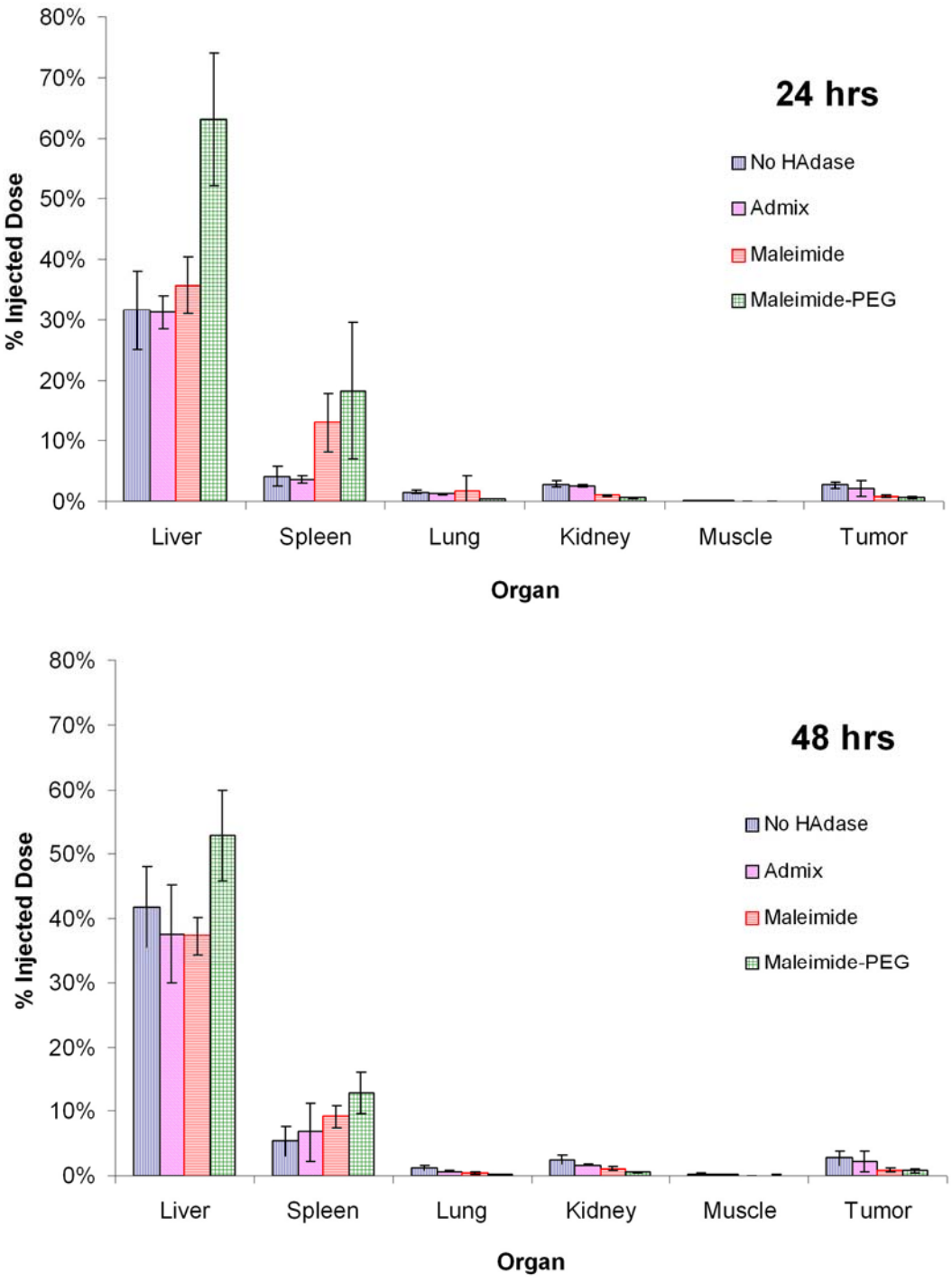


Figure 5-6. Biodistribution of Hyaluronidase-Liposomes at 24 and 48 hours post-intravenous injection into BALB/c mice bearing C26 subcutaneous flank tumors. Liposomes contained tritiated cholesteryl hexadecyl ether for radioactive measurements. (n=4)

24 hrs	No HAdase	Admixed	Maleimide	Maleimide-PEG
Liver	315537 ± 64791	312041 ± 27193	357511 ± 46473	631609 ± 108705
Spleen	41631 ± 16036	36776 ± 5870	130026 ± 47776	182622 ± 111889
Lung	15888 ± 2563	12745 ± 1024	17004 ± 24817	4027 ± 395
Kidney	28782 ± 6086	25041 ± 2305	10221 ± 1322	6198 ± 1064
Muscle	1446 ± 189	1247 ± 243	641 ± 236	387 ± 88
Tumor	27060 ± 4608	21462 ± 13782	8625 ± 1438	5772 ± 1800

48 hrs	No HAdase	Admixed	Maleimide	Maleimide-PEG
Liver	418157 ± 63042	375851 ± 76915	372878 ± 29054	528654 ± 70559
Spleen	53555 ± 23317	67878 ± 44786	91814 ± 17320	128705 ± 32702
Lung	11524 ± 4116	6816 ± 1151	3720 ± 2685	2059 ± 947
Kidney	24635 ± 6702	16885 ± 870	10583 ± 3367	5804 ± 1137
Muscle	2199 ± 897	1071 ± 95	638 ± 157	847 ± 368
Tumor	27926 ± 10936	22488 ± 15605	8728 ± 2571	7276 ± 2579

Table 5-4. Amount of Tritiated Hyaluronidase-Liposome Per Organ in BALB/c tumor-bearing mice at 24 and 48 hours. Values are reported as the average DPM (disintegrations per minute) per organ. (n=4)

5.5 Discussion

Hyaluronidase can degrade the HA-rich extracellular matrix of tumors in a way that improves the uptake and diffusion of macromolecules (*8, 10-12*). Nanoparticles, high-molecular weight saccharides and small molecule dyes had increased intratumoral dispersion when co-injected intratumorally with hyaluronidase (*10, 12*). Liposomes in the presence of hyaluronidase could exploit increased permeability of the tumor extracellular matrix (*8, 12*) to permeate further into the tumor.

To determine if hyaluronidase bound to the surface of liposomes could directly mediate tumor targeting or intratumoral translocation in animals, I engineered three types of hyaluronidase-containing liposomes: hyaluronidase-his_{10} which non-covalently associated with NTA-liposomes, hyaluronidase conjugated to the liposome surface via a maleimide and hyaluronidase conjugated to the liposome via a PEG(2000) linker. I characterized the effect of hyaluronidase-liposome attachment on hyaluronidase activity and determined if hyaluronidase present on the liposome surface could mediate diffusion of liposomes within an HA-gel or cause binding of the liposomes to HA-expressing cells in culture. With mice bearing a subcutaneous, HA-expressing colon carcinoma, I evaluated hyaluronidase-liposome clearance from the blood and tumor accumulation.

Hyaluronidase modified to contain sulfhydryls was active in a solution containing refiltered fetal calf serum at 37 ºC for 24 hours (Figure **5-2A**). When the enzyme was attached to the surface of PEGylated liposomes, it retained full enzymatic activity (Table **5-2**), whether the hyaluronidase was non-covalently associated or covalently attached

(Figure **5-1**). Liposome-attachment did not prevent hyaluronidase from interacting with, and degrading, the HA-gel substrate (Figure **5-3**). Liposomes with surface associated or attached hyaluronidase could diffuse through the HA-gel at approximately the same rate as liposome admixed with free, unmodified hyaluronidase. Further, hyaluronidase-liposomes conjugated via a PEG(2000) spacer were able to bind HA expressing C26 colon carcinoma cells while in culture (Figure **5-4A**).

Without a carrier, intravenously injected hyaluronidase (500 or 5000 U/kg) had a circulation half-life of 2-10 minutes (*18, 19*). At lower doses (500 U/kg) in dogs and humans the half life was 2-3 minutes. At higher doses (5000 U/kg) in dogs, the half-life of hyaluronidase exhibited two phases. The half-life was 2 minutes for the first 7 minutes and then increased to 9 minutes at later time points (*18*). We sought to determine if attaching hyaluronidase to the surface of a liposome could increase hyaluronidase half-life in circulation. Attaching proteins, such as superoxide dismutase, to liposomes improved their therapeutic efficacy by increasing half-life in circulation (*20, 21*). In the case of superoxide dismutase, circulation increased from minutes to hours and the protein accumulated in inflamed tissues, improving its therapeutic effect (*21*).

Control liposomes and liposomes admixed with hyaluronidase had half-lives of 10.4 and 10.2 hours, respectively. Hyaluronidase-liposomes, conjugated directly to the surface or via a PEG(2000) linker, were cleared with a half-life of approximately 45 minutes (Figure **5-5**, Table **5-3**). Although, the presence of hyaluronidase decreased the circulation half-life of conjugated liposomes 10-fold, the circulation of conjugated

hyaluronidase is 2-10 fold longer than the reported values for free hyaluronidase (*18*). Liposome attachment may improve circulation time compared to the free protein. However, the comparison between free protein and liposome-conjugated protein was not directly made in this study. Non-covalent association of proteins with NTA-liposomes did not decrease liposome half-life in circulation; however, tris-NTA-liposomes did not increase the circulation time of his-tagged protein (**Chapter 3**). Thus, the behavior of hyaluronidase-liposome formed using non-covalent association was not studied *in vivo*.

Fewer liposomes with covalently-attached hyaluronidase trafficked from circulation into the tumor than control liposomes, potentially due to rapid clearance from the blood (Figure **5-5, 5-6**). Liposomes accumulated primarily in the liver regardless of hyaluronidase conjugation. Approximately 3% of the total dose of control liposomes and liposomes admixed with hyaluronidase accumulated in the tumor at 48 hours. Less than 1% of the total liposome dose accumulated in the tumor of animals injected with hyaluronidase-conjugated liposomes (Figure **5-5,** Table **5-4**).

Our results indicate that hyaluronidase-liposomes are active *in vitro* but are cleared rapidly from circulation when injected intravenously. Though shielded below the mPEG(2000)-DSPE, hyaluronidase conjugated directly to the liposome surface was cleared as rapidly as hyaluronidase conjugated via a PEG(2000) spacer (Figure **5-1** and Figure **5-5**). Both liposomes degraded a hyaluronan gel and diffused at approximately the same rate as admixed liposomes (Figure **5-4**).

Direct PEGylation of recombinant human hyaluronidase increased blood circulation from 1 hour to over 20 hours in mice and increased elimination of tumor extracellular HA in murine PC3 models of prostate cancer (*22*). Multiple intravenous injections of high hyaluronidase doses (150,000 U/kg or approximately 4 mg/kg) decreased growth of PC3 prostate cancer tumors in a manner that was related to the loss of extracellular matrix HA (*23*). PEGylated hyaluronidase was administered with Doxil, a long-circulating, PEGylated liposome doxorubicin formulation. Hyaluronidase treatment decreased the interstitial fluid pressure within HA expressing tumors but not HA negative, control tumors. Repeated intravenous dosing of PEGylated hyaluronidase (7 doses of 10,000 U/mouse at 2 day intervals) with three doses of Doxil (6 mg/kg at weekly intervals) prevented tumor growth as compared to Doxil or hyaluronidase treatment alone (*24*). The prolongation of hyaluronidase half-life by incorporating PEG suggests that macromolecular carriers may also be a feasible route for increasing hyaluronidase circulation time.

It is encouraging that attachment of the hyaluronidase to the surface of liposomes increases the circulatory lifetime of the enzyme. However the half-life of the liposome was greatly decreased. The consequence is that the amount of liposomes accumulating in the tumor was greatly reduced compared to unmodified liposome. Thus, we were not able to determine if there was enhancement of tumor penetration by degradation of the HA-matrix due to hyaluronidase attachment to the liposome.

Studies which utilized multi-day intravenous injections of high hyaluronidase doses (10,000 U/kg) improved Doxil uptake in a manner which decreased tumor growth (*24*). Lower hyaluronidase doses injected either intratumorally or intravenously increased accumulation and dispersion of macromolecules in tumors. The hyaluronidase doses used in these studies were typically 1500-1600 U per animal (*8, 9, 11, 12*). Studies in which fewer units (0.5 – 25 U per animal) were used increased the penetration of co-injected dye, adenoviral expression cassettes and nanoparticles compared to treatments without hyaluronidase (*10*).

Although we injected fewer units of hyaluronidase (approximately 700 U per animal) than was used in many of the previous studies, direct conjugation of the hyaluronidase to the surface of the liposome may be effective at inducing intratumoral motility because the surface-attached hyaluronidase will remove HMW-HA directly around the liposome. Thus, hyaluronidase-liposomes may not require as high a concentration as studies in which the hyaluronidase was injected separately from the macromolecule (*9, 11, 12*). Although only 1% of the administered hyaluronidase-liposome dose reached the tumor in this study, that accounts for approximately 7 U hyaluronidase within the tumor. This is a similar dose to studies which achieved improved spreading of nanoparticles and high molecular weight saccharides (*10*). Reducing the amount of hyaluronidase conjugated to the liposome surface may reduce liposome clearance from circulation and still exhibit HA targeting or degradation activity to improve intratumoral translocation.

5.6 Acknowledgements and Author Contributions

Our greatest appreciation is extended to Katherine Jerger for her assistance with cell culture and animal experiments, Doug Watson for supplying the maleimide-polyhistidine and Kareen Riviere for synthesizing the FITC-DSPE lipid.

5.7 Literature Cited

(1) Toole, B. P. (2004) Hyaluronan: from extracellular glue to pericellular cue. *Nat Rev Cancer 4*, 528-39.

(2) Tammi, R., Saamanen, A. M., Maibach, H. I., and Tammi, M. (1991) Degradation of newly synthesized high molecular mass hyaluronan in the epidermal and dermal compartments of human skin in organ culture. *J Invest Dermatol 97*, 126-30.

(3) Zhou, B., Weigel, J. A., Fauss, L., and Weigel, P. H. (2000) Identification of the hyaluronan receptor for endocytosis (HARE). *J Biol Chem 275*, 37733-41.

(4) Harris, E. N., Kyosseva, S. V., Weigel, J. A., and Weigel, P. H. (2007) Expression, processing, and glycosaminoglycan binding activity of the recombinant human 315-kDa hyaluronic acid receptor for endocytosis (HARE). *J Biol Chem 282*, 2785-97.

(5) Naor, D., Nedvetzki, S., Golan, I., Melnik, L., and Faitelson, Y. (2002) CD44 in cancer. *Crit Rev Clin Lab Sci 39*, 527-79.

(6) Stern, R., and Jedrzejas, M. J. (2006) Hyaluronidases: their genomics, structures, and mechanisms of action. *Chem Rev 106*, 818-39.

(7) Shuster, S., Frost, G. I., Csoka, A. B., Formby, B., and Stern, R. (2002) Hyaluronidase reduces human breast cancer xenografts in SCID mice. *Int J Cancer 102*, 192-7.

(8) Brekken, C., and de Lange Davies, C. (1998) Hyaluronidase reduces the interstitial fluid pressure in solid tumours in a non-linear concentration-dependent manner. *Cancer Lett 131*, 65-70.

(9) Brekken, C., Hjelstuen, M. H., Bruland, O. S., and de Lange Davies, C. (2000) Hyaluronidase-induced periodic modulation of the interstitial fluid pressure increases selective antibody uptake in human osteosarcoma xenografts. *Anticancer Res 20*, 3513-9.

(10) Bookbinder, L. H., Hofer, A., Haller, M. F., Zepeda, M. L., Keller, G. A., Lim, J. E., Edgington, T. S., Shepard, H. M., Patton, J. S., and Frost, G. I. (2006) A recombinant human enzyme for enhanced interstitial transport of therapeutics. *J Control Release 114*, 230-41.

(11) Erikson, A., Tufto, I., Bjonnum, A. B., Bruland, O. S., and de Lange Davies , C. (2008) The impact of enzymatic degradation on the uptake of differently sized therapeutic molecules. *Anticancer Res 28*, 3557-66.

(12) Eikenes, L., Tari, M., Tufto, I., Bruland, O. S., and de Lange Davies, C. (2005) Hyaluronidase induces a transcapillary pressure gradient and improves the distribution and uptake of liposomal doxorubicin (Caelyx) in human osteosarcoma xenografts. *Br J Cancer 93*, 81-8.

(13) Szoka, F., Olson, F., Heath, T., Vail, W., Mayhew, E., and Papahadjopoulos, D. (1980) Preparation of unilamellar liposomes of intermediate size (0.1-0.2 μmol) by a combination of reverse phase evaporation and extrusion through polycarbonate membranes. *Biochim Biophys Acta 601*, 559-71.

(14) Reissig, J. L., Storminger, J. L., and Leloir, L. F. (1955) A modified colorimetric method for the estimation of N-acetylamino sugars. *J Biol Chem 217*, 959-66.

(15) Hunnicutt, G. R., Mahan, K., Lathrop, W. F., Ramarao, C. S., Myles, D. G., and Primakoff, P. (1996) Structural relationship of sperm soluble hyaluronidase to the sperm membrane protein PH-20. *Biol Reprod 54*, 1343-9.

(16) Szepfalusi, Z., Nentwich, I., Dobner, M., Pillwein, K., and Urbanek, R. (1997) IgE-mediated allergic reaction to hyaluronidase in paediatric oncological patients. *Eur J Pediatr 156*, 199-203.

(17) Afify, A. M., Stern, M., Guntenhoner, M., and Stern, R. (1993) Purification and characterization of human serum hyaluronidase. *Arch Biochem Biophys 305*, 434-41.

(18) Wolf, R. A., Chaung, L. Y., O'Hara, D., Smith, T. W., and Muller, J. E. (1982) The serum kinetics of bovine testicular hyaluronidase in dogs, rats and humans. *J Pharmacol Exp Ther 222*, 331-7.

(19) Earnshaw, J. S., Curtis, C. G., Powell, G. M., Dodgson, K. S., Olavesen, A. H., and Gacesa, P. (1985) The fate of intravenously administered highly purified bovine testicular hyaluronidase (Hyalosidase) in the rat. *Biochem Pharmacol 34*, 2199-203.

(20) Turrens, J. F., Crapo, J. D., and Freeman, B. A. (1984) Protection against oxygen toxicity by intravenous injection of liposome-entrapped catalase and superoxide dismutase. *J Clin Invest 73*, 87-95.

(21) Gaspar, M. M., Boerman, O. C., Laverman, P., Corvo, M. L., Storm, G., and Cruz, M. E. (2007) Enzymosomes with surface-exposed superoxide dismutase: in vivo behaviour and therapeutic activity in a model of adjuvant arthritis. *J Control Release 117*, 186-95.

(22) Thompson, C., Osgood, R., Jiang, P., Kadhim, S., Wang, S., Symons, R., Quimbon, A., Radi, A., Bee, W., and Frost, G. I. (2008) Intravenous administration of recombinant human hyaluronidase (rHuPH20 modulates tumor interstitial fluid pressure and pericellular hyaluronan in a human prostate carcinoma xenograft model. *American Association for Cancer Research Annual Meeting San Diego, CA*, Halozyme Poster 2292.

(23) Kadhim, S., Jiang, P., Fu, G., Araiza, F., Symons, R., Bahn, J., Osgood, R., Quimbon, A., Radi, A., Thompson, C., O'Connor, P. M., and Frost, G. I. (2009) PEGPH20: PEGylated Human Recombinant PH20 Hyaluronidase shows significant antitumor activity concomitant with hyaluronan reduction in the PC3 hormon refractory prostate cancer model. *American Association for Cancer Research Annual Meeting Denver, CO*, Halozyme Poster 8569.

(24) Kadhim, S., Fu, G., Thompson, C., Jiang, P., Osgood, R., Nekoroski, T., Radi, A., Bee, W., and Frost, G. I. (2008) Synergistic anti-tumor effect of pegylated recombinant human hyaluronidase (PEGrHuPH20) with cytotoxic agents following intravenous administration in a hormone refractory prostate cancer xenograft model. *American Association for Cancer Research Annual Meeting San Diego, CA* Halozyme Poster A45.

Chapter 6

Conclusions and Future Outlook

6.1 Summary of Finding

The goal of this dissertation project was to investigate methods to develop liposomal anti-cancer drugs that take advantage of abnormal hyaluronan (HA) biology. In some cancers, the extracellular matrix HA and cell-surface CD44 are expressed differently than in healthy tissue and these differences can be used to target anti-cancer therapeutics (*1*). Overexpression of CD44 on the surface of cancer cells can be targeted by hyaluronan-modified liposomes (*2-5*). The HA-rich extracellular matrix surrounding tumors is overexpressed in some cancers (*6*). This multivalent ligand is accessible to matrix-targeted liposomes in circulation due to the compromised capillaries found in tumors (*7, 8*). In this dissertation, I have described methods to target liposomes to cancer using hyaluronan oligosaccharides (**Chapter 2**) or the protein hyaluronidase (**Chapter 5**). To simplify the processes used to form protein-functionalized liposomes, I investigated the utility of nitrilotriacetic acid (NTA)-liposomes for non-covalent, his-tagged protein association (**Chapters 3** and **4**).

To better understand the HA oligosaccharide length necessary for specific targeting of liposomes to CD44 overexpressed on the surface of cancer cells, I formulated liposomes containing HA-lipid conjugates of defined oligosaccharide number. In **Chapter 2**, I describe the synthesis and characterization of mono-dispersed HA oligosaccharide-lipid conjugates. These lipid conjugates contained HA-O from 4 to 8 monosaccharides in length; the minimum estimated HA saccharide that binds CD44 is below 10 saccharides.

The yield for lipooligosacchrides was 40 – 60 % after purification. However, specific binding of liposomes containing these lipooligosaccharides to CD44-overexpressing cell types was not attained. This study contributed to our understanding of the minimum HA/CD44 binding length when the oligosaccharide is conjugated to a drug carrier but did not synthesize a ligand with a sufficient HA-O number to determine an exact minimum binding length. Advanced conjugation methods will need to be developed that resolve the diverse solubility requirements of the oligosaccharide/lipid conjugation pair. These ligands are necessary to determine the minimum saccharide number required for HA-mediated liposome binding to CD44-overexpressing cancer cell types.

To improve the ease of formulating protein/drug carriers, I studied his_6-proteins associated with multivalent-NTA liposomes in **Chapters 3** and **4**. In **Chapter 3,** I evaluated the stability and longevity of the interaction between his_6-proteins and NTA-liposomes *in vitro* and *in vivo*. Mono- and tris-NTA liposomes robustly associated two types of his-tagged proteins, mKate and yCD, without decreasing protein activity. When challenged with a surrogate biological condition, liposomes containing either of two tris-NTA lipids retained proteins for a longer period than mono-NTA liposomes. His-tagged proteins of differing affinities for tris-NTA could exchange for NTA positions on the liposome surface, revealing the dynamic nature of the his_6/tris-NTA interaction. Despite the higher affinity of tris-NTA than mono-NTA for his-tagged proteins (K_D ~ 0.2 nM and 10 μM, respectively), tris-NTA-liposomes did not increase the circulation time of associated protein, compared to free protein.

To determine if avidity of the his_6-protein/NTA-liposome interaction influences the magnitude of immune response to his-tagged antigens in mice, I evaluated several formulations of strong and weak antigens with liposomes. In **Chapter 4**, I compared the adjuvant capabilities of liposomes containing mono-NTA or tris-NTA lipids to the capability of liposomes in which antigens were covalently-attached to or admixed with the liposomes. A peptide derived from the membrane proximal region (MPR) of the HIV envelope protein was synthesized with an additional his_6. Ovalbumin, a model antigen, was modified to contain a his_{10} by non-specific sulfhydryl addition followed by covalent modification with a maleimide-his_{10} peptide. Ovalbumin-his_{10} associated with NTA-liposomes. Non-covalent association of his-tagged antigens with liposomes containing either mono- or tris-NTA increased the immune response in mice of the peptide antigen N-MPR over admixed antigen with liposomes. For both ovalbumin- and MPR-containing liposome formulations, covalent-conjugation of the adjuvant to the liposome resulted in higher immune responses to the antigen. Non-covalent association with liposomes did elicit immune response to the antigen but there was not a significant difference of the immune response when the antigen/liposome formulation included either mono-NTA or tris-NTA lipids. Antigen association with the liposome was important for immune response generation; however the strength of interaction between the his-tagged antigen and the NTA-liposome did not appear to directly correlate to the strength of immune response.

To establish the effect of surface-attached hyaluronidase on the behavior of conjugated liposomes in a HA-rich environment and to see if these liposomes could be used as a tumor targeting agent, I formulated and characterized hyaluronidase-liposomes. In

Chapter 5, I functionalized liposomes with hyaluronidase using both non-covalent and covalent modification techniques. Hyaluronidase was modified to include additional sulfhydryls. Maleimide-lipids were then used to conjugate the hyaluronidase to the liposome. Alternately, the sulfhydryls were used to conjugate a maleimide-his_{10} to engineer non-covalent association with NTA-liposomes. Hyaluronidase on the surface of liposomes retained activity in solution and was able to degrade an HA-gel. When the covalently-attached hyaluronidase was spaced away from the surface of the liposome with a PEG(2000) linker, the liposomes could bind to the surface of hyaluronan expressing cells in culture. Covalent surface attachment of the sulfhydryl modified hyaluronidase to liposomes successfully increased the length of circulation time of hyaluronidase in mice.

6.2 Future Directions

Two methods to target liposomes to tumors were investigated in this dissertation: hyaluronan oligosaccharides and the protein hyaluronidase. Proteins are available which may target to CD44 overexpressed on the surface of cancer cells or directly to the HA-rich extracellular matrix.

Hyaluronidase may act as both a targeting ligand to the HA-rich extracellular matrix and an aid to increasing liposome permeability into tumors. The work done in **Chapter 5** suggests that hyaluronidase, which remains active when covalently conjugated to the liposome surface, could aid in intratumoral diffusion after it has reached the tumor extracellular matrix from the blood circulation. Future studies should work toward

further increasing the hyaluronidase-liposome circulation, which may involve further shielding the surface attached hyaluronidase or utilizing PEGylated hyaluronidase (*9*).

Other proteins could be used to target the blood-accessible, HA-rich extracellular matrix surrounding cancer cells. TSG6-Link consists of the hyaluronan binding domain of the protein of tumor necrosis factor stimulated gene 6 (TSG-6) (*10*). This hyaluronan binding protein was produced as a fusion construct with yCD, the prodrug converting enzyme used in **Chapter 3**, and injected intratumorally into mice with C26 flank tumor. Mice receiving 5-FC prodrug in their drinking water and the fusion protein had reduced tumor size compared to animals who received 5-FC and an intratumoral injection of yCD alone (*7*). On the surface of liposome in circulation, TSG6-Link could help traffic the liposome to the HA-rich tumor extracellular matrix.

Proteins which specifically target CD44, or CD44 variants (CD44v), overexpressed on cancers could also be a viable option with which to target liposomes. An antibody-radioisotope conjugate, which specifically targeted a splice-variant of CD44, CD44v6, stabilized the progression of cancer or regressed cancer growth in some patients with head and neck squamous cell carcinoma and metastatic breast cancer (*11, 12*). Anti-CD44v6 antibody-radioisotopes stabilized tumor growth at the maximum tolerated dose in half (3 of 6) patients with head and neck squamous cell carcinoma (*12*). Clinical trials of antibody conjugated to the cytotoxic drug mertansine, showed that the antibody-drug conjugate stabilized disease in 2 of 7 patients but were stopped due to severe toxic epidermal necrolysis; this off-target effect results in the epidermis detaching from the

dermis and was fatal in one case (*13*). In patients with early-stage breast cancer, the antibody-radioisotope accumulated in CD44v6 overexpressing tumors, but the accumulation was not correlated to CD44v6 expression or tumor diameter. The tumor to non-tumor tissue ratio was low (*11*). For some cancers, conjugation of the CD44v6-specific antibody to liposomes may avoid off-target effects in the skin while accumulating in tumors due to the EPR effect. Furthermore, fewer antibodies may be needed to target liposomes to CD44v6 overexpressing tumors than were needed to exhibit a therapeutic effect when the antibodies are used directly as conjugate drug-carrier.

Ideally, formulation of recombinant proteins with liposomes may be accomplished through a non-covalent interaction. Incorporating multivalent NTA-head group displays into liposomes increases the retention time of proteins with the liposome in fetal calf serum but did not appear to directly increase circulation time of the protein (**Chapter 3**). Improving this technology may involve improving retention of the chelated metal. This can potentially be done by 'caging' the metal with a novel lipid to prevent loss to endogenous chelators present in the biological system (*14*). However, if the therapeutic protein is removed in circulation due to competition with endogenous multihistidine containing proteins, the strength of interactions between the his-tag and the NTA-liposome will need to be increased, possibly to the sub-picomolar range.

Non-covalent protein association technology is reaching the stage where *in vivo* particulate functionalization is possible but it has yet to breach that threshold. Universal methods to functionalize particles would expand the functions of protein therapeutics to anti-cancer applications and beyond.

6.3 Literature Cited

(1) Naor, D., Nedvetzki, S., Golan, I., Melnik, L., and Faitelson, Y. (2002) CD44 in cancer. *Crit Rev Clin Lab Sci 39*, 527-79.

(2) Eliaz, R. E., Nir, S., Marty, C., and Szoka, F. C., Jr. (2004) Determination and modeling of kinetics of cancer cell killing by doxorubicin and doxorubicin encapsulated in targeted liposomes. *Cancer Res 64*, 711-8.

(3) Eliaz, R. E., Nir, S., and Szoka, F. C., Jr. (2004) Interactions of hyaluronan-targeted liposomes with cultured cells: modeling of binding and endocytosis. *Methods Enzymol 387*, 16-33.

(4) Peer, D., and Margalit, R. (2004) Tumor-targeted hyaluronan nanoliposomes increase the antitumor activity of liposomal Doxorubicin in syngeneic and human xenograft mouse tumor models. *Neoplasia 6*, 343-53.

(5) Peer, D., and Margalit, R. (2004) Loading mitomycin C inside long circulating hyaluronan targeted nano-liposomes increases its antitumor activity in three mice tumor models. *Int J Cancer 108*, 780-9.

(6) Toole, B. P. (2004) Hyaluronan: from extracellular glue to pericellular cue. *Nat Rev Cancer 4*, 528-39.

(7) Park, J. I., Cao, L., Platt, V. M., Huang, Z., Stull, R. A., Dy, E. E., Sperinde, J. J., Yokoyama, J. S., and Szoka, F. C. (2009) Antitumor therapy mediated by 5-fluorocytosine and a recombinant fusion protein containing TSG-6 hyaluronan binding domain and yeast cytosine deaminase. *Mol Pharm 6*, 801-12.

(8) Maeda, H., Seymour, L. W., and Miyamoto, Y. (1992) Conjugates of anticancer agents and polymers: advantages of macromolecular therapeutics in vivo. *Bioconjug Chem 3*, 351-62.

(9) Thompson, C., Osgood, R., Jiang, P., Kadhim, S., Wang, S., Symons, R., Quimbon, A., Radi, A., Bee, W., and Frost, G. I. (2008) Intravenous administration of recombinant human hyaluronidase (rHuPH20 modulates tumor interstitial fluid pressure and pericellular hyaluronan in a human prostate carcinoma xenograft model. *American Association for Cancer Research Annual Meeting San Diego, CA*, Halozyme Poster 2292.

(10) Mahoney, D. J., Blundell, C. D., and Day, A. J. (2001) Mapping the hyaluronan-binding site on the link module from human tumor necrosis factor-stimulated gene-6 by site-directed mutagenesis. *J Biol Chem 276*, 22764-71.

(11) Koppe, M., Schaijk, F., Roos, J., Leeuwen, P., Heider, K. H., Kuthan, H., and Bleichrodt, R. (2004) Safety, pharmacokinetics, immunogenicity, and biodistribution of (186)Re-labeled humanized monoclonal antibody BIWA 4 (Bivatuzumab) in patients with early-stage breast cancer. *Cancer Biother Radiopharm 19*, 720-9.

(12) Borjesson, P. K., Postema, E. J., Roos, J. C., Colnot, D. R., Marres, H. A., van Schie, M. H., Stehle, G., de Bree, R., Snow, G. B., Oyen, W. J., and van Dongen, G. A. (2003) Phase I therapy study with (186)Re-labeled humanized monoclonal antibody BIWA 4 (bivatuzumab) in patients with head and neck squamous cell carcinoma. *Clin Cancer Res 9*, 3961S-72S.

(13) Tijink, B. M., Buter, J., de Bree, R., Giaccone, G., Lang, M. S., Staab, A., Leemans, C. R., and van Dongen, G. A. (2006) A phase I dose escalation study with anti-CD44v6 bivatuzumab mertansine in patients with incurable squamous cell carcinoma of the head and neck or esophagus. *Clin Cancer Res 12*, 6064-72.

(14) Bell, S. G., and Vallee, B. L. (2009) The metallothionein/thionein system: an oxidoreductive metabolic zinc link. *Chembiochem 10*, 55-62.

Publishing Agreement

It is the policy of the University to encourage the distribution of all theses, dissertations, and manuscripts. Copies of all UCSF theses, dissertations, and manuscripts will be routed to the library via the Graduate Division. The library will make all theses, dissertations, and manuscripts accessible to the public and will preserve these to the best of their abilities, in perpetuity.

Please sign the following statement:

I hereby grant permission to the Graduate Division of the University of California, San Francisco to release copies of my thesis, dissertation, or manuscript to the Campus Library to provide access and preservation, in whole or in part, in perpetuity.

Virginia Platt

Author Signature

1/11/10

Date